Dynamics of the Coupled System Troposphere/Stratosphere in the Extratropics

Dissertation
zur Erlangung des Doktorgrades
der Mathematisch-Naturwissenschaftlichen Fakultät
der Christian-Albrechts-Universität zu Kiel
vorgelegt von

Nour-Eddine Omrani

IFM-GEOMAR
Leibniz-Institut für Meereswissenschaften
an der Universität Kiel

Kiel 2007

Contents

0.1 Zusammenfassung

In dieser Studie wurde die Dynamik des gekoppelten Systems Troposphäre/Stratosphäre mit dem atmosphärischen Zirkulationsmodell MAECHAM5, gekoppelt mit einem Deckschicht-Ozeanmodell, untersucht. Der Schwerpunkt lag auf dem Einfluß der Stratosphäre auf die Troposphäre. Bezüglich des Modells konnte festgestellt werden, dass die Januar-MAECHAM5-Klimatologie gut mit der beobachteten Klimatologie übereinstimmt. Am besten ist die Übereinstimmung in den Extratropen und unterhalb der obersten Modellschichten (wo der Sponging-Effekt stark ist). Weitere Untersuchungen zeigten, daß sowohl Dynamik als auch dreidimensionale Struktur des 'Northern Annular Mode' (NAM) in MAECHAM5 gut mit vorherigen Studien übereinstimmen. Bezüglich der Kopplung konnte durch MAECHAM5-Daten festgestellt werden, dass die NAM-Muster nicht nur die troposphärische und stratosphärische Variabilität, sondern auch die Kovariabilität zwischen Troposphäre und Stratosphäre nördlich von 20°N dominieren.

Eine zeitverschiebende 'Composite' Analyse basierend auf dem 50hPa-NAM-Index (NAMI), ein Maß für die Stärke des 'stratosphärischen Modes', zeigte, daß stark positive stratosphärische NAM-Phasen mit einem starken anomalen Westwind in hohen Breiten und einem Temperatur-Quadrupol zwischen Troposphäre und unterer Mesosphäre verbunden sind. Der untere Teil dieses Quadrupols hat eine Dipolstruktur mit einer anomal kalten (warmen) Tropo- und Stratosphäre an den Polen (in den mittleren Breiten) und ist mit einer anomal positiven vertikalen Windscherung assoziiert. Dieser Dipol wird zusammen mit den Westwind-Anomalien in der NAM-Zunahme (Abnahme) Phase stärker (schwächer). Der obere Teil des Temperatur-Quadrupols zeigt einen Dipol mit einer anomal warmen (kalten) oberen Strato- und Mesosphäre an den Polen (in den mittleren Breiten) und ist mit einer anomal negativen vertikalen Windscherung verbunden. Der warme Pol in Mesosphäre und oberer Stratosphäre verstärkt sich zusammen mit den Ostwind-Anomalien besonders in der NAM-Abnahmephase und breitet sich nach unten aus.

Unter Anwendung des Impuls-Erhaltungssatzes in der TEM-Formulierung (Transformed Eulerian Mean) wurde außerdem die Dynamik während des starken stratosphärischen Wirbels analysiert. Die Analyse der Wellen-, Coriolis- und Residualforcings aus dem Impuls-Erhaltungssatz zeigt, dass die NAM-Strukturen der Temperatur, des Windes und der Geopotential-Höhe, sowie ihre abwärts gerichteten Ausbreitungen, aus der Antwort der 'Stretching Vorticity' auf Änderungen des Coriolisforcings und eine quasigeostrophische Anpassung der Troposphäre an diese Änderungen resultieren. Das Coriolis-Forcing wiederum wird durch das Wellen- und das Residualforcing verursacht. Persistenz, Zunahme, und abwärtsgerichtete Ausbreitung der NAM-Anomalien werden durch eine Rückkopplung zwischen planetaren Wellen und polarem Wirbel verstärkt, die den Westwind innerhalb des gekoppelten Systems Troposphäre/Stratosphäre beschleunigt. Dabei verstärken sich die anormale äquatorwärts gerichtete Ausbreitung der planetaren Wellen und der starke polare Wirbel gegenseitig. Abnahme und Modulation der starken NAM-Anomalien werden dagegen durch zwei negative Rückkopplungen erhöht, die den Westwind an der oberen und unteren Grenze des gekoppelten Systems Troposphäre/Stratosphäre verlangsamen: (1) Rückkopplung zwischen polarem Wirbel und Residualforcing in der oberen Stratosphäre und unteren Mesosphäre, die durch das Filtern der Schwerwellen

durch den polaren Wirbel erklärt werden kann. (2) Rückkopplung zwischen Zonalwind und der Summe aus Residual- und planetarem Wellenforcing.

Eine zeitverschiebende 'Composite' Analyse basierend auf dem 1000hPa-NAMI ('troposphärischer Mode') zeigte, dass tropo- und stratosphärischer NAM zwei verschiedene Modes sind, die von unterschiedlichen Forcings angetrieben werden. Im troposphärischen Mode werden die troposphärischen Westwinde durch starke interne Forcings ausgelöst, die sich innerhalb der Troposphäre in den synoptischen Zeitskalen entwickeln. Dies resultiert in stärkeren troposphärischen Westwinden. Die Stratosphäre ist für den troposphärischen Mode ebenfalls wichtig: sie führt zu niederfrequenten Änderungen in der oberen Troposphäre, die mit einer Verstärkung des troposphärischen Wellen-, Coriolis- und Residual-Forcings verbunden sind. Diese Verstärkung des Forcings führt dann zu troposphärischen Zirkulationsanomalien, die zu einer starken anomalen Aufwärtsbewegung führen und damit zu einem starken Vortex, der ca. 4-5 Tage später sein Maximum erreicht. Der starke Vortex trägt durch den 'Stretching Vorticity' Mechanismus und die Rückkopplung zwischen Vortex und planetaren Wellen dazu bei, dass die Westwinde und die Abkühlung in der Tropo- und Stratosphäre andauern. Die stratosphärischen Westwinde sind im troposphärischen Mode schwächer als im stratosphärischen, da die planetaren Wellen im ersteren einen wesentlich geringeren Beitrag zu den stratosphärischen Windanomalien leisten als im stratosphärischen Mode.

0.2 Abstract

In this study the dynamics of the coupled troposphere/stratosphere system was investigated using the atmospheric circulation model MAECHAM5/ocean mixed layer coupled model. The focus was on the impact of the stratosphere on the troposphere. The January climatology of the model agrees well with the observations, especially in the extratropical region and below the uppermost model levels (where the sponging effect is strong). The dynamics that maintains the middle atmospheric circulation in MAECHAM5 is consistent with the middle atmospheric dynamics known from previous studies. The three-dimensional structure of the Northern Annular Mode (NAM) in MAECHMA5 agrees well with that observed. The NAM dominates not only the variability in but also the covariability between troposphere and stratosphere north of 20°N.

A lag composite analysis based on the 50hPa NAM-Index (NAMI), a measure of the strength of the 'stratospheric mode', shows that strongly positive stratospheric NAM-phases are associated with strong anomalous westerlies in high latitudes and a temperature quadrupole between troposphere and lower mesosphere. The lower part of this quadrupole shows a dipole structure with an anomalous cold (warm) polar (mid-latitude) troposphere and stratosphere and is associated with a positive shear of the anomalous westerlies there. This dipole strengthens (weakens), together with the anomalous westerlies, in the NAM-increase (decrease) phase. The upper part of the temperature quadrupole shows a coherent dipole with an anomalous warm (cold) polar (mid-latitude) upper stratosphere and lowermost mesosphere and is associated with a negative shear of the anomalous zonal flow there. The warm pole in mesosphere and upper stratosphere strengthens and propagates downward together with anomalous easterlies, especially in the NAM-decrease phase.

The dynamics during strong vortex is analyzed by computing the wave, residual Coriolis, and non-resolved (residual) forcing in the Transformed Eulerian Mean formulation (TEM). NAM temperature, zonal flow and geopotential height patterns and their downward propagation can be explained by the response of the stretching vorticity to residual Coriolis forcing changes, which are caused by the resolved and non-resolved wave forcing, and by quasigeostrophic adjustment of the troposphere to these changes. The persistence, increase, and downward propagation of the NAM-patterns is enhanced mainly by the planetary wave-vortex feedback that accelerates the westerlies within the coupled troposphere/stratosphere system. Thereby the strong vortex is strengthened further by the equatorward propagation of planetary waves and vice versa. The decrease and modulation of the strong NAM-anomalies is enhanced by two negative feedbacks that decelerate the westerlies in the upper and lower boundaries of the coupled troposphere/stratosphere system. The first feedback is a vortex-residual forcing feedback acting in upper stratosphere and lower mesosphere and can be explained by the filtering of gravity waves by the stratospheric jet. The second feedback acts near the lower boundary and is driven by both residual and planetary wave forcing.

A lag composite analysis based on the 1000hPa-NAMI, a measure of the strength of the 'tropospheric mode', showed that tropospheric and stratospheric NAM are two different modes driven by two different forcings. In the tropospheric mode the tropospheric

westerlies are induced by a strong internal wave forcing, which develops inside the troposphere on a synoptical time scale. This results in stronger tropospheric westerlies in the tropospheric mode. The stratosphere is also important in the tropospheric mode: It provides the upper troposphere with a low frequency westerly wind and wind shear and thus with enhanced baroclinicity that are associated with an amplification of the upper tropospheric wave, Coriolis and residual forcing. This forcing amplification leads then to an increase of the tropospheric circulation anomalies, which results in anomalous ascent and cooling in the Arctic and thus in a strong vortex that reaches its maximum 4-5 days later. The strong vortex contributes, through the stretching vorticity mechanism and the vortex-planetary waves forcing, to the persistence of both tropospheric and stratospheric westerlies and cooling. The stratospheric westerlies are much weaker in the tropospheric than in the stratospheric mode due to the much lower contribution of the planetary waves to the stratospheric wind anomalies in the tropospheric mode.

0.3 Abbreviations and list of figures

Abbreviations

AM	Annular Mode
AO	Arctic Oscillation
EOF	Empirical Orthogonal Function
EP-flux	Eliassen-Palm-Flux
GCM	General Circulation Model
H - L	High minus Low composite
(MA)ECHAM5	(Middle Atmospheric) Hamburg version of the ECMWF model
ML	Mixed Layer
NAM(I)	Northern Annular Mode (Index)
NAO(I)	North Atlantic Oscillation (Index)
TEM(E)	Transformed Eulerian Mean (Equation)
SVD	Singular Value Decomposition
PC(A)	Principal Component (Analysis)
PV	Potential Vorticity
QBO	Quasi Biannual Oscillation
SAM(I)	Southern Annular Mode (Index)
SPARC	Stratospheric Processes And their Role in Climate
SSA	Singular Spectrum Analysis
SST	Sea Surface Temperature
STE	Stratosphere-Troposphere Exchange
STT	Stratosphere-Troposphere-Transport
TST	Troposphere-Stratosphere-Transport
TTL	Tropical-Tropopause-Layer

List of Figures

1 Introduction

1.1 Overview of this study

The purpose of this work is to understand the dynamics of the coupling between troposphere and stratosphere with the help of the middle atmosphere model MAECHAM5 coupled to an ocean mixed layer model, which was used without any external forcing. This makes the interpretation of the results easy, since the effects on ocean dynamics and/or natural and anthropogenic forcings are not considered. In this first chapter a general introduction into the different modes of coupling between troposphere and stratosphere is given. The focus is on the dynamical mode of the coupling. In the second chapter, the accuracy of MAECHAM5 is described by comparing its climatology to observational data and by looking at the consistency of its dynamics. The focus is on the meridional residual circulation and on its forcing. In the third chapter, the leading modes of the month-to-month winter variability and covariability in the stratosphere/troposphere coupled system are identified. The dominant intraseasonal time scales of the tropospheric and stratospheric NAM are also investigated. In the fourth chapter the dynamics of the coupled system stratosphere/troposphere during strong stratospheric Northern Annular Mode -NAM- or vortex (in the following: 'stratospheric mode') are examined. The following fundamental questions are addressed in chapter four:

- What drives the temperature, wind, and geopotential patterns during strong stratospheric NAM-phases?
- Which mechanisms control the strengthening of the polar vortex and its impact on the troposphere?

- Which processes contribute to the weakening and decay of the polar vortex?

Finally, in chapter 5, the dynamics of the coupling between troposphere and stratosphere during strong tropospheric NAM (in the following 'tropospheric mode') is investigated briefly. The focus is on the differences between the stratospheric and tropospheric modes. The results of this study are discussed in chapter 6.

1.2 The vertical structure of the atmosphere

The conventional dividing of the atmosphere is based on the vertical structure of the temperature field (Fig. 1.1). The lowermost atmospheric layer is the troposphere, and it extends from the surface to the tropopause (10-16 km depending on latitude). The troposphere is characterized by a temperature decrease with height. The stratosphere extends from the tropopause to the stratopause (about 50 km) and is characterized by a temperature increase with height. The mesosphere is located between stratopause and mesopause (about 80 km) and shows, like the troposphere, a temperature decrease with height. The thermosphere is characterized by a temperature increase with height and extends from the mesosphere to about 500 km. The region between the tropopause and approximately 110km (homopause) is termed 'middle atmosphere'.

The troposphere contains about 85% of the atmospheric mass and nearly all of the water vapor. Almost all human activities and weather phenomena occur in this layer. The strongest absorption of the solar radiation that reaches the troposphere is found at the surface. The absorption of the short wave radiation in the free troposphere is weak, so that the vertical thermal structure of the troposphere results mainly from the balance among infrared radiative cooling, vertical turbulent transport of sensible and latent heat from the surface, and heat transport by synoptic eddies. This results in the maximum tropospheric temperature near the surface that decreases vertically with a lapse rate of about 6°C/km, and in low static stability leading to enhanced vertical mixing. The term troposphere originates from the Greek word 'tropos',

which means 'mixing' and thus reflects the main property of the troposphere. The

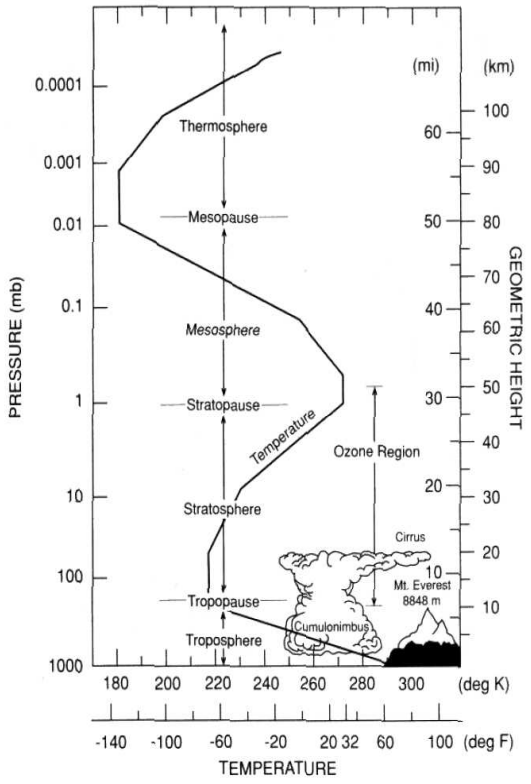

Figure 1.1: Vertical profile of the temperature as defined in U.S. Standard Atmosphere [1976]. The tropopause level is represented for mid-latitude conditions. The clouds in the tropics extend to about 18 km, which corresponds to the tropical tropopause. Figure taken from *Brasseur et al.* [1999].

thermal structure of the middle atmosphere results mainly from the balance between the infrared radiative cooling by the stratospheric gases and the radiative heating due to the absorption of the solar ultraviolet (UV) radiation by ozone. The latter induces an increase of the stratospheric temperature with height, which results in a strong static stability suppressing rapid vertical mixing so that horizontal mixing becomes more important. The term stratosphere stems from the Latin word 'stratum', which means 'layered' and reflects the layered structure of the stratosphere.

1.3 The meridional circulation in the middle atmosphere

The middle atmospheric meridional circulation (Fig. 1.2) results mainly from the dynamical response to the seasonal radiative heating. The imbalance between the UV-absorption by ozone and cooling (caused mainly by greenhouse gases) throughout the middle atmosphere determines to a very large degree the middle atmospheric

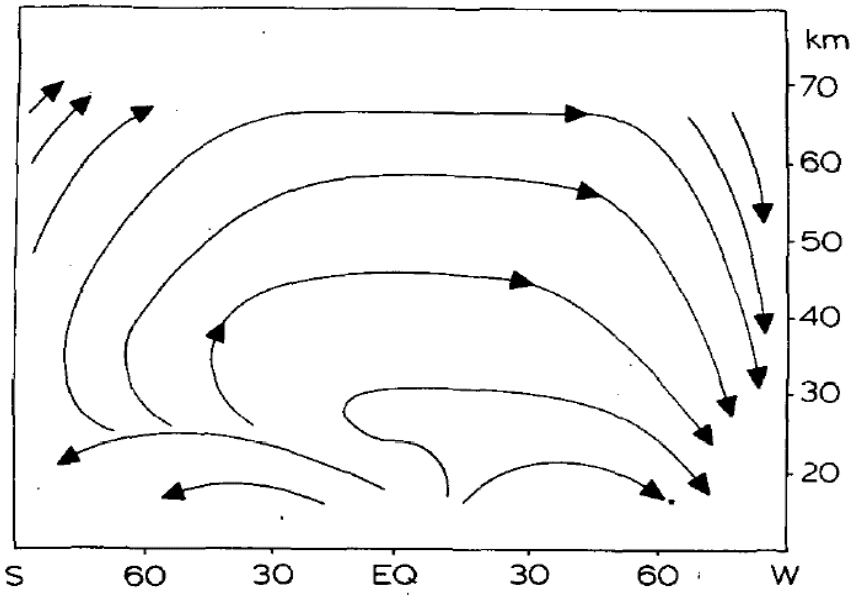

Figure 1.2: Schematic streamlines of the meridional residual circulation during northern winter [After *Dunkerton*, 1978]

temperature pattern. The structure of the temperature that results from the radiative equilibrium (without dynamics) shows a strong temperature decrease from the summer to the winter pole e.g. [e.g. *Andrews et al.*, 1987; *Holton*, 1992]. This results, by thermal wind balance, in very strong radiatively induced westerlies (easterlies) in the winter (summer) hemisphere of the middle atmosphere. The radiatively induced temperature in the poles deviates strongly from the observed temperature, which

results from both radiative and dynamical heating.

The role of the middle atmospheric circulation, i.e. dynamics, consists in the compensation of the radiative heating (by vertical motion), a damping of the radiatively induced meridional temperature gradients and a reduction of the radiatively induced strong zonal flow. In this way, the temperature and zonal flow structures become comparable to observations. The middle atmospheric circulation of the summer pole is dominated by upward motion and thus an adiabatic cooling that compensates the strong radiative heating and weakens the radiatively induced meridional temperature gradients and easterlies there. The winter pole part of the meridional circulation is dominated by downward motion and thus by an adiabatic warming that compensates the radiative cooling and weakens the radiatively induced meridional temperature gradient and westerlies there. A meridional motion from winter to summer hemisphere is thus induced across the equator leading to the so-called Murgatroyd-Singleton circulation [*Murgatroyd and Singleton*, 1961; *Dunkerton*, 1978]. This one-cell circulation structure dominates in the upper part of the middle atmosphere. The lower and middle stratosphere is dominated by a quasi-symmetric two-cell circulation known as Brewer-Dobson circulation. Both Brewer-Dobson and Murgatroyd-Singleton circulation are driven by tropospheric waves that propagate into the middle atmosphere inducing a circulation change by wave-meanflow interactions. The Brewer-Dobson circulation is strongest in the winter pole, where planetary wave activity is strong.

1.4 The Annular Mode (AM)

The most recent investigations of the coupling between stratosphere and troposphere use the Annular Mode (AM) [*Thompson and Wallace*, 1998; 2000; *Baldwin and Dunkerton*, 1999]. The AM in the Northern (Southern) Hemisphere is referred to as the Northern (Southern) Annular Mode, i.e. NAM (SAM), and defined as the leading Empirical Orthogonal Function (EOF) of the monthly winter geopotential height north of $20°N$ (south of $20°S$). The AM pattern is nearly zonally

symmetric. Its structure is characterized by a meridional dipole in the geopotential height between the arctic basin and the surrounding zonal ring [e.g. *Thompson and Wallace*, 1998]. The Principal Component (PC) corresponding to the NAM (SAM) is called NAM- (SAM-) Index, i.e. NAMI (SAMI). The NAM at the surface is strongly related to the North Atlantic Oscillation (NAO) [*Thompson and Wallace*, 1998]. The NAM-associated zonally averaged zonal wind anomalies show a north-south dipole structure centered on 40°-45°N; the zonally averaged temperature shows cold (warm) anomalies in the polar stratosphere and upper troposphere at positive (negative) NAM-phase [*Baldwin and Dunkerton*, 1999; *Thompson and Wallace*, 2000]. The NAM describes the strength of the polar vortex, which is a large-scale cyclone near the winter pole that persists in the middle and upper troposphere and in the stratosphere during the whole winter. Because of the enhanced wave activities, caused by the winter hemispheric distribution of land masses, the Arctic polar vortex is less pronounced and more variable than the Antarctic one. During positive (negative) NAMI, the polar vortex is strong (weak) through convention, and the jet is shifted poleward (equatorward) [e.g. *Limpasuvan and Hartmann*, 1999]. The structure and the amplitude of the AM can be obtained from a model run in climatological mode, indicating that it results from the internal atmospheric dynamics [e.g. *Limpasuvan and Hartmann*, 1999].

1.5 The coupling between troposphere and middle atmosphere

There are three modes of coupling between middle atmosphere and troposphere that interact with each other: A radiative, a dynamical, and a chemical mode (Fig. 1.3). This study concentrates on the dynamical mode with the focus on the impact of the middle atmosphere on the troposphere.

1.5.1 The chemical mode of coupling

The abundance and distribution of ozone, which is the major source of the diabatic heating and causes the main temperature distribution in the middle atmosphere, is determined by a large number of photochemically active species. These originate to a large extent from the troposphere (e.g. oxygen, hydrogen, chlorine and bromine

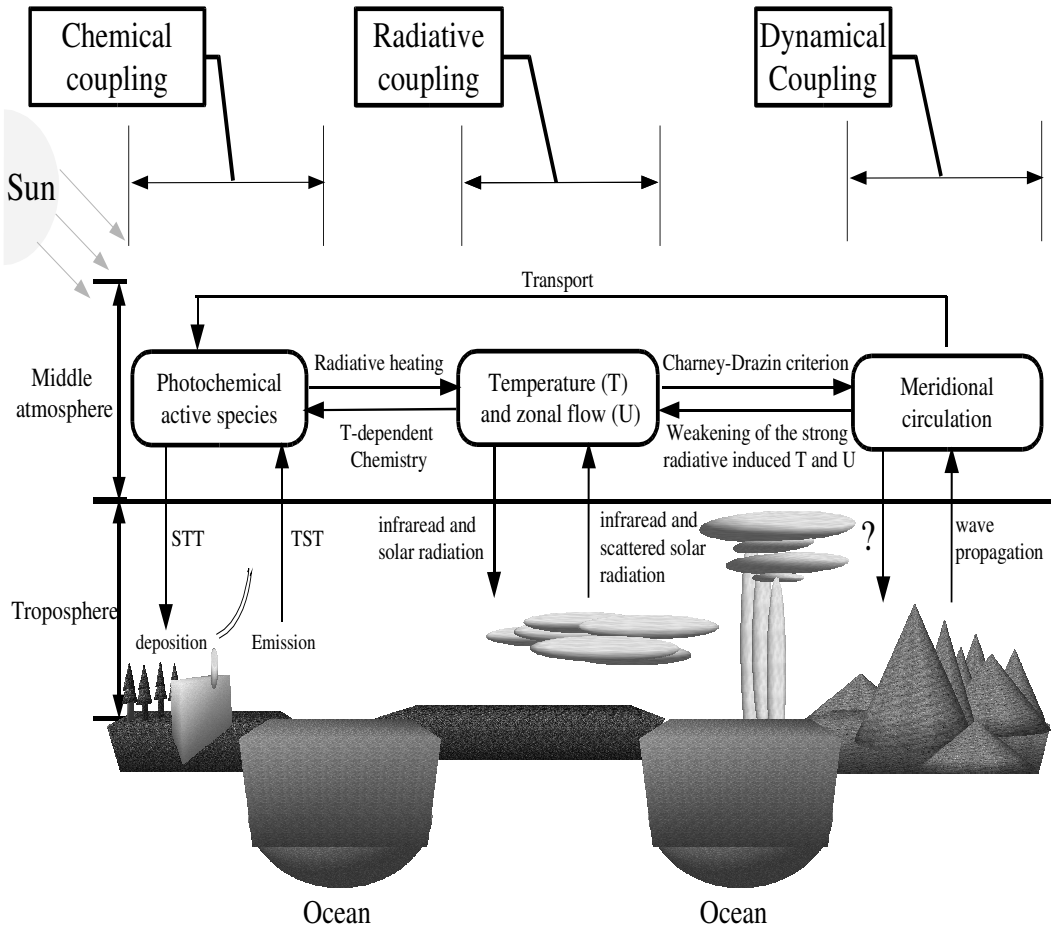

Figure 1.3: Schematic representation of the chemical, radiative and dynamical modes of coupling between the middle atmosphere and troposphere and their interactions with each other.

compounds).

Troposphere and middle atmosphere are coupled chemically through the Stratosphere-Troposphere Exchange (STE) of the photochemically active gases. The troposphere impacts the middle atmosphere chemically by the Troposphere-to-Stratosphere Transport of tropospheric gases (TST), while the middle atmosphere impacts the troposphere by the loss of chemical species through the Stratosphere-to-Troposphere-Transport (STT). The global scale of STE is due to the Brewer-Dobson circulation (Fig. 1.2). It transports the tropospheric air, which reaches the stratosphere by tropical convection, into the winter hemisphere and pushes the stratospheric air through the extratropical tropopause into the troposphere causing STT. At smaller scales the STE is dominated by the synoptic scale eddy processes, which cause a three-dimensional deformation of the tropopause associated with the so-called tropopause folds [e.g. *Danielsen et al.*, 1970] and filamentation [e.g. *Appenzeller et al.*, 1996]. The STE can also occur by tropopause erosion through the mesoscale exchange inside convective systems [e.g. *Rood et al.*, 1997] and so-called cut-off cyclones [e.g. *Gouget et al.*, 2000]. The distribution and formation of photochemical species and ozone in the middle atmosphere is determined not only by STE (i.e. STT and TST) but also by temperature-dependent chemical reactions and transport-processes occurring in the middle atmosphere itself. Most of the tropospheric species that are transported into the stratosphere by TST are the direct result of emissions at the earth's surface mainly by oceans, soils, biosphere and human activities.

1.5.2 The radiative mode of coupling

The troposphere can influence the thermal structure of the middle atmosphere radiatively (Fig. 1.3) by infrared radiation originating in the troposphere and also by the solar radiation backscattered from the surface and clouds. The middle atmosphere, on the other hand, impacts the troposphere radiatively by the absorption and thus the filtering of short wave radiation and the direct emission of infrared radiation by various trace gases. The radiatively induced temperature is mainly controlled by the abundance and distribution of ozone, which is determined by the photochemically active species. The seasonal radiative heating is associated through

the thermal wind balance with radiatively induced westerly and easterly jets in the high latitude winter and summer stratosphere, respectively. In both hemispheres, the radiatively induced jets are stronger than the observed jets, as described above.

1.5.3 The dynamical mode of coupling

1.5.3.1 The dynamical impact of the troposphere on the stratosphere

The troposphere affects the middle atmosphere dynamically in the high and middle latitudes (Fig. 1.3) through planetary and gravity waves. Both waves propagate upward and change the zonal flow in such a way that the Coriolis force response results in the meridional residual circulation shown in Fig 1.2.

The upward propagation of the planetary waves [e.g. *Charney and Drazin*, 1961; *Matsuno*, 1970] changes the zonal mean flow through eddy heat and momentum fluxes. This results in a westward acceleration of the zonal mean flow as well as in an eastward Coriolis force and thus in a poleward motion. The net result of these changes are the Brewer-Dobson circulation and an adiabatic warming by downward motion, which weakens the polar vortex and damps the strong radiatively induced meridional temperature gradient and zonal flow. The planetary waves can be generated in the troposphere by land-sea heat contrasts and topography. They break into the middle atmosphere, if the background wind is westerly but, weaker than a threshold value, and the propagating waves have a large horizontal wavelength. This so-called 'Charney-Drazin criterion' can occur in the Northern Hemisphere during the boreal winter, when the stratospheric wind is westerly and the tropospheric planetary wave activity is strong.

The wave driven Brewer-Dobson circulation transports the chemical species from the tropical troposphere into the winter part of the middle atmosphere and then downward into the lower stratosphere. This explains the enhanced spring ozone concentration in the high latitude middle and lower stratosphere. It also explains the extreme dryness of the stratosphere, since the tropospheric air is strongly dehydrated in the extremely cold tropical tropopause before reaching the stratosphere.

One of the most important stratospheric events is the major stratospheric warming, which is driven by planetary waves. This event occurs typically in the Northern Hemisphere about every two years, when the wave breaking into the stratosphere is large enough to drive a strong Brewer-Dobson circulation and thus a strong adiabatic warming that reverses the stratospheric meridional temperature gradient and the westerlies into easterlies. The major stratospheric warming was observed in the Southern Hemisphere in the winter of 2002 for the first time [e.g. *Orsolini et al.*, 2005; *Krüger et al.*, 2005].

The annual appearance of the Antarctic ozone hole in the last decades and its virtual absence in the arctic is related to weaker orography-induced waves in the Southern compared to the Northern Hemisphere. The reduced wave breaking in the Antarctic stratosphere leads to a weaker Brewer-Dobson circulation and thus to less adiabatic warming by downward motion and a stronger polar vortex. This favors the colder antarctic temperatures, less ozone transport into the Antarctic and the formation of the polar stratospheric clouds. The latter accelerate the conversion of the anthropogenic bromine and chlorine from photochemically inactive to active forms. The net effect is the formation of the Antarctic ozone hole in spring, when the sunlight returns and bromine and chlorine catalyze photochemical reactions that destroy the stratospheric ozone. During the transition from winter westerlies to summer easterlies the polar vortex breaks up and the Antarctic ozone-poor air is mixed with ozone-rich air from lower latitudes, which causes a ‘filling up‘ of the ozone hole.

Not only the stationary waves are active in the middle atmosphere, but also the transient growing waves, which are induced by baroclinic and barotropic instabilities associated with the vertical and horizontal shear of the zonal flow, respectively. The climatology of the zonal wind in the winter hemisphere is characterised by a strong subtropical jet in the troposphere as well as strong westerlies in the mid latitude stratosphere and mesosphere, with a maximum near the stratopause. This results in a strong westerly wind shear and thus baroclinic instability in both stratosphere and troposphere [e.g. *Charney*, 1947; *Green*, 1960; *Hartmann*, 1979; *Strauss*, 1981;

Mechoso and Hartmann, 1982]. The strong tropospheric vertical wind shear is associated with a shallow baroclinic mode called 'Charney mode', which has the largest amplitude in the troposphere and decreases strongly in the lower stratosphere. The strong stratospheric westerly shear is associated with a deep baroclinic mode called 'Green Mode', the amplitude of which shows a very rapid increase from the troposphere to the stratosphere. *Tanaka and Tokinaga* [2002] showed that the anomalous strong high latitude stratospheric vortex is associated with a deep baroclinic mode called 'monopole Charney mode' (M_1). The M_1-mode extends from the troposphere into the stratosphere and transfers the momentum poleward in such a way that the stratospheric jet is strengthened. A positive feedback between polar vortex and M_1-mode that contributes to the persistence of the strong polar vortex was proposed by the same authors. The summer hemisphere is characterised by strong easterlies throughout the mid latitude stratosphere and lower mesosphere, with a maximum near the stratopause. This leads to negative (positive) wind shear and thus to reduced (enhanced) baroclinicity in the stratosphere (mesosphere). The inversion of the stratospheric zonal wind and its vertical shear in the summer hemisphere and during the sudden stratospheric warming (in the northern winter hemisphere) result in an absence of the baroclinic mode in the stratosphere [*Zhang and Sasamori*, 1985]. The strong westerly wind shear in the summer mesosphere results in enhanced baroclinic wave activities [e.g. *Rodgers and Prada*, 1981; *Plumb*, 1983; *Pfister*, 1985].

1.5.3.2 Gravity waves

Gravity waves can be generated by mountain barriers, deep convection, and shear instability of the tropospheric jet. They break non-linearly towards the upper middle atmosphere due to the exponential increase of their amplitude with altitude. They tend to preserve their energy density during their upward propagation and become dominant in the mesosphere. Several observational studies show that the major stratospheric warming is associated with a compensating cooling in the mesosphere [e.g. *Quiroz*, 1969; *Labitzke*, 1972a;b; *Hirota and Barnett*, 1977]. The mesospheric cooling has been attributed to the effect of the gravity wave drag [e.g. *Lindzen*, 1981;

Matsuno, 1982; *Holton*, 1983]. Although the planetary waves are important for the stratospheric temperature change, *Holton* [1983] showed that a realistic warming in the polar upper stratosphere can be simulated by using only the gravity wave drag, tuned to ensure a realistic mesosphere. Using observational data, *Duck et al.* [2001] found high gravity wave activity in the vortex jet after late December, which was related to a strengthening of the jet. Their calculations suggested that the drag induced in late December drives a warming observed in the vortex core and weakens the vortex-jet. They deduced a feedback mechanism between vortex-jet and gravity waves that regulates the strength of the arctic stratospheric vortex.

1.5.3.3 The dynamical impact of the middle atmosphere on the troposphere

While the dynamical impact of the troposphere on the middle atmosphere through planetary and gravity waves has been well accepted, there are still many debates about the impact of the middle atmosphere on the troposphere. Many observational and model studies show an impact of the stratosphere on the tropospheric circulation. One of the first to present evidence of this was *Quiroz* [1977], who showed that a large increase of the tropospheric temperature was associated with the sudden stratospheric warming of 1976-1977. The downward propagation of the low frequency signal of the zonally averaged zonal wind was shown e.g. by *Kodera et al.* [1990]. *Baldwin and Dunkerton* [1999] showed that the NAM anomalies first appear in the stratosphere and then propagate downward into the troposphere on time scales of few weeks. The tropospheric anomalies induced persist up to two months after the extreme stratospheric circulation anomalies [e.g. *Baldwin and Dunkerton*, 2001]. *Baldwin et al.* [2003] used an empirical statistical model to demonstrate the possibility of extended-range forecasts of the NAM at the surface (called Arctic Oscillation, AO). They showed that the best extended-range prediction of the AO occurs in winter using the lower stratospheric NAM as predictor. The low frequency NAM at 150hPa accounted for 20% of the variance of the AO in the time lags of 10 to 40 days and was a better predictor of the AO than the AO itself. The stratospheric influence on the troposphere was shown in both relatively simple models and more

complex general circulation models [*Boville*, 1984; *Christiansen*, 2001; *Polvani and Kushner*, 2002; *Norton*, 2003].

Three different mechanisms have been proposed to explain the dynamical impact of the stratosphere on the troposphere. The first mechanism is the direct influence on tropospheric wind and temperature of the stratospheric potential vorticity change. *Black* [2002] used the quasi-geostrophic piecewise potential vorticity inversion to show the forcing of tropospheric wind anomalies by localized stratospheric potential vorticity anomalies. A strong stratospheric polar vortex is associated with enhanced positive stratospheric potential vorticity anomalies, which cause both a rise of the tropopause and stretching of the tropospheric column at the pole [e.g. *Ambaum and Hoskins*, 2002] resulting in a lower pressure and an increase of the tropospheric westerlies. This mechanism explains how tropospheric wind anomalies can be generated by stratospheric potential vorticity anomalies. A strong polar vortex is also associated with an enhanced anomalous equatorward propagation of tropospheric planetary waves, which means less wave breaking in the stratospheric jet and thus its strengthening [e.g. *Ambaum and Hoskins*, 2002]. An equivalent approach to the non-local effect of the potential vorticity inversion is the 'downward control' shown by *Haynes et al.* [1991] and *Holton et al.* [1995]. In this mechanism, the meridional circulation is non-locally controlled by wave-induced forcing and short-wave heating. At timescales greater than the radiative damping timescale of the stratosphere (about 10 days), the wave-induced forcing becomes more important than the short-wave heating, and the non-locally induced meridional circulation becomes deeper and narrower. The second proposed mechanism is the indirect effect of the refraction index on the wave propagation. The change of the low stratospheric polar vortex induces a change of the tropospheric vertical wind shear and of the vertical and meridional wind curvature, and thus a change in wave refraction [*Hartmann et al.*, 2000; *Lorenz and Hartmann*, 2003]. This affects both the tropospheric and the stratospheric zonal wind. The third mechanism is the vertical reflection of the Rossby waves in the upper stratosphere into the troposphere [e.g. *Perlwitz and Harnik*, 2003; 2004]. Here a reflecting surface, which results from the vertical wind curvature, is formed around 5hPa, if the polar night jet peaks.

None of the proposed mechanisms include the impact of the upper stratosphere and mesosphere. There is observational evidence of a compensating cooling in the mesosphere during the sudden stratospheric warming [*Quiroz*, 1969; *Labitzke*, 1972a;b; *Hirota and Barnett*, 1977], which has been attributed to the gravity wave drag [*Lindzen*, 1981; *Matsuno*, 1982; *Holton*, 1983]. The impact of such compensating mesospheric temperature changes on the stratosphere-troposphere coupling has not yet been considered.

2 The dynamics of the middle atmosphere in MAECHAM5

This chapter examines the accuracy of the MAECHAM5 model used to understand the dynamics of the coupling between troposphere and middle atmosphere. First, the model is compared with observations and then the consistency of its dynamics in the middle atmosphere is investigated. The focus is on the meridional residual circulation and its forcing agents.

2.1 Model and observational data

2.1.1 Model

The following results are based on a 45-years simulation performed with the Middle Atmospheric version of the ECHAM5 general circulation model (MAECHAM5) coupled to an ocean mixed layer model. MAECHAM5 is an atmospheric model developed to simulate the general circulation of troposphere, stratosphere, and lower mesosphere. The vertical domain ranges from the surface to 0.01 hPa (about $80km$) and allows the investigation of the impacts of the evolution of the upper stratosphere and the lower mesosphere on the life cycle of the polar vortex. Differences between the standard ECHAM5 and MAECHAM5 include: The vertical resolution and the location of the model top, the parameterization of the momentum flux due to gravity waves, and a few modifications in the representation of the horizontal diffusion. Both MAECHAM and ECHAM exist in two cycles, 4 and 5, respectively. A detailed description of the ECHAM4 model is given by *Roeckner et al.* [1996]. A

description as well as a climatology of ECHAM5 are given by *Roeckner et al.* [2003] and *Roeckner et al.* [2004]. A summary of the MAECHAM4 model parameterizations and the model structure is given by *Manzini and McFarlane* [1998]. We used the model with a T42 horizontal resolution and 39 levels in the vertical.

The mixed layer (ML) ocean ice model has a 50m constant depth and a seasonally varying Q-flux. The model heat budget is calculated separately for ice-free and ice-covered regions. The distributions of ozone, well-mixed greenhouse gases, and aerosols are prescribed from the climatology, and the solar effect is included only in the seasonal time scales. In this way, several external natural and anthropogenic forcings affecting the atmosphere on inter-annual and interdecadal time scales were excluded.

2.1.2 Observational data (SPARC)

The MAECHAM5-January climatology of the zonally averaged zonal wind and temperature is validated using the 'Stratospheric Processes And their Role in Climate' (SPARC) climatology (SPARC Report No.3). The temperature in the SPARC data set is derived using the United Kingdom Meteorological Office's (UKMO) analysis over 1000-1.5hPa, combined with the 'Halogen Occultation Experiment' (HALOE) temperature between 50°S-50°N and over 1.5-0.0046hPa (about 85km). The mesospheric temperature poleward of 50°N and 50°S is derived from the Microwave Limb Sounder (MLS) climatology. The UKMO analysis consists in a stratosphere-troposphere version of the UK Meteorological Office data assimilation system [*Swinbank and O'Neill*, 1994] that has been used since October 1991 to produce daily stratospheric data. The HALOE instrument on the Upper Atmosphere Research Satellite (UARS) provides temperatures in the altitude range of about 45-85 km [*Russell et al.*, 1993; *Hervig et al.*, 1996]. The MLS instrument is also set on UARS [*Fishbein et al.*, 1996]. The data are obtained from a retrieval described in *Wu et al.* [2003]. The valid altitude range is 20-90 km, with large uncertainties at the two ends. The monthly zonal wind climatology of the SPARC data (over 0-85 km) is derived from the 'Reference Atmosphere Project' (URAP) [*Swinbank and Ortland*,

2003], which is based primarily on UKMO, UARS and 'High Resolution Doppler Imager' (HRDI) [*Hays et al.*, 2003] data. In order to provide smooth monthly estimates, the harmonic analysis of the available time series over 1992-1997 was used, including annual and semi-annual harmonic components.

2.2 The Transformed Eulerian Mean (TEM) formulation of the momentum budget

The Transformed Eulerian Mean (TEM) formulation of the momentum and heat budget [e.g. *Andrews et al.*, 1987; *Holton*, 1992] provides all forcings driving the change of the zonally averaged wind and temperature. The momentum budget in the quasigeostrophic form of the TEM-formulation (equation 2.1) was used to test the dynamics of MAECHAM5 that maintains the wind climatology and drives the residual meridional circulation and thus the temperature deviations from the radiative equilibrium. Because of the small Rossby number, the quasigeostrophic flow evolves slowly compared to the rotation period of the earth. In the quasigeostrophic approximation, the horizontal acceleration and advection are supposed to be geostrophic, and the vertical advection is neglected. Near the strong jet the three-dimensional wind becomes stronger, and the non-quasigeostrophic components in the primitive equations become important.

$$\bar{u}_t = f\bar{v^*} + (a\,\cos\phi)^{-1}\underline{\nabla}\cdot\underline{F} + \bar{X} \tag{2.1}$$

$$\bar{v}^* = \bar{v} - \left(\frac{\overline{v'\theta'}}{\bar{\theta}_p}\right)_p \quad and \quad \bar{\omega}^* = \bar{\omega} + \frac{1}{a\,\cos\phi}\left(\cos\phi\,\frac{\overline{v'\theta'}}{\bar{\theta}_p}\right)_\phi \tag{2.2}$$

$$F^\phi = -a\,\cos\phi\,\overline{u'v'} \;\; and \;\; F^p = af\cos\phi\left(\frac{\overline{v'\theta'}}{\overline{\theta_p}}\right) \tag{2.3}$$

In these equations t, ϕ, and p denote time, latitude, and pressure, and subscripts denote derivations, respectively. The bars denote the zonal mean, the prime denotes the deviation from the zonal mean. $\bar{u}$ is the zonal mean of the zonal wind, $\overline{T}$ the zonal mean of the temperature, and $\bar{v}^*$ ($\bar{\omega}^*$) the horizontal (vertical) residual velocity.

The vector $\underline{F}$ is the Eliassen-Palm-Flux (EP-flux), F^{ϕ} and F^{p} the meridional and vertical components of the EP-flux, f the Coriolis parameter, κ=R/$C_p = 2/7$. θ is the potential temperature and a is the earth's radius.

The first term on the right side of equation (2.1) is the residual Coriolis forcing, and the second term is the wave forcing. The residual Coriolis forcing strengthens (weakens) the westerlies by poleward (equatorward) motion and the wave forcing strengthens (weakens) the westerlies by the divergence (convergence) of the EP-flux. The third term is the residual forcing, which was computed from zonal averaged wind tendency, Coriolis forcing, wave forcing and advection terms [e.g. *Andrews et al.*, 1987; *Holton*, 1992]. In this way, the residual forcing includes all non-resolved forcings such as gravity wave drag, forcing of non-quasigeostrophic EP-flux and frictional forcing. The orographic gravity wave drag in MAECHAM5 is parameterized using *Lott and Miller* [1997], as in ECHAM5. Unlike ECHAM5, MAECHAM5 additionally includes the parameterization of the momentum flux deposition from the spectrum of non-orographic gravity waves [*Hines*, 1997b;a]. Both orographic and non-orographic gravity wave drag depend on the vertical structure of the background wind. The frictional forcing is important near the surface.

2.3 The structure of the zonally averaged zonal wind and temperature

Fig. 2.1 shows the radiatively induced temperature in the middle atmosphere in mid-January from a radiative-convective-photochemical model [*Fels*, 1985]. Fig. 2.2a(1) (2.2b(1)) shows the January climatology of the zonally averaged temperature (zonal wind) from the MAECHAM5 simulation, and Fig. 2.2a(2) (2.2b(2)) shows the corresponding SPARC observational data.

The radiatively determined temperature of the middle atmosphere in Fig. 2.1 is caused only by the imbalance between infrared radiative cooling (due to emissions by the middle atmospheric gases) and short-wave radiative heating (due to the absorption of the solar ultraviolet (UV) radiation by ozone). This temperature

shows a strong seasonal dependence, with maximum heating in the summer pole (due mainly to the absorption of the solar radiation by ozone) and maximum cooling in the winter pole (due mainly to the longwave emission by the middle atmospheric gases including ozone). The structure of the radiatively determined temperature shows an almost uniform decrease from the summer to the winter pole.

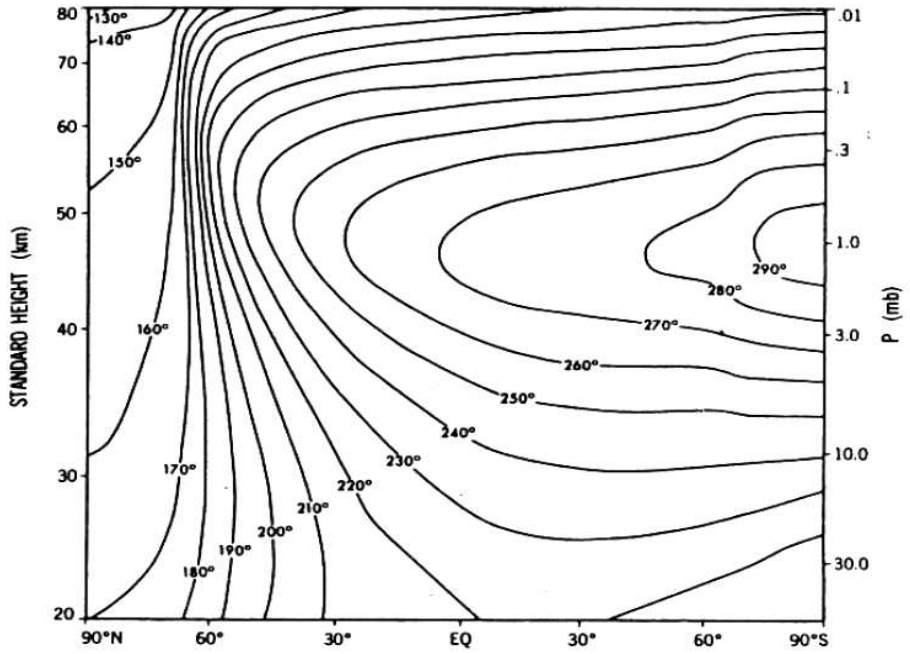

Figure 2.1: The radiatively determined temperature in mid-January from a radiative-convective-photochemical model that was driven by the annual cycle. The tropospheric lapse rate was set to 6.5 $°K/km$. The cloudiness and ozone below 25 km were prescribed at the annual mean values. The ozone above 25 km was computed by a detailed photochemical model. Figure taken from *Fels* [1985].

Although the temperature and wind structures in the MAECHAM5 simulation and observational data are quite similar in most regions, there are some differences, especially in the uppermost model levels where the nudging is strong and the vertical resolution is low. In several regions, the temperature in both MAECHAM5 and observational data differs strongly from that in Fig. 2.1. The reversed temper-

ature gradient near the summer and winter poles between upper stratosphere and mesosphere can be seen only in the observations and MAECHAM5 and can thus be attributed to dynamical and not radiative processes. The middle atmosphere near the summer pole is much colder and near the winter pole much warmer than the radiative equilibrium. Large differences from the radiative equilibrium can also be seen in the equatorial stratosphere, with much warmer temperatures than the radiatively determined on . The dynamics damp hence the radiatively determined temperature gradient and thus the zonal flow.

The structure of the zonally averaged zonal wind simulated by MAECHAM5 is quite similar to that observed. It shows a strong easterly (westerly) jet in the summer (winter) hemisphere near the stratopause that results from the prevailing temperature structures by thermal wind balance. Westerly subtropical jets are seen in both the summer and winter troposphere and are comparable in both location and strength in the MAECHAM5 and observational data.

In summary, much colder (warmer) temperatures are present in the summer (winter) pole than expected from radiative equilibrium throughout the middle atmosphere. In the equatorial stratosphere, the temperatures are also lower than the radiative equilibrium, and the zonal flow is in thermal wind balance with the temperature in both data sets.

2.4 The structure of the meridional residual circulation in MAECHAM5

Fig. 2.3a shows the January climatology of the meridional residual circulation from the MAECHAM5-simulation. Fig. 2.3b shows the net adiabatic temperature change associated with the vertical motion. The MAECHAM5-model reproduces the most important features of the middle atmospheric meridional residual circulation except for the uppermost model levels. It shows the lower part of the Murgatroyd-Singleton circulation [*Murgatroyd and Singleton*, 1961; *Dunkerton*, 1978], which is characterized by one global cell-structure between the upper stratosphere and mesosphere

a) Zonally averaged temperature in MAECHAM5 (1) and SPARC-Data (2)

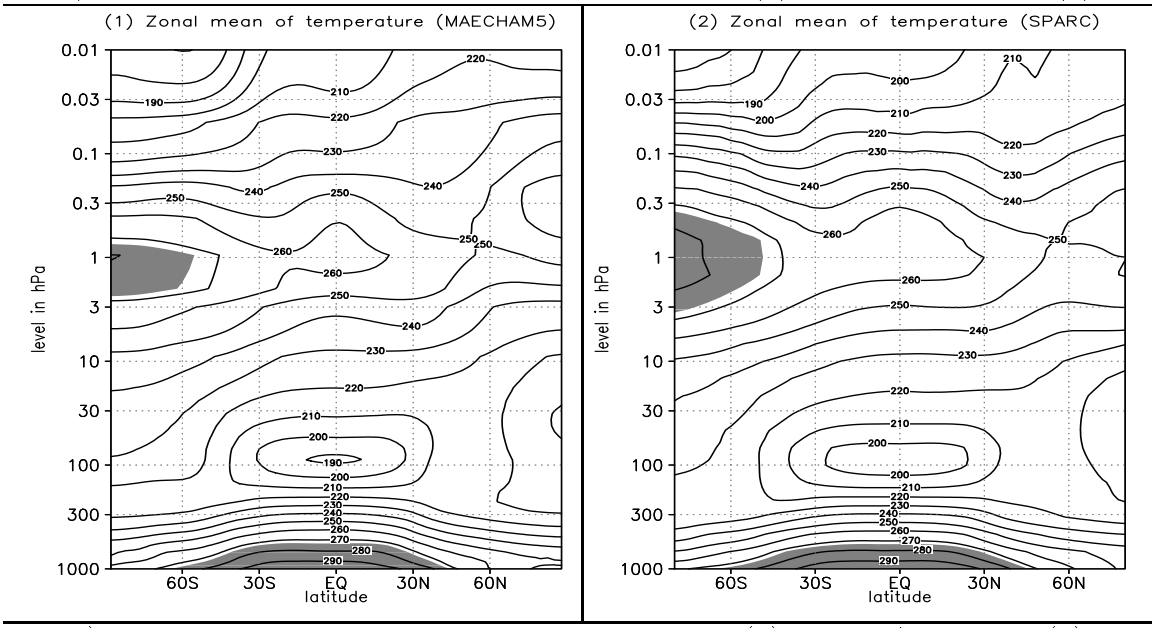

b) Zonally averaged zonal wind in MAECHAM5 (1) and SPARC-Data (2)

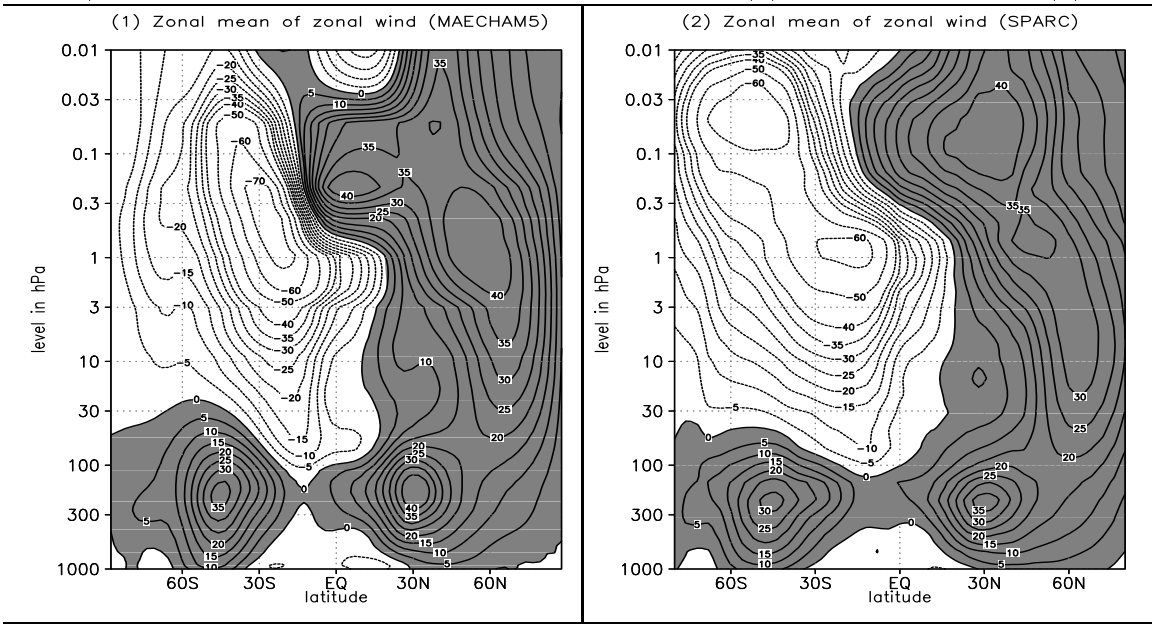

Figure 2.2: a(1) and a(2) represent the January climatology of the zonally averaged temperature in MAECHAM5 and SPARC-data, respectively. The contour interval is 10 $^{\circ}K$ (to allow comparison with Fig. 2.1). Dark grey (no) shading indicates positive (negative) temperature values in $^{\circ}C$. b(1) and b(2) represent the January climatology of the zonally averaged zonal wind in MAECHAM5 and SPARC-data, respectively. The contour interval is 10 m/s for values above (below) 10 (-10) m/s, and 2 m/s for values between -10 and 10 $(m/s)/day$. Dark grey (no) shading indicates positive (negative) wind values.

showing an upward motion in the summer hemisphere, a meridional motion from the summer into the winter pole across the equator and downward motion in the high latitudes of the winter hemisphere.

The model also reproduces the Brewer-Dobson circulation, which is characterised by a quasi-symmetric two-cell circulation structure showing a rising of equatorial air into the lower and middle stratosphere, a poleward transport of this air and a subsidence near both poles. The winter hemispheric branch of the Brewer-Dobson circulation is much deeper and stronger than the summer hemispheric part.

The structure of the meridional residual circulation in the troposphere is characterised by a quasi symmetric four-cell structure showing two cells in each hemisphere. The tropospheric cells in the winter hemisphere are much stronger and deeper than in the summer hemisphere.

The deep convection in the equatorial troposphere joins the upward branch of the Brewer-Dobson circulation. The latter transports the tropospheric air further into the winter pole and then down into the troposphere across the high latitude tropopause. The stratospheric residual circulation is thus associated with Troposphere-Stratosphere-Transport (TST) in the equatorial region and Stratosphere-Troposphere-Transport (STT) in the high latitudes. Hence, it induces Troposphere-Stratosphere-Exchange (TSE) and mixing on a global scale. TSE and mixing of tropospheric and stratospheric air masses can also occur on regional scales, especially by synoptic weather patterns that are associated with the tropospheric Rossby wave activity [*Holton et al.*, 1995] and the coexistence of surface cold and warm fronts centered at low pressure. The cold front is associated with an equatorward motion near the surface, which advects cold polar air southwards and is compensated by poleward motion near the tropopause. This poleward motion leads to an intrusion of ozone-poor tropospheric air from the upper troposphere into the lowermost stratosphere and thus to TST. The warm front, on the other hand, is associated with a poleward motion near the surface, which advects warm equatorial air poleward and is compensated by an equatorward motion near the tropopause. This leads to an intrusion of the ozone-rich stratospheric air from the lowermost stratosphere

a) Meridional residual circulation (January)

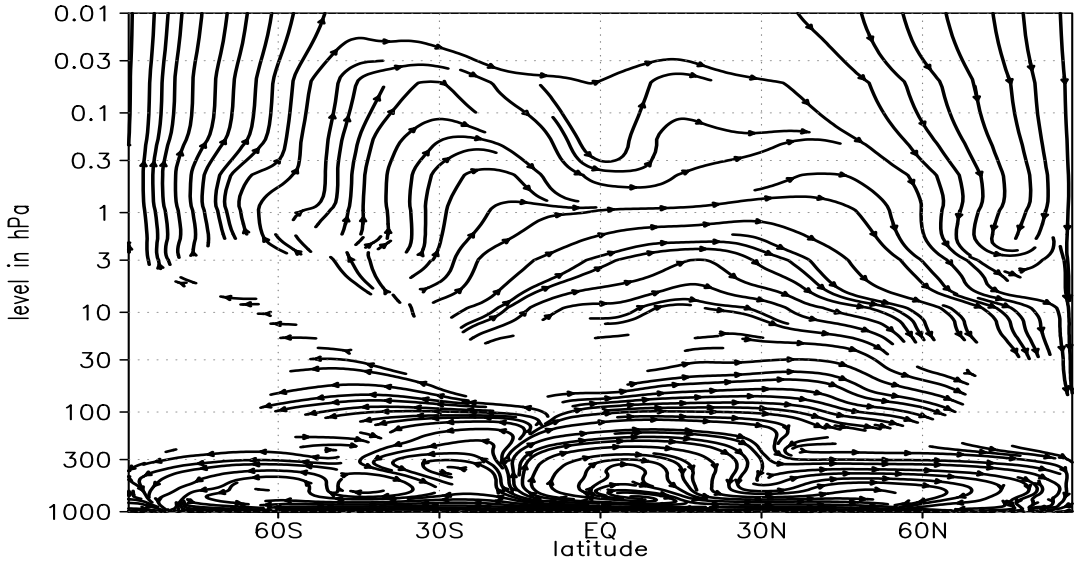

b) Adiabatic temperature change by vertical motion (January)

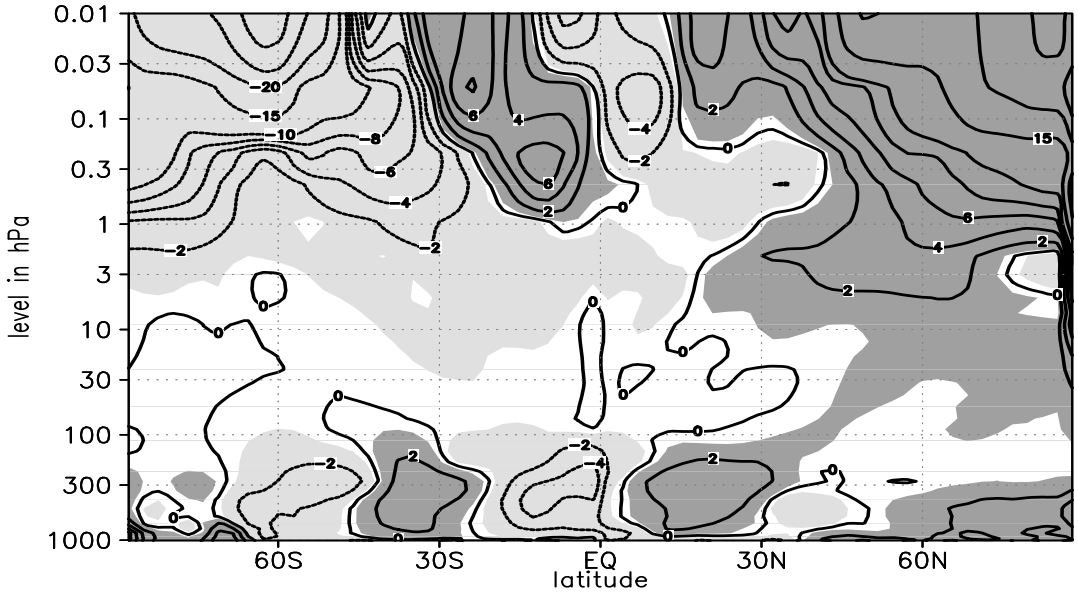

Figure 2.3: (a) January MAECHAM5-climatology of the meridional residual circulation in stream representation. The residual circulation was computed in pressure coordinates. The vertical residual velocity was scaled by the density and then multiplied by -1. b) Adiabatic temperature change by vertical motion. The contour interval is 5 $(°K/s)/day$ for values above (below) 10 (-10) $(°K/s)/day$, and 2 $(°K/s)/day$ for values between -10 and 10 $(°K/s)/day$. Dark (light) grey shading indicates values greater (smaller) than 0.5 (-0.5) $(°K/s)/day$.

into the upper troposphere and thus to STT. The TSE by synoptic waves is known as 'tropopause folds', since the tropopause is destroyed by the associated mixing processes.

The role of the middle atmospheric circulation (i.e. dynamics) can be seen in Fig. 2.3b, which shows the adiabatic temperature change by vertical motion. As expected, the upward motion in the summer stratosphere and mesosphere is associated with an adiabatic cooling that damps the radiative heating due to the absorption of solar radiation by ozone. The downward motion in the winter troposphere and stratosphere is associated with an adiabatic warming that damps the radiative cooling due to the emission of infrared radiation by atmospheric gases. The tropical deep convection between troposphere and lower stratosphere is associated with a strong adiabatic cooling that compensates the strong latent heat release. The upwelling in the Tropical-Tropopause-Layer (TTL) leads, depending on the strength of tropical convection and Brewer-Dobson circulation, to extremely low temperatures enhancing the dehydratation of air and explaining the dryness of the TTL.

2.5 The forcings driving MAECHAM5 meridional residual circulation

The quasigeostrophic TEM formulation of the momentum budget provides the most important forcings that drive the global meridional residual circulation. The meridional residual Coriolis forcing responds to the wave and residual forcing so that the momentum remains conserved (Equation 2.1). The response of the Coriolis forcing results in a meridional movement and thus, by continuity, in vertical motion; these too together determine the structure of the meridional residual circulation.

Fig. 2.4 shows the January climatologies of the planetary wave (Fig. 2.4(1)), residual (Fig. 2.4(2)) and residual Coriolis (Fig. 2.4(3)) forcing. Fig. 2.4(4) shows the EP-flux vector in stream representation and as vector. The residual forcing includes frictional, gravity and non-quasigeostrophic wave forcing. While the frictional forcing is important near the surface, gravity and non-quasigeostrophic wave

forcing are important in the free atmosphere.

The middle atmospheric planetary wave forcing is strong and decelerates the westerlies only in the high latitude winter hemisphere (Fig. 2.4(1)). In this region the wave activity, as shown by the EP-flux (Fig. 2.4(4)), is enhanced. The upward vertical component of the EP-flux is associated with an equatorward eddy-transport of the westerly momentum. The poleward meridional component of the EP-flux is associated with a poleward eddy heat transport (equation 2.3). The net effect is the deceleration of the westerlies by planetary wave forcing as shown in Fig 2.4(1). This result is consistent with the 'Charney-Drazin criterion', in which the planetary waves break into the middle atmosphere and change the zonal flow there, if the background stratospheric wind is westerly. As shown in Fig. 2.2, this condition occurs only in the winter hemisphere. The enhanced easterly planetary wave forcing in the lower and middle winter-stratosphere is associated with a westerly residual Coriolis forcing in such a way that the momentum remains conserved. The westerly Coriolis drag in turn induces a meridional motion from the equator into the winter pole and thus, by continuity, the Brewer-Dobson circulation shown in Fig. 2.3.

The residual forcing between upper stratosphere and lower mesosphere (Fig. 2.4(2)) is due mainly to the non-orographic gravity wave drag [Fig. 2.5, computed after *Hines*, 1997b;a]. It is similar to the structure shown by *Holton* [1983], which is characterised by an enhanced negative drag in the winter and a positive drag in the summer hemisphere, showing the strongest values in the uppermost mesosphere. The effect and structure of the gravity wave drag in the middle atmosphere can be understood with the help of the basic gravity wave parameterization by *Lindzen* [1981]. According to this parameterization, the gravity wave drag is proportional to $\left(-\left(\bar{u}-c\right)+3H(\bar{u})_z\right)$; where c is the phase velocity. In the mesosphere and upper stratosphere, the gravity waves with westerly (easterly) phase speed are absorbed in the regions with westerly (easterly) background wind. In this way almost only gravity waves with easterly (westerly) phase speed break into the winter (summer) mesosphere and upper stratosphere. The gravity wave drag thus depends on phase speed, strength, and vertical structure of the background zonal flow. The strong

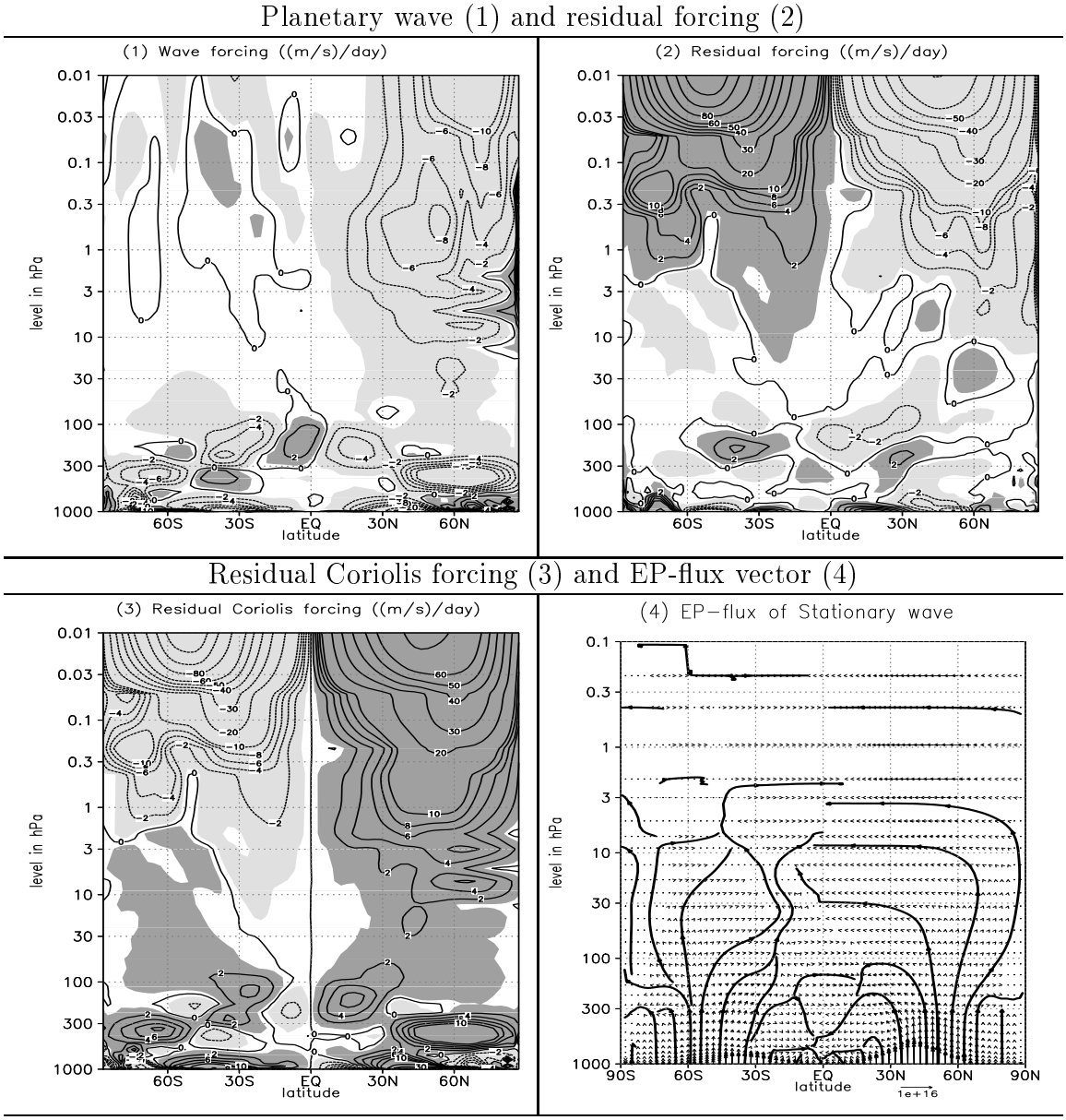

Figure 2.4: The January climatology of (1) planetary wave forcing, (2) residual forcing, and (3) residual Coriolis forcing in MAECHAM5. The forcing interval is 10 $(m/s)/day$ for values above (below) 10 (-10) $(m/s)/day$, and 2 $(m/s)/day$ for values between -10 and 10 $(m/s)/day$. Light (dark) shading indicates values less (greater) than -0.5 (+0.5) $(m/s)/day$. (4) shows the EP-flux vector in both stream and vector representations.

Non-orographic gravity wave drag

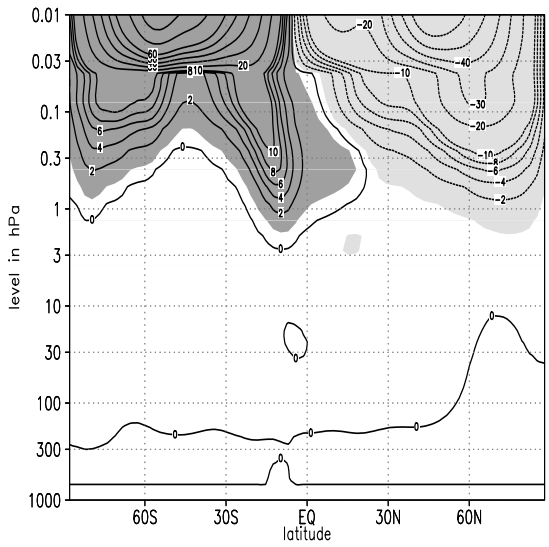

Figure 2.5: The January climatology of the non-orographic gravity wave drag [after Hines parameterization, 1997a;b] in MAECHAM5. The forcing interval is 10 $(m/s)/day$ for values above (below) 10 (-10) $(m/s)/day$, and 2 $(m/s)/day$ for values between -10 and 10 $(m/s)/day$. Light (dark) shading indicates values less (greater) than -0.5 $(+0.5)$ $(m/s)/day$.

westerlies and the negative wind shear above the stratospheric jet in the winter hemisphere (Fig 2.2) are associated with enhanced negative wave drag in the mesosphere and upper stratosphere by both the first $(-\bar{u})$ and third $(3H(\bar{u})_z)$ terms of Lindzen's parameterization. Since the gravity waves with westerly phase speed are filtered and those with easterly phase speed break into the winter mesosphere and upper stratosphere, the phase speed term (c) is also associated with a negative gravity wave drag. This explains the enhanced negative residual forcing that weakens the strong radiatively induced westerlies. A strong positive Coriolis drag is induced in the winter mesosphere and upper stratosphere in such a way that both stationary and gravity wave drag are balanced. The strong positive Coriolis forcing is in turn associated with an enhanced meridional motion into the winter pole, which leads, by continuity, to downward motion in the polar mesosphere and upper stratosphere. This explains the winter hemispheric branch of the Murgatroyd-Singleton residual circulation. The net effect is an adiabatic warming by downward motion that counteracts the radiatively induced cooling near the winter pole. The contribution of the residual forcing by the gravity wave drag to the winter branch of the Murgatroyd-Singleton residual circulation and to the resulting adiabatic warming is much larger than that of the stationary waves. This contribution shows the importance of the gravity wave drag in the upper stratosphere, and it is consistent with *Holton* [1983], who showed that a realistic warming in the polar upper stratosphere can be simulated by using only gravity wave drag, tuned to ensure a realistic mesosphere.

The strong easterlies and the resulting positive wind shear above the summer stratospheric jet (Fig. 2.2) are associated with an enhanced positive gravity wave drag. Since the gravity waves with easterly phase speed are filtered and those with westerly phase speed break into the summer mesosphere and upper stratosphere, the phase speed term is also associated with positive gravity wave drag. This explains the enhanced positive residual forcing in the summer mesosphere and upper stratosphere (Fig. 2.4(2)), which weakens the strong radiatively induced easterlies and drives a strong negative Coriolis drag (Fig. 4.2(3)). The easterly Coriolis drag is in turn associated with an equatorward motion near the summer pole, which leads, by continuity, to upward motion in the polar mesosphere and upper stratosphere.

This explains the summer hemispheric branch of the Murgatroyd-Singleton residual circulation. The net effect is an adiabatic cooling by upward motion that weakens the radiatively induced warming near the summer pole. The residual forcing between the troposphere and stratosphere can be explained by other effects such as the non-quasigeostrophic component of the EP-flux and the orographic gravity wave drag, which also depends on the vertical structure of the background wind above the wave source [*Lott and Miller*, 1997].

In summary, the dynamics that maintains the middle atmospheric circulation in MAECHAM5 is consistent with previous studies. In accordance with the Charney-Drazin criterion, the planetary waves propagate up- and poleward in the winter hemisphere into the high latitude middle atmosphere and decelerate the strong radiatively induced westerlies. This results in a poleward motion and drives the Brewer-Dobson circulation. Both planetary waves and residual forcing contribute to the winter part of the Murgatroyd-Singleton residual circulation. The strong residual forcing in the winter mesosphere and upper stratosphere can be explained by the gravity wave drag, which contributes much more to the Murgatroyd-Singleton circulation than the planetary wave drag. The summer branch of the Murgatroyd-Singleton residual circulation is induced exclusively by the residual forcing, which can be explained mainly by the gravity wave drag.

3 The leading statistical modes in the Northern Hemisphere

In this chapter the three-dimensional structure of the leading modes of the intraseasonal variability and covariability in the stratosphere/troposphere coupled system will be examined. The focus is on the winter season, where the coupling between troposphere and stratosphere through enhanced wave activity is strong. The dominant time scales of the leading mode of the intraseasonal variability will also be investigated.

3.1 Methods

First, the statistical methods used in this study are described. Additionally, a list of references for detailed descriptions and applications of these methods is given. More detailed descriptions of the multivariate methods used can be found in *von Storch and Zwiers* [1999] and *von Storch and Navarra* [1995].

3.1.1 Empirical Orthogonal Function (EOF) analysis

The EOF analysis, also known as Principal Component Analysis (PCA), is one of the multivariate techniques most often used. It provides a compact description of the spatial structures in terms of orthogonal function or spatial modes. In general, most of the variance of multivariate time series can be explained by the first few EOFs. EOF analysis is used here to find the dominant mode of geopotential height variability north of 20°N, known as the Northern Annular Mode (NAM). EOF anal-

ysis can also be used to reduce the spatial degrees of freedom of multivariate time series. It was first introduced in fluid dynamics by *Lorenz* [1957], and has been widely applied in climate research. The input of the EOF-analysis are the realizations $\vec{X}_t$ at different times $t = 1, 2...., N$ of the M-dimensional random vector $\vec{X}$ (in our case M represents the number of grid points). The realizations $\vec{X}_t$ of field $\vec{X}$ are represented by the $N \times M$ matrix

$$\mathcal{X} = (\vec{X}_1 \mid \vec{X}_2 \mid ..... \mid \vec{X}_N) = \begin{pmatrix} & \rightarrow t: & time & \\ x_{1,1} & x_{1,2} & .. & x_{1,N} \\ x_{2,1} & x_{2,1} & .. & x_{2,N} \\ . & . & .. & . \\ . & . & .. & . \\ x_{M,1} & x_{M,2} & .. & x_{M,N} \end{pmatrix} \downarrow l: \; locations \quad (3.1)$$

having the vectors $\vec{X}_t$ in its rows. The EOF analysis yields at each mode k the eigenvalues λ_k and eigenvectors $\vec{p}_k$ of the covariance matrix R_{XX} of $\vec{X}$. The time coefficients $a_k(t)$ are obtained by projecting the original data on the $\vec{p}_k$. The eigenvectors $\vec{p}_k$ are called EOFs, and the time coefficients are called Principal Components (PCs). The eigenvalue λ_k measures the amount of variance explained by mode k.

3.1.2 Singular Value Decomposition (SVD)

Singular Value Decomposition, also called Maximum Covariance Analysis (MCA), was developed to investigate the covariability of two multivariate fields. It has been also widely used in climate research [e.g. *Wallace et al.*, 1992; *Bretherton et al.*, 1992]. This technique maximizes the covariance between two input fields, and it was used here to investigate the coupling between troposphere and stratosphere. The input files of the SVD-analysis are the realizations $\vec{X}_t$ and $\vec{Y}_t$ of the M-dimensional random vectors $\vec{X}$ and $\vec{Y}$ at times $t = 1, 2...., N$. For each mode k, the output of this method is: The left and right vectors $\vec{p}_k^X$ and $\vec{p}_k^Y$, the singular value γ_k, and the left and right coefficients $a_k^X(t)$ and $a_k^Y(t)$. The left and right vectors and the singular values are computed from the left and right singular vectors and from the

singular values using the SVD decomposition of the cross covariance matrix R_{XY} between $\vec{X}$ and $\vec{Y}$, respectively. The singular value γ_k measures the amount of the explained squared covariance between the two input fields. The pattern $\vec{p}_k^X$ of vector $\vec{X}$ can be interpreted as the structure of field $\vec{X}$ that is maximally coupled to $\vec{Y}$; the patterns $\vec{p}_k^Y$ of vector $\vec{Y}$ can be interpreted as the structure of field $\vec{Y}$ that is maximally coupled to $\vec{X}$. The strength of the coupling between the two fields $\vec{X}$ and $\vec{Y}$ is given by the correlation between the time coefficients $a_k^X(t)$ and $a_k^Y(t)$.

3.1.3 Wavelet analysis

Wavelet analysis is a two-dimensional time-frequency spectral analysis. Compared to classical spectral analysis, which computes the spectrum as a function of frequency only, wavelet analysis enables the investigation of the local power as a function of both time and frequency (or period). This analysis can thus detect the time evolution of the local power at each frequency and hence the non-stationary behavior of a time series. Several geophysical studies deal with the application of wavelet analysis [e.g. *Wang and Wang*, 1996; *Lau and Weng*, 1995; *Torrence and Compo*, 1998]. The local power $|W_{ab}|^2$ at the time scale a and time b (displacement) is the square of the magnitude of the complex function W_{ab} defined as convolution of the time series x_t with the wavelet ψ :

$$W_{ab} = \sum_{t=1}^{N} x_t \psi^* \left(\frac{t-b}{a} \right) \quad t = 1, .., N,$$

where * describes the complex conjugate. The time scale a describes the period of the oscillation. Here the so-called Morlet wavelet is used, which is sinusoidal of period a and modulated by a Gaussian function. The latter enables the localization of the local power.

3.2 The leading modes of the intraseasonal variability

3.2.1 The Northern Annular Mode (NAM)

An EOF analysis of the monthly geopotential height anomalies north of 20°N in winter (JFM) was performed at different levels between troposphere and stratosphere. The data were weighted using the square of the cosine of the latitude before computing the EOFs. All monthly anomalies were obtained by removing the monthly climatology. The first EOF-mode at each level describes the Northern Annular Mode (NAM) of this level. The daily NAM-index at each level is computed by projecting the daily geopotential height anomalies on the corresponding NAM pattern. All daily anomalies used in this thesis were obtained by removing the climatology of 30-day low pass filtered data from the daily data.

The vertical profiles of the variances explained by the first four EOF-modes are shown in Fig. 3.1. Fig. 3.2 shows the NAM pattern at different levels. About 37% of the entire variance is explained by the first EOF mode at the surface. This value decreases to the minimum of about 29% in the middle troposphere and increases strongly with height to about 77% in the middle stratosphere.

The second EOF mode explains about 11% of the variance at the surface. This value remains almost constant in the whole troposphere, decreases slightly with height to about 8% at the lowermost stratosphere, and increases again to about 14% at 1hPa. The third EOF mode explains about 10% of the variance at the surface and has a similar vertical structure as the second EOF mode. The fourth mode is important only in the lower troposphere, with an explained variance of 8% at the surface.

The first EOF-mode of the geopotential height north of 20°N, which represents the NAM, explains the most variance in both troposphere and stratosphere and is thus the most important Northern Hemispheric mode. This mode explains much more variance in the stratosphere than in the troposphere.

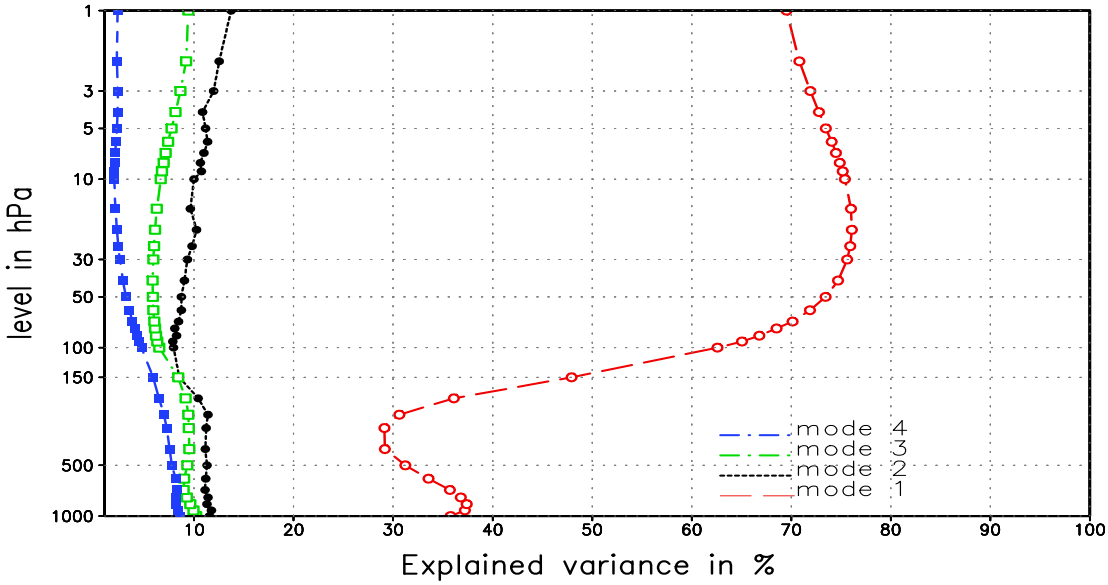

Figure 3.1: Vertical profiles of the explained variance by the first (red), second (black), third (green), and fourth (blue) EOF-modes of the geopotential height north of $20°N$.

The vertical and horizontal structure of the NAM-patterns (Fig 3.2) are quite similar to the observational patterns shown by *Thompson and Wallace* [1998; 2000] and *Baldwin and Dunkerton* [1999]. The NAM-pattern is almost barotropic and zonally symmetric. It is characterized by a meridional dipole in the geopotential height, with opposite polarity over the Arctic and the midlatitudes. By convention, the positive pole is taken over the Arctic so that a positive NAMI describes strong westerlies. While the strong NAM-anomalies show a localized structure in the troposphere, the NAM-anomalies in the stratosphere are more annular.

Since the vertical and horizontal structure of the NAM are obtained from a general circulation model coupled to an ocean mixed layer model without any external forcing, the NAM results from the internal dynamics of the coupled system atmosphere-ocean. However, the NAM may be strongly influenced by both external and internal forcings, like Quasi Biannual Oscillation (QBO), solar cycle, volcano eruptions, and ENSO. The strong sensitivity of the middle atmosphere to the dif-

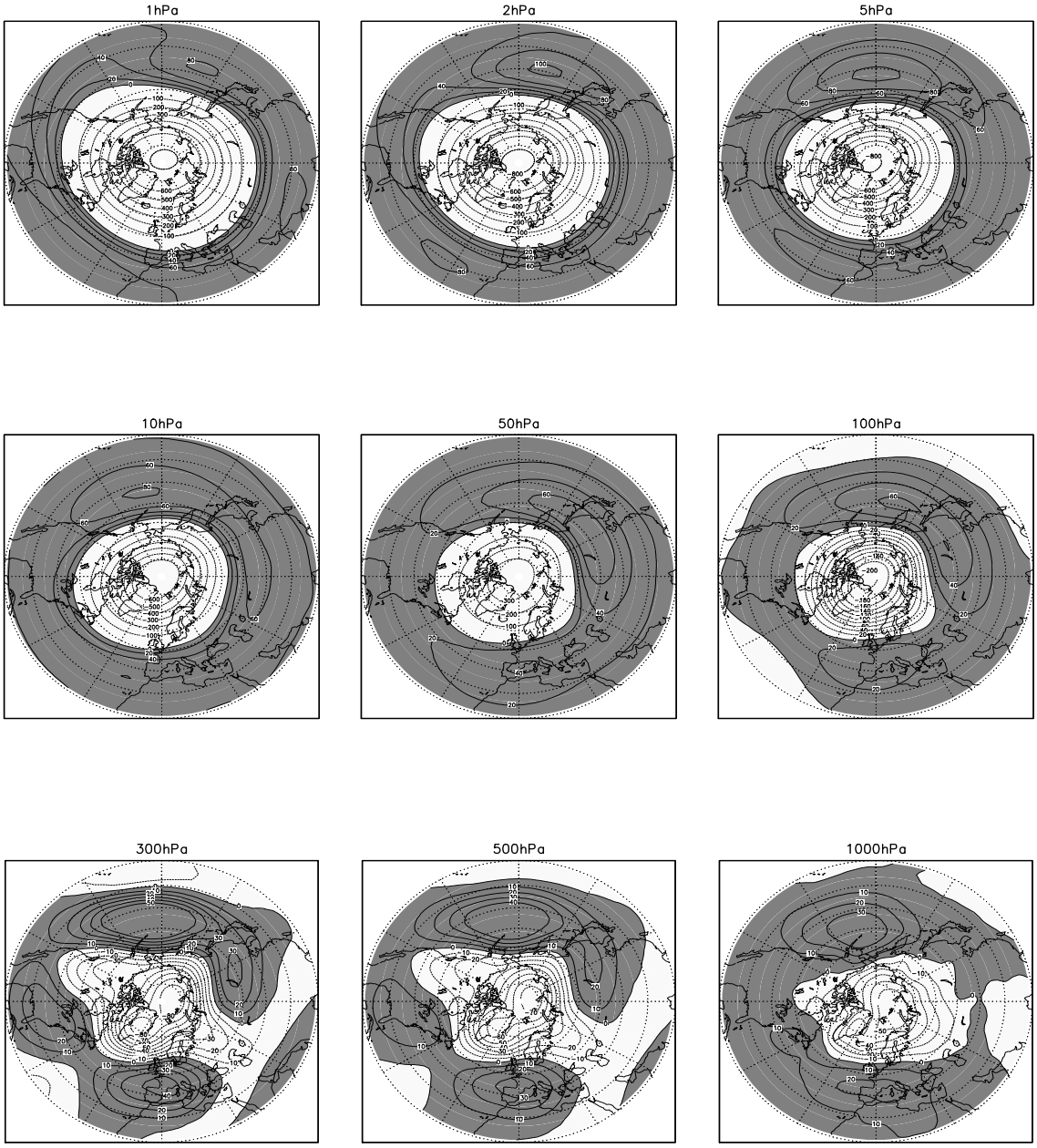

Figure 3.2: Vertical structure of the NAM (in m), which is the leading mode of the geopotential height north of $20°N$. Shading indicates positive anomalies. The structures are given at 1, 2, 5, 10, 50, 100, 300, 500; and 1000hPa levels.

ferent forcings, the non-linear nature of the atmospheric dynamics, and the lack of long-term measurements make the understanding of the effect of individual external forcings very difficult. The ENSO impact on the NAO and Europe was studied e.g. by *Brönnimann et al.* [2004], *Brönnimann* [2006], and *Brönnimann et al.* [2007]. The tropical-extratropical interaction through the QBO-vortex connection was investigated e.g. by *Holton and Tan* [1980]. In both cases a change in wave propagation and thus in the Brewer-Dobson circulation, which eventually leads to a change in the stratospheric NAM, seems to be important. The latter change can then propagate downward and impact the troposphere over both Pacific and Atlantic sectors.

3.2.2 The dominant time scales of the intraseasonal NAM variability

Fig. 3.3 shows the local wavelet power of the daily NAMI at 1000, 200 and 10hPa for winter. The local wavelet power was first computed for each winter and then averaged over all winter seasons. The NAM at 10hPa is dominated by low frequency variability (period above 40 days) over the whole winter season. Singular Spectrum Analysis (SSA) shows that the low frequency time scales explain about 92% of the winter variance at 10hPa. The stratospheric wavelet power shows also considerable variability at quasistationary time scales (periods between 15 and 40 days). The dominance of low frequency time scales in the stratosphere reflects the large-scale and hemispheric structure of stratospheric circulation and its variability . The low frequency power spectrum is much smaller in the troposphere. The low frequency variability of the NAMI at 1000hPa peaks in January and February, when the coupling between troposphere and stratosphere through planetary wave propagation is strong. The local wavelet power at the quasistationary and synoptical time scales (periods less than 15 days) is much higher in the troposphere than in the stratosphere. An SSA-analysis (not shown) shows that the quasistationary and synoptical time scales together explain about 34% of the winter variability at 1000hPa, as opposed to about 8% at 10hPa. This reflects the smaller scales and the much more localized structures of tropospheric circulation and its variability as compared to

a) The winter local wavelet power at 10hPa and 200hPa

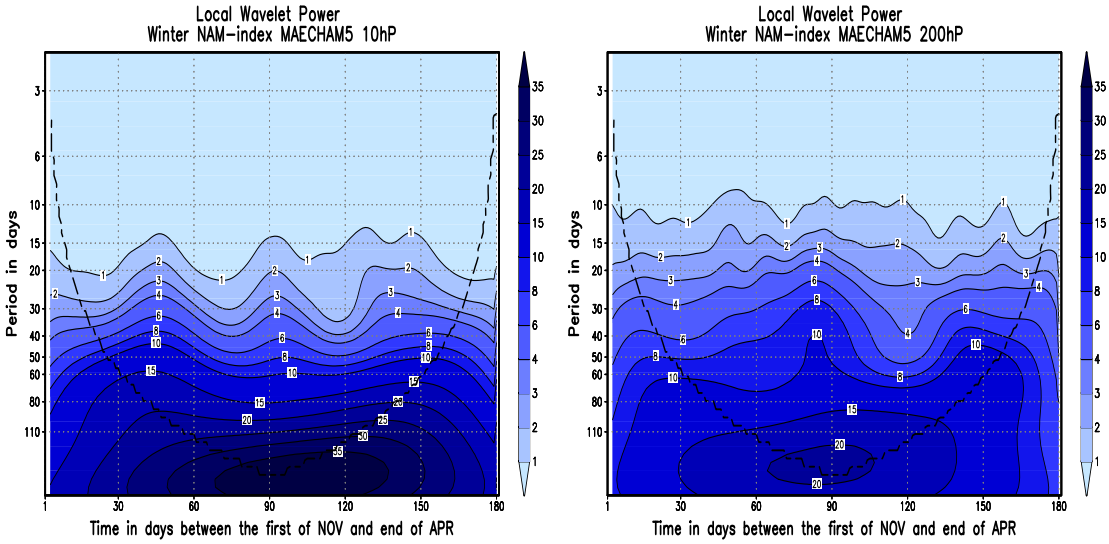

b) The winter local wavelet power at 1000hPa

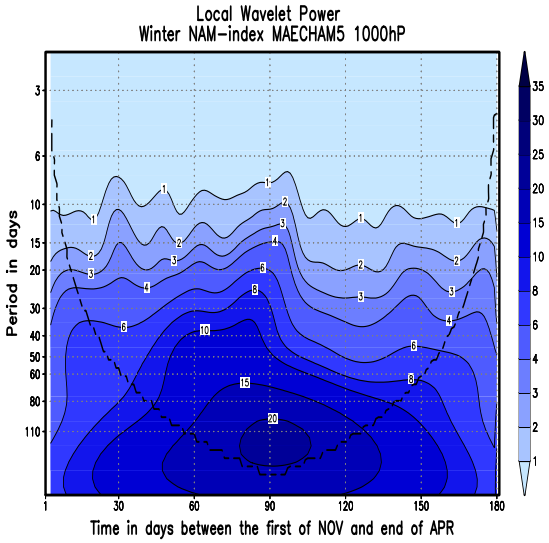

Figure 3.3: The winter (NOV-APR) average of the local wavelet power of the NAMI at 10 and 200hPa (a) and at 1000hPa (b). The bold dashed line is the cone of influence within which the side effect becomes important.

the large-scale and much hemispheric structures in the stratosphere.

3.3 The leading modes of the troposphere/stratosphere covariability

An SVD analysis was performed north of 20°N between the geopotential height at 34 levels located between 1000 and 1hPa, and that at the 10hPa-level. This yields for each mode 34 left vectors (coefficients) and 34 right vectors (coefficients). Fig.

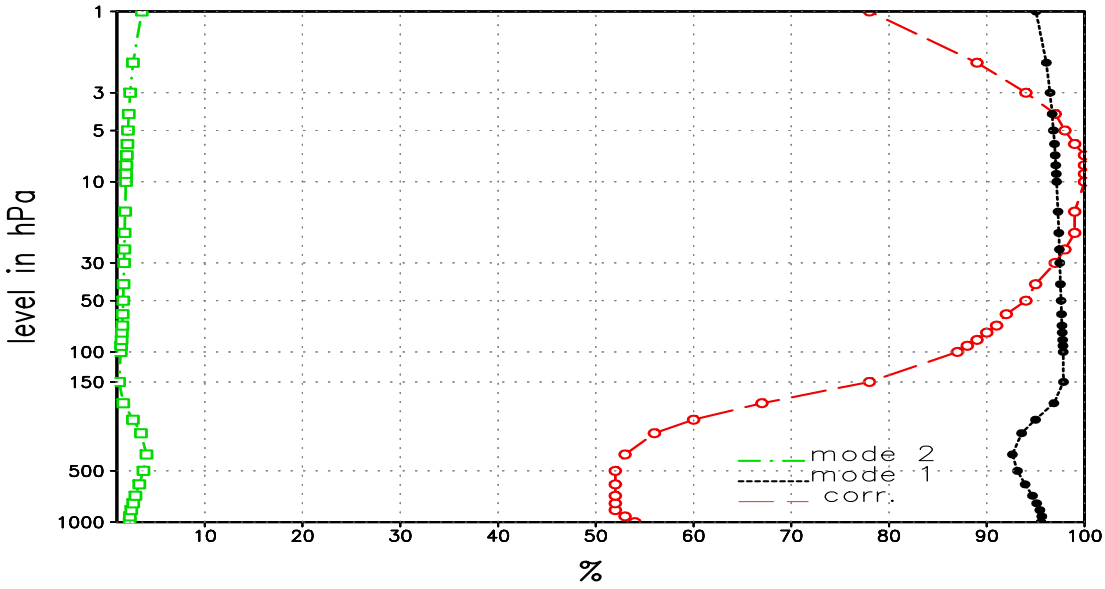

Figure 3.4: The vertical profile of the explained squered covariance by the first (black) and second (green) modes of SVD between 10hPa and the 34 levels taken between 1000hPa and 1hPa. The vertical profile of the correlation between the right and left coefficients of the first SVD-modes is plotted in red.

3.4 shows the vertical structure of amounts of squared covariances between 10hPa and the other 34 levels explained by the first and second mode, and the correlation between the left and right coefficients of the first mode. The explained squared covariance amounts to about 92% in the middle troposphere and to about 98% in the whole stratosphere. The correlation between the left and right coefficients

is above 0.5 at all lower tropospheric levels and increases strongly in the upper troposphere (to about 0.77). In the stratosphere, the correlation increases from about 0.8 at 150hPa to 1 at 10hPa and decreases again to about 0.8 at 1hPa. The enhanced correlation between the first mode left coefficients in the troposphere and the first mode right coefficients at 10hPa indicates, together with the high fraction of the explained squared covariance by this mode, a strong coupling between the troposphere and stratosphere. This coupling is explained almost completely by the first SVD mode.

Fig. 3.5 shows the left vectors at the same levels as those shown in Fig. 3.2. All 34 right vectors (not shown) strongly resemble the NAM pattern at the 10hPa level shown in Fig. 3.2. As we can see, all left vectors are very similar to the corresponding NAM-patterns. An SVD-analysis between the same 34 levels and the 1000hPa level (not shown) yields the NAM patterns as left vectors and the NAM pattern of the 1000hPa level as right vectors. Thus, the tropospheric NAM-patterns can be interpreted as the patterns that are maximally correlated with those in the stratosphere.

In summary, the three-dimensional structure of the NAM in MAECHAM5 is quite similar to that observed. The NAM is much more important in the stratosphere than in the troposphere. The stratospheric NAM variability is dominated by low frequency time scales and reflects the large-scale and hemispheric structure of the stratospheric circulation. The synoptical and quasistationary time scales are much more important in the troposphere. This reflects the relatively small-scale and local structure of the tropospheric circulation. The stratosphere and troposphere are strongly coupled by their corresponding NAM-patterns.

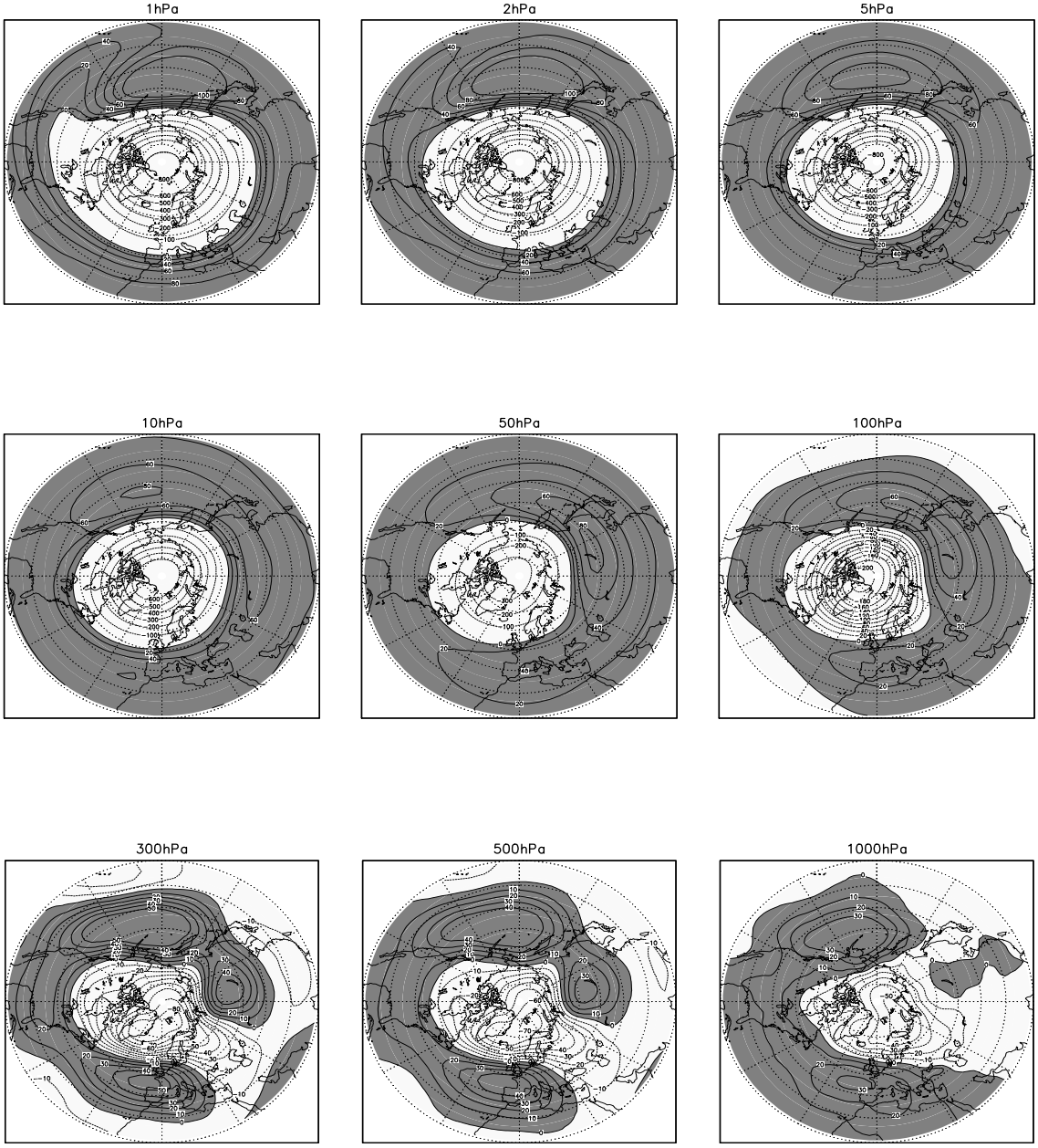

Figure 3.5: The left vectors of the first SVD-mode (in m). These vectors represent the geopotential patterns at 1, 2, 5, 10, 50, 100, 300, 500, and 1000hPa that are maximally correlated with the 10hPa-geopotential height through the first SVD-mode. Shading indicates positive geopotential anomalies.

4 The coupled system stratosphere/troposphere at strong polar vortex

In this chapter, the dynamics of the coupling between troposphere and stratosphere during a strong stratospheric Northern Annular Mode (in the following: 'stratospheric mode') is investigated. The focus will be on the mechanisms driving the pattern and downward propagation of the NAM-anomalies and on the processes controlling the different phases of the life cycle of the polar vortex.

4.1 Methods and theoretical background

4.1.1 Composite analysis

The input in composite analysis are univariate time series x_t and the realization $\vec{X}_t$ $(t = 1, ..., N)$ of a random vector $\vec{X}$. This method is based on averaging a subset $\mathcal{K}$ of patterns from the multivariate field $\vec{X}_t$ that meet certain conditions. The conditions used to form the subset $\mathcal{K}$ are computed using the time series x_t. In this study, all events with $x_t^{'} > 2\sigma_x$ and $x_t^{'} < -2\sigma_x$ were taken to build the subsets $\mathcal{K}_H$ and $\mathcal{K}_L$ for high and low index phases, respectively. Thereby $x_t^{'}$ is the anomaly time series and σ_x is the standard deviation of x_t. The high composite pattern was defined as:

$$\vec{X}_H = \frac{1}{K_H} \sum_{t \in \mathcal{K}_H} \vec{X}_t,$$

and the low composite pattern as:

$$\vec{X}_L = \frac{1}{K_L} \sum_{t \in \mathcal{K}_L} \vec{X}_t,$$

where K_H and K_L are the number of patterns in the subsets $\mathcal{K}_H$ and $\mathcal{K}_L$, respectively. The significance of the composite was tested by performing a multivariate Student's t-test of the difference $\vec{X}_H - \vec{X}_L$. Here the difference between high and low composite will be denoted by $H - L$. In contrast to the 'associated pattern' approach, which is based on the correlation and/or regression patterns and thus on linear assumption between $\vec{X}_t$ and x_t, composite analysis is a non-parametric approach, which means that no assumption about a relationship between $\vec{X}_t$ and x_t is made. Composite analysis can thus capture even non-linear relationships [e.g. *Hoerling et al.*, 1997]. Most of the results in this study are based on the lag composite analysis using the winter NAMI at 50hPa. The NAMI was computed by projecting the daily anomalies of the geopotential height at 50hPA on the NAM pattern at the same level (Fig. 3.2). All anomalies were obtained by removing the climatology of 30-day low pass filtered data from the daily data. Anomalies from 60 days before to 60 days after the NAMI peak were also computed.

4.1.2 Dynamical background

The dynamics of the wind and temperature anomalies during strong NAM-phase were investigated by diagnosing the anomalous residual circulation and EP-flux vectors (equation 2.2 and 2.3), the Transformed Eulerian Mean (TEM) formulation of the momentum budget in pressure coordinates (equation 2.1), and the anomalies of the terms of the refraction index depending on the spatial structure of the zonally averaged zonal wind (equations 4.1 and 4.2) [*Matsuno*, 1970; *Limpasuvan and Hart-*

mann, 2000; *Lorenz and Hartmann*, 2003]. Waves are refracted from regions with a low to regions with a high refraction index. In equations 4.1 and 4.2, z denotes the log pressure coordinate, q denotes the potential vorticity and k is the wave number. N^2 is the buoyancy frequency, H the scale height (ca.7km) and Ω the earth's angular frequency. All notations and non-described parameters in 4.1 and 4.2 are similar to those of equations 2.1, 2.2, and 2.3.

The first term on the right of equation 4.1 is proportional to the meridional potential vorticity gradient. It represents the contribution of the planetary effect (first term of 4.2), the effect of meridional (second term) and vertical wind curvature (fourth term), and the effect of vertical wind shear (third term). The strengthening of the polar jet leads to a decrease in the refraction index through the planetary term. If we neglect the change of stability (N^2), high positive vertical and meridional wind curvatures cause a negative refraction index, while a high positive vertical wind shear leads to a positive refraction index. The anomalies of the refraction index depend only on the terms that contain the zonal wind. The division by very small zonal flow in 4.1 makes the result very noisy. To avoid this problem, it was divided by the 60 days running mean of the zonally averaged zonal wind.

$$n^2 = \frac{\bar{q}_\phi}{\overline{u}} - \left(\frac{k}{a\cos\phi}\right)^2 - \left(\frac{f}{2NH}\right)^2 \tag{4.1}$$

$$\bar{q}_\phi = \frac{2\Omega}{a}\cos\phi - \frac{1}{a}\left(\frac{(\bar{u}\cos\phi)_\phi}{\cos\phi}\right)_\phi + \frac{f^2}{N^2}\bar{u}_z\left(\left(\ln N^2\right)_z + \frac{1}{H}\right) - \frac{f^2}{N^2}\bar{u}_{zz} \tag{4.2}$$

According to *Ambaum and Hoskins* [2002], the downward propagation of stratospheric wind anomalies into the troposphere results from the change of the tropopause height and thus from the stretching of the stratospheric column. The contraction (stretching) of the stratosphere can lead to a stretching (contraction) of both troposphere and mesosphere and thus to temperature, pressure and wind changes through the resulting vertical motion there. Understanding the processes that drive the stretching of an atmospheric layer will help to understand not only the troposphere-stratosphere, but also the stratosphere-mesosphere coupling. The stretching and

contraction of an atmospheric layer can be described by the stretching vorticity q_s, the zonal mean of which (in log-pressure coordinates) is defined as follows [e.g. *Andrews et al.*, 1987; *Holton*, 1992]:

$$\overline{q_s} = \frac{f_0}{\rho_0}\left(\frac{\rho_0}{N^2}\left(\overline{\Phi}_z\right)\right)_z \ . \tag{4.3}$$

In this equation ρ_0 is the background air density. Using the hydrostatic equation ($\overline{\Phi}_z = \frac{R}{H}\bar{T}$) we get:

$$\overline{q_s} = \frac{f_0 R}{\rho_0 H}\left(\frac{\rho_0}{N^2}\bar{T}\right)_z \ . \tag{4.4}$$

The vertical integration between the top and the bottom of an atmospheric layer ($\langle x\rangle = \int_{bot}^{top} x\delta z$) and the time derivation of (4.4) lead to:

$$\langle\overline{q_s}\rangle_t = \frac{f_0 R}{\rho_0 H}\left(\left(\frac{\rho_0}{N^2}\bar{T}_t\right)(top) - \left(\frac{\rho_0}{N^2}\bar{T}_t\right)(bot)\right) \ . \tag{4.5}$$

For small diabatic heating we get thus a contraction of an atmospheric layer ($\langle\overline{q_s}\rangle_t > 0$) by:

- 1a) adiabatic warming by downward motion at the top and adiabatic cooling by upward motion at the bottom
- 1b) strong adiabatic warming by downward motion at the top and small adiabatic cooling by upward motion or no temperature change at the bottom
- 1c) small adiabatic warming by downward motion or no temperature change at the top and strong adiabatic cooling by upward motion at the bottom

The stretching of an atmospheric layer ($\langle\overline{q_s}\rangle_t < 0$) can be caused by:

- 1a') adiabatic cooling by upward motion at the top and adiabatic warming by downward motion at the bottom
- 1b') strong adiabatic cooling by upward motion at the top and small adiabatic warming by downward motion or no temperature change at the bottom

- 1c') small adiabatic cooling by upward motion or no temperature change at the top and strong adiabatic warming by downward motion at the bottom

Using some basic equations in the quasigeostrophic formulation (see Appendix A), we can derive the following tendency equation for the zonally averaged stretching vorticity:

$$(\overline{q_s})_t = (f_0 \bar{v}^*)_y + f_0 \rho_0^{-1} \left(\rho_0 \frac{\bar{Q}}{\bar{\theta}_{0z}} \right)_z . \tag{4.6}$$

The first term on the right is the meridional divergence of the meridional residual Coriolis forcing and depends, according to the TEME (equation 2.1), on the resolved and unresolved wave forcing and the frictional forcing. Due to its f-dependence, it causes strong (small) changes of the stretching vorticity near the pole (in mid-latitudes). The meridional convergence (divergence) of the meridional residual Coriolis forcing leads to a stretching (contraction) of an atmospheric layer. Fig. 4.1 shows the possible cases if the residual Coriolis forcing acts in the middle of this layer. The contraction of an atmospheric layer can be induced by (see Fig. 4.1):

- 2a) poleward decrease of the westward residual Coriolis forcing
- 2b) poleward increase of the eastward residual Coriolis forcing
- 2c) poleward transition from westward to eastward residual Coriolis forcing

The stretching of an atmospheric column can be caused by (Fig. 4.1):

- 2a') poleward increase of the residual westward Coriolis forcing
- 2b') poleward decrease of the residual eastward Coriolis forcing
- 2c') poleward transition from eastward to westward residual Coriolis forcing

The second term of equation 4.6 reflects the effect of the diabatic heating. Strong vertical convergence (divergence) of the diabatic heating leads to the stretching (contraction) of an atmospheric layer.

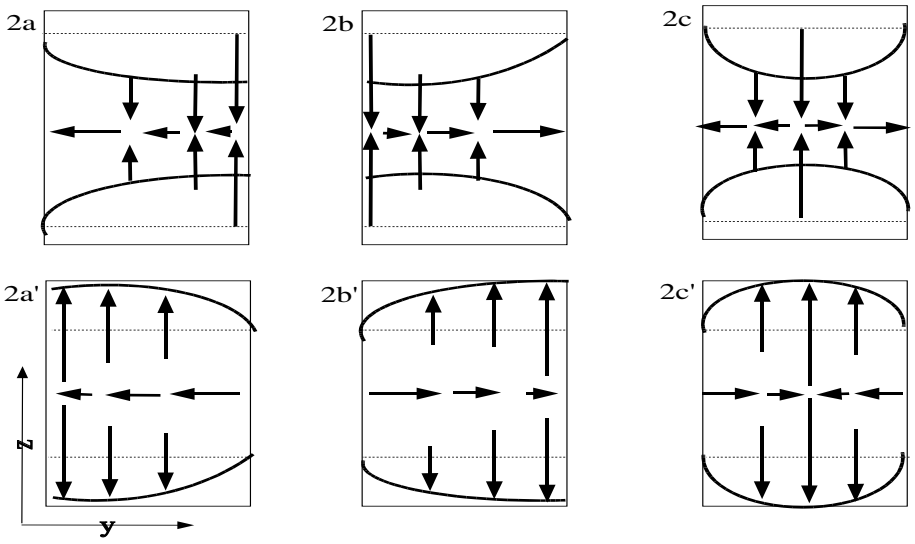

Figure 4.1: The effect of the meridional structure of the residual Coriolis forcing on the stretching and contraction of a free atmospheric layer according to cases 2a, 2b, 2c, 2a', 2b', and 2c'(see text). Horizontal arrows represent the meridional component of the residual velocity, which is proportional to the residual Coriolis forcing. Vertical arrows represent the vertical residual velocity, which causes adiabatic warming (cooling) by upward (downward) motion. Dashed (solid) curves correspond to the initial (final) position of the upper and lower layer boundaries.

According to the equation 4.6, a change in radiative and/or wave forcing leads to a change of the stretching vorticity and thus to a change of the potential vorticity (see also Appendix A, equations A-4 and A-3). The potential vorticity inversion mechanism, in which the non local circulation change is controlled by the potential vorticity anomalies [*Black*, 2002; *Ambaum and Hoskins*, 2002], and the downward control mechanism [*Haynes et al.*, 1991; *Holton et al.*, 1995], in which the circulation change is controlled by the radiative and wave induced dynamical forcing, thus describe the same mechanism. All analyses done in this study are based on anomalous changes, which were computed by removing the seasonal cycle. Since the model is driven by the climatology of radiatively active elements and no coupling to chemistry is performed, the anomalous change of the short wave radiative heating in the stratosphere and its impact on the stretching vorticity can be neglected. In the following, only the dynamical effect on the stretching vorticity is considered, since the dynamical damping time in the stratosphere is much higher than the radiative one and the winter stratospheric circulation is driven mainly by wave dynamics. Figs. 4.2 and 4.3 sketch the anomalous changes that drive the vertical structure of the temperature and wind anomalies during the evolution of strong positive and negative NAM-phases. The NAM temperature and wind anomalies and their downward propagation can be understood as the response of the stretching vorticity to the meridional structure of the Coriolis forcing and quasigeostrophic adjustment of the troposphere to these changes. During strong stratospheric positive NAM-phase (Fig. 4.2a), an enhanced stratospheric anomalous westward Coriolis forcing centered near 60-70°N is induced by reduced planetary wave breaking. This results in a poleward decrease (increase) of the westward Coriolis forcing north (south) of 60-70°N and leads -as in case 2a (2a') of Fig. 4.1- to a contraction (stretching) of the stratospheric layer in the high (mid) latitudes. These changes contribute, by continuity, to an anomalous stretching of the high latitude troposphere and lower mesosphere and a contraction of the mid-latitude troposphere and lower mesosphere.

The lower mesosphere responds during enhanced positive NAM-phase with an anomalous eastward residual Coriolis forcing, centered in mid and high latitudes (Fig. 4.3a). This is balanced mainly by the residual forcing (or gravity wave drag).

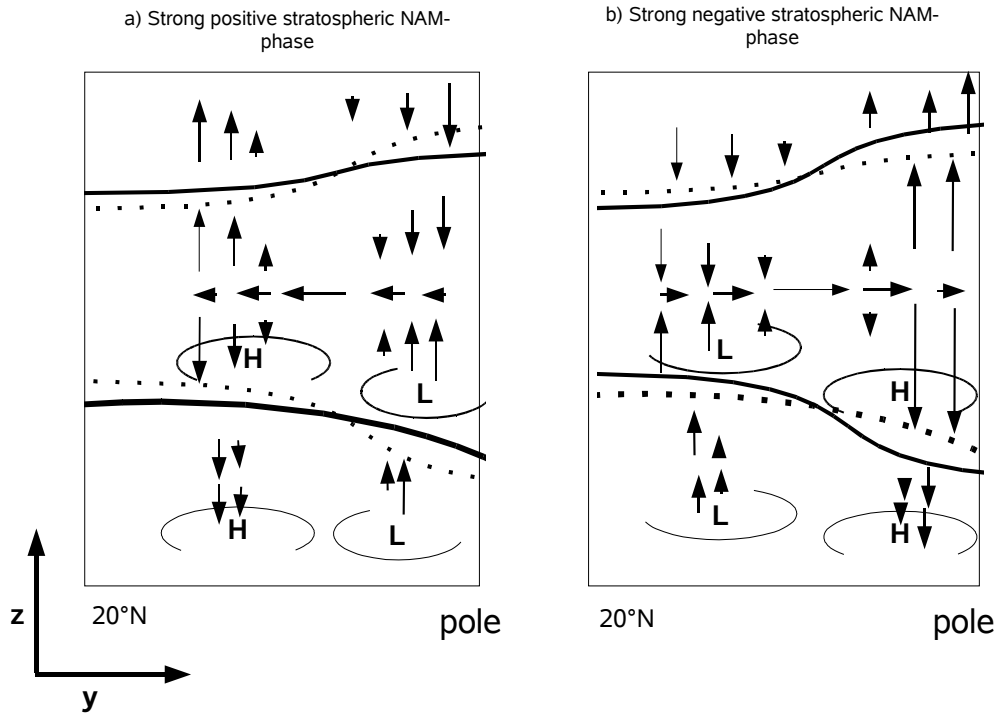

Figure 4.2: (a) illustrates the effect of the stretching vorticity of the stratospheric column during strong positive NAM-phase as a result of the meridional structure of the anomalous residual Coriolis forcing. Horizontal arrows represent the meridional residual velocity, which is proportional to the residual Coriolis forcing. Vertical arrows represent the vertical residual velocity, which causes adiabatic warming (cooling) by upward (downward) motion. Dashed (solid) curves correspond to the initial (final) position of the upper and lower boundaries of the stratosphere. (b) illustrates the effect of the stretching vorticity of the stratospheric column during strong negative NAM-phase. H (L) illustrates positive (negative) anomalous changes of pressure.

The net result is a poleward decrease of the eastward Coriolis forcing in high latitudes which leads - as in case 2b' of Fig. 4.1 - to a stretching of the lower mesosphere near the pole. This contributes to the contraction of the upper stratosphere and an increase of the anomalous downward motion in both lower mesosphere and upper stratosphere. The vertical structure of the temperature and wind anomalies during the strong NAM-phases and the associated downward propagations result mainly from adiabatic temperature changes by the vertical motions, sketched in Figs. 4.2a and 4.3a. Figs 4.2b and 4.3b describe the situation during negative stratospheric NAM-phase. In the following, the TEM formulation is used to get further insight into the processes sketched in Figs. 4.2 and 4.3.

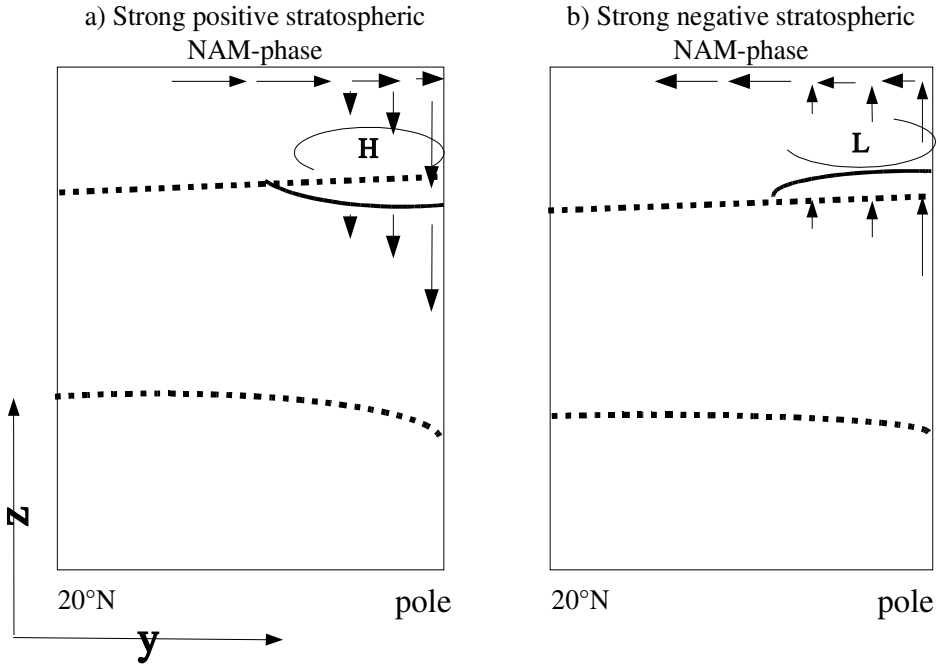

Figure 4.3: a (b) like Fig. 2a (2b) but illustrating the effect of the stretching vorticity of the lower mesosphere column during strong positive (negative) NAM-phase as a result of the meridional structure of the anomalous residual Coriolis forcing.

4.2 Wind and temperature anomalies during strong stratospheric NAM-phases

The evolution of the high minus low (H - L) lag composites of the NAMI at 50hPa is shown in Fig. 4.4a. In Fig. 4.4b, the evolution of the H - L lag composites of the anomalous zonally averaged zonal wind between 55 and 70°N is shown as a function of height. Statistical significance was estimated with a t-test. Fig. 4.4c shows the anomalous zonally averaged temperature between 60 and 90°N. The evolution of the stratospheric polar jet is well described by the NAMI. The slow increase of the 50hPa-NAMI between lag -60 and lag -40 days characterizes the onset phase of the development of the stratospheric polar jet. The faster increase of the NAMI between lag -30 and 0 describes the growth and mature phases, while the decrease of the NAMI at positive lags indicates the decline and decay phases.

The growth and the mature phases of the stratospheric polar jet are associated with a strengthening and downward propagation of negative temperature and positive wind anomalies in the stratosphere and troposphere (Figs. 4.4b and 4.4c). These anomalies strongly decrease in the decline and decay phases. The evolution of the stratospheric jet after lag -30 is associated with an enhanced warming in the upper polar stratosphere and lower mesosphere and thus, according to the thermal wind balance, with a negative shear of the zonal flow and a weakening of the anomalous westerlies. The warming and the associated change in the zonal flow become stronger and propagate downward towards the lower stratosphere, especially during the decline and decay phases.

Figs. 4.5 and 4.6 show the two-dimensional structure of the H - L lag composites of the zonally averaged zonal wind and temperature anomalies, respectively. Six time lags (-60, -50, -10, 0, 20 and 50) are shown. Both Figs. 4.5 and 4.6 show a strengthening of the zonally averaged zonal wind and of temperature anomalies in the stratosphere during the growth and mature phases. They also show downward propagation of both anomalies into the troposphere, especially during the mature phase. The wind and temperature anomalies in the troposphere and the lower

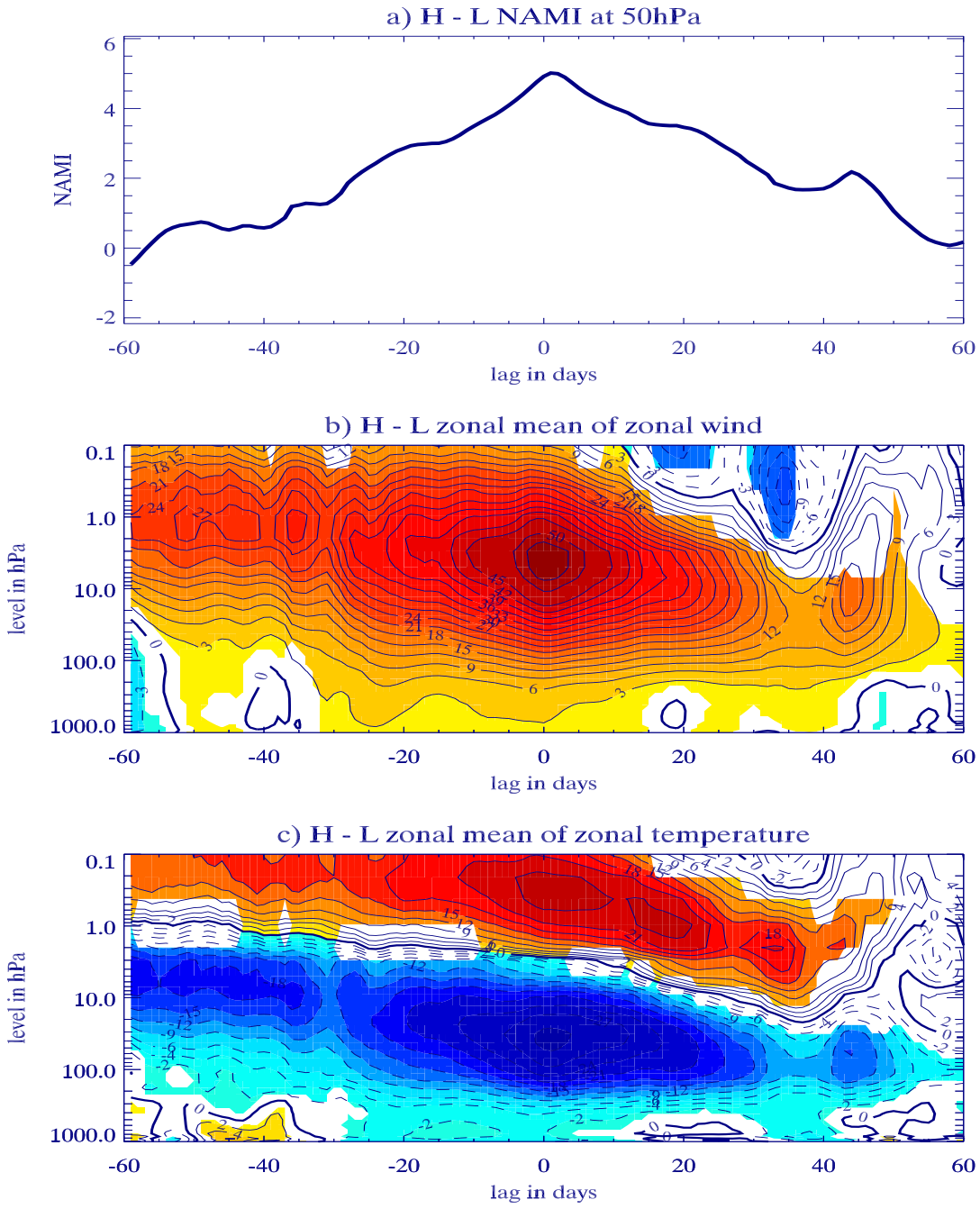

Figure 4.4: The difference between the high and low lag composite (H - L) of (a) the NAMI at 50hPa, (b) the zonally averaged zonal wind between 55 and 70°N and (c) the zonally averaged temperature north of 60°N. Positive (negative) values are represented by solid (dashed) lines and zero by a thick line. Color indicates significance at 95% level according to a t-test.

to middle stratosphere weaken considerably during the decline and decay phases. The growth and mature phases of the stratospheric polar jet are associated with a temperature quadrupole between the troposphere and mesosphere (Fig. 4.6). The lower part of this quadrupole has a deep cold pole in the high latitude and a warm pole in the mid-latitude troposphere and stratosphere. This dipole strengthens in the NAM-strengthening phase and weakens in the decay phase. It is in thermal wind balance with the wind shear and explains the positive vertical shear of the anomalous zonal flow between the surface and the middle stratosphere. The upper part of the temperature quadrupole has a warm pole in the high latitudes between the upper stratosphere and lower mesosphere and a cold pole in the mid latitudes. The warm pole strengthens and propagates downward, especially in the NAM-decline and decay phase. Consistent with the thermal wind balance, a negative vertical shear and a weakening of the anomalous zonal flow are found in the upper stratosphere and lower mesosphere. The temperature anomalies of the quadrupole are generally stronger in the polar region than in the mid latitudes. The vertical inversion of the temperature anomalies between stratosphere and mesosphere at extreme NAM-phases is consistent with the observations [*Quiroz*, 1969; *Labitzke*, 1972a;b; *Hirota and Barnett*, 1977].

In summary the strongly positive stratospheric NAM-phases are associated with strong anomalous westerlies in high latitudes and a temperature quadrupole between troposphere and lower mesosphere. The zonal wind pattern results, by thermal wind balance, from the quadrupole structure of the temperature.

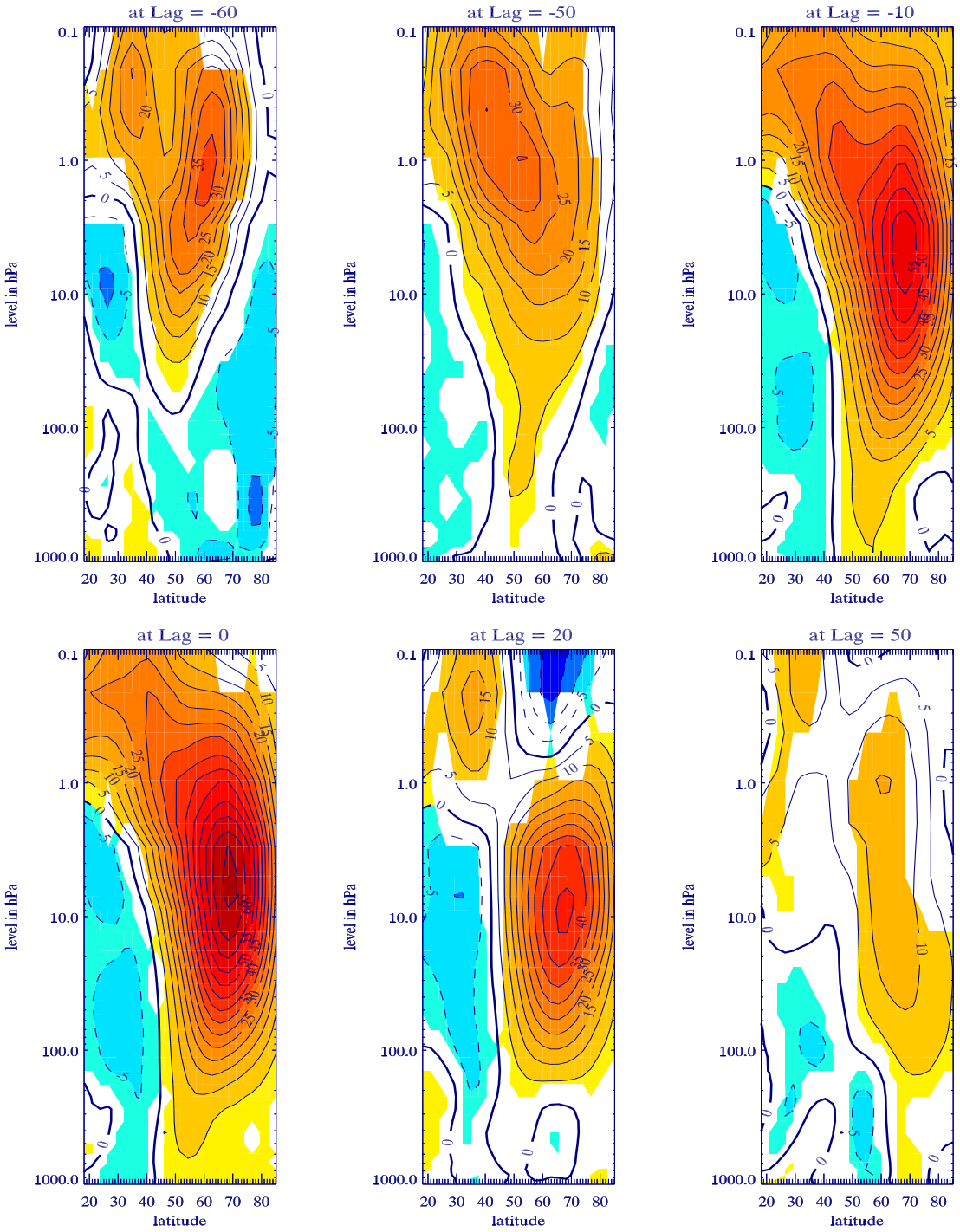

Figure 4.5: The differences between high and low composite (H - L) of the zonally averaged zonal wind at six different time lags. Positive (negative) values are represented by solid (dashed) lines and zero by a thick line. Color indicates significance at the 95% level according to a t-test.

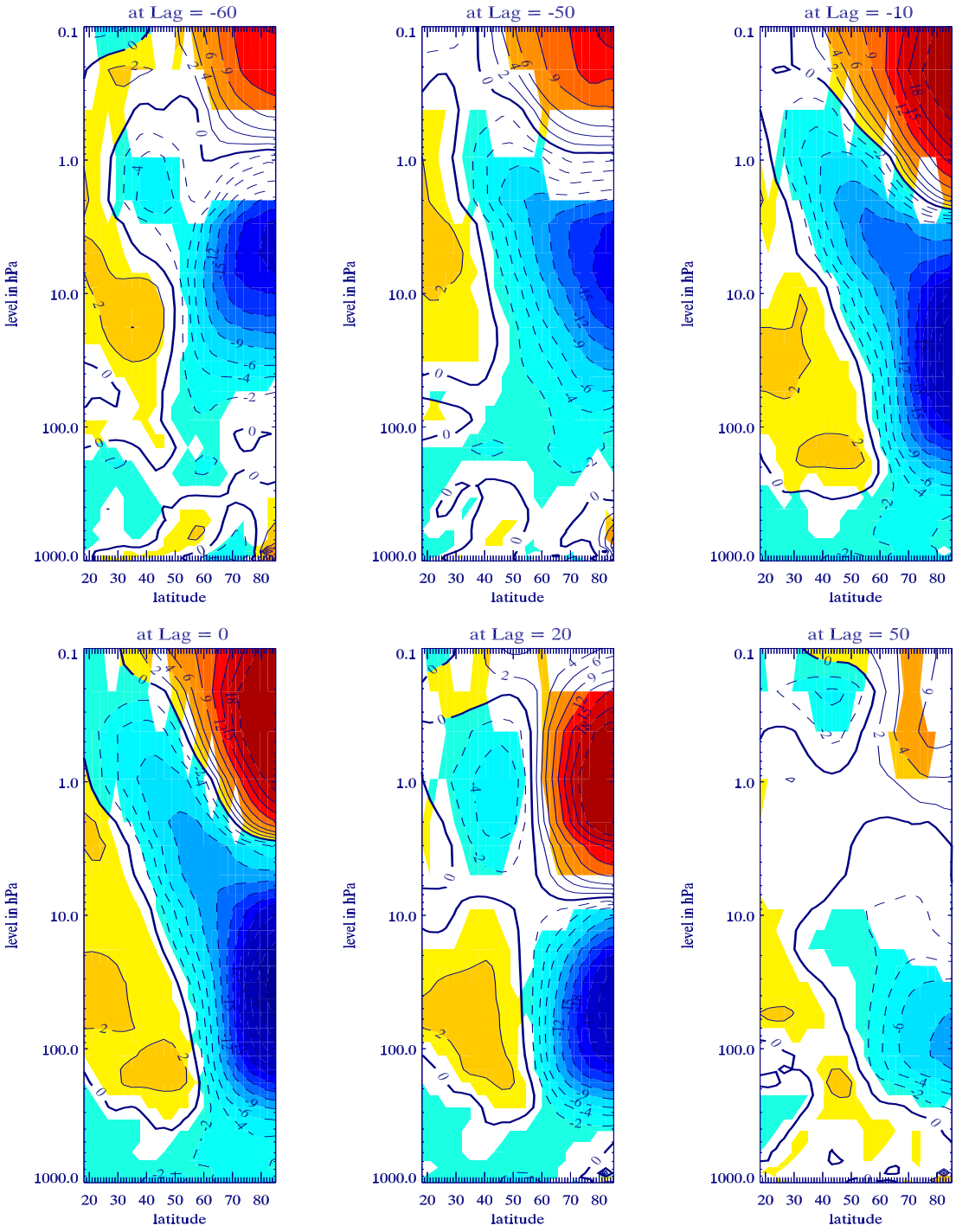

Figure 4.6: The differences between high and low composite (H - L) of the zonally averaged temperature at six different time lags. Positive (negative) values are represented by solid (dashed) lines and zero by a thick line. Color indicates significance at the 95% level according to a t-test.

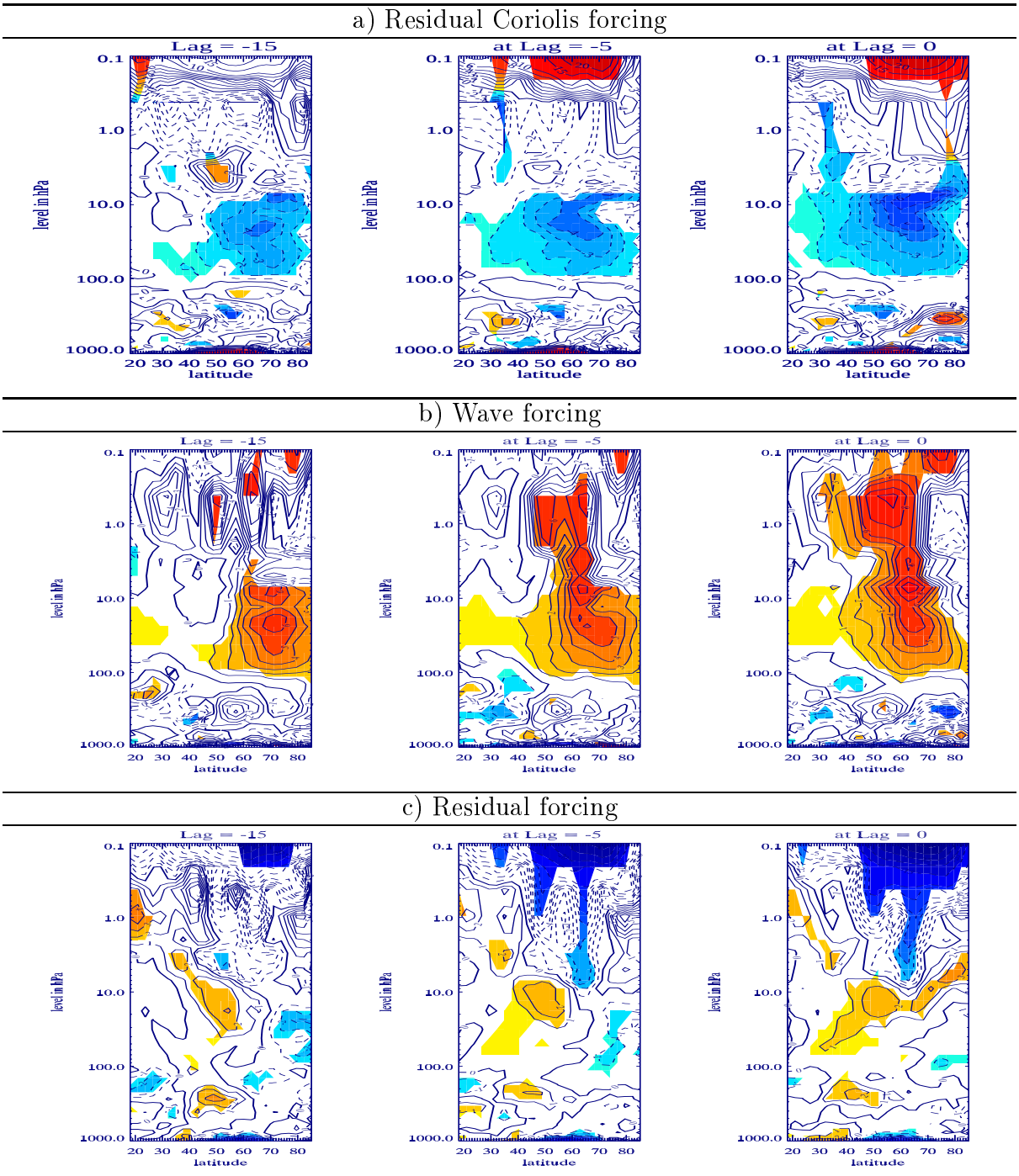

Figure 4.7: The differences between high and low composite (H - L) at lag -15, -5 and 0 of (a) residual Coriolis forcing, (b) wave forcing, and (c) residual forcing. Positive (negative) values are represented by solid (dashed) lines and zero by a thick line. Color indicates significance at the 95% level according to a t-test.

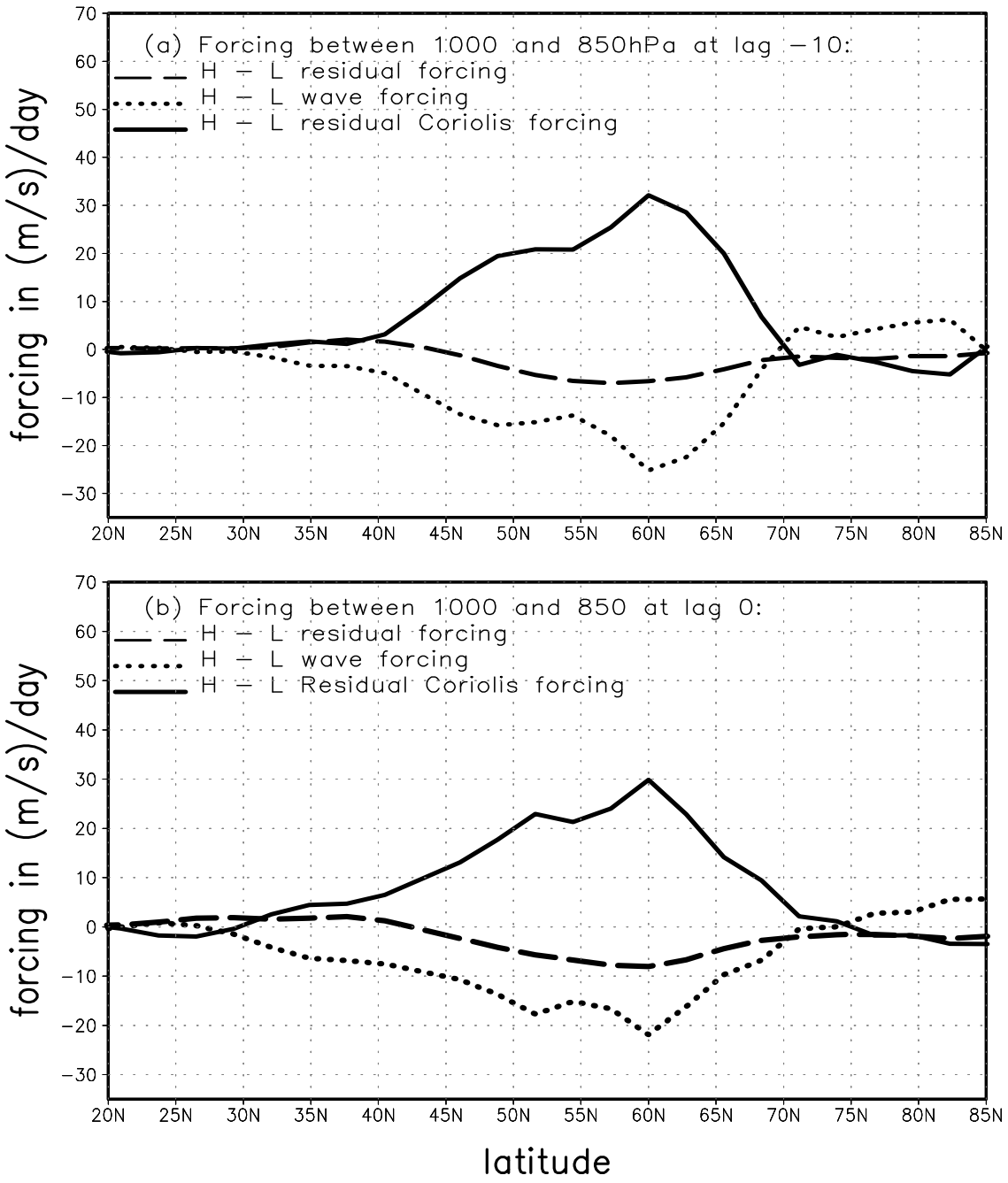

Figure 4.8: a (b) shows the differences between high and low composite at lag -10 (0) of the following forcings acting near the bottom: Residual Coriolis forcing (solid line), wave forcing (dotted line), and residual forcing (dashed line).

a) Non-orographic gravity wave drag

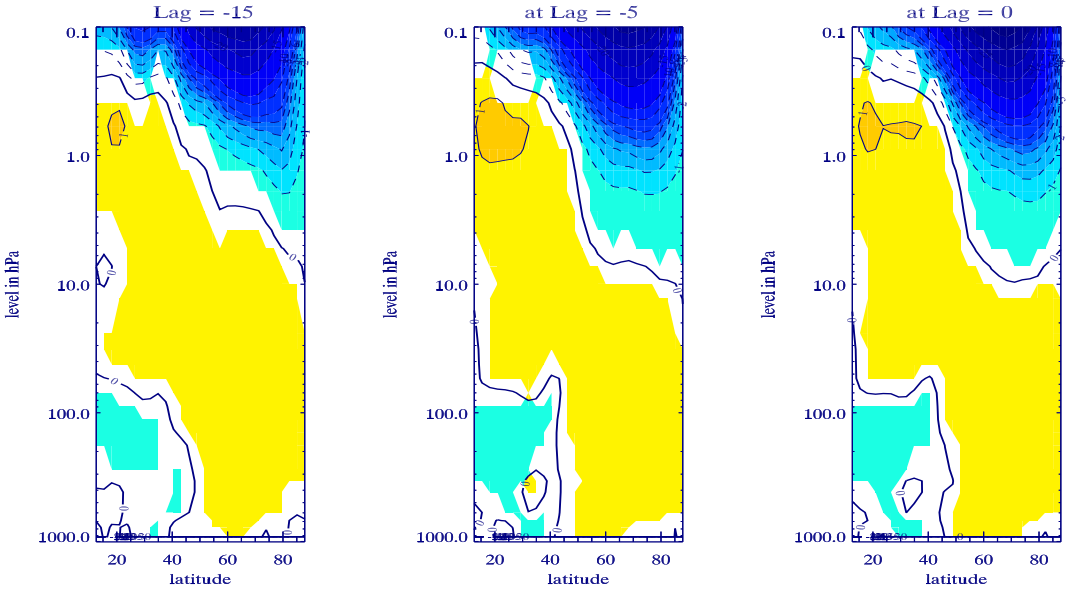

b) Residual meridional circulation and vertical velocity

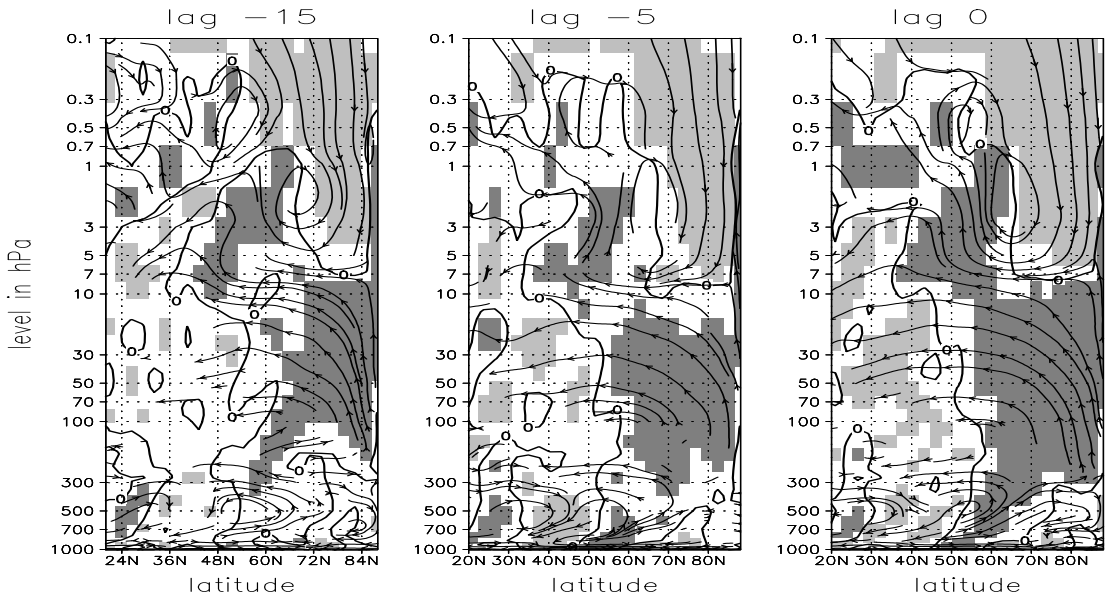

Figure 4.9: (a) is like Fig. 4.7 but it shows the non-orographic gravity wave drag. (b) shows the differences between high and low composite (H - L) at lag -15, -5 and 0 of the inverted omega residual velocity in p-coordinate. The stream plot represents the meridional residual circulation. Shading indicates significant values at the 95% level according to a t-test. Dark (light) grey indicates upward (downward) motion.

4.3 Dynamical coupling and spatial structure in the mature phase

4.3.1 Transformed Eulerian Mean (TEM) forcings and the NAM-pattern

The TEM formulation provides the forcing that drives both the wind anomalies and the structure of the Coriolis forcing, which (according to equation 4.6) is important for the change of a layer thickness. Fig. 4.7 shows the H - L lag composites of the anomalous residual Coriolis (Fig. 4.7a), planetary wave (Fig. 4.7b), and residual (Fig. 4.7c) forcing at lags -15, -5 and 0. The anomalous residual vertical velocity and the meridional circulation are plotted in Fig 4.9b. Fig. 4.8a (4.8b) shows the same forcings at lags -10 (0), but averaged near the bottom. The enhanced anomalous westerlies in the lower and middle stratosphere are maintained against the westward Coriolis forcing mainly by the eastward planetary wave forcing and partly by the much weaker residual forcing. Since the eastward planetary wave forcing is generated during a strong vortex and strengthens it, there is a positive feedback between the NAM wind-pattern and the planetary wave forcing. The enhanced anomalous westward Coriolis forcing and equatorward motion in the middle and lower stratosphere (Figs. 4.7a and 4.9b) weaken the Brewer-Dobson circulation and are strongest near 60-70°N. This results in a divergence (convergence) of the anomalous meridional Coriolis forcing in the high (mid) latitudes as in cases 2a (2a') of Fig. 4.1 and thus in a contraction (stretching) of the stratospheric layer north (south) of 60°-70°N. By continuity, the contraction of the polar stratosphere contributes to a stretching of the polar troposphere [*Ambaum and Hoskins*, 2002] and mesosphere, while the stretching of the stratosphere contributes to a contraction of the troposphere and mesosphere in the mid-latitudes. The net effect is the vertical motion shown in Fig. 4.9b explaining the temperature quadrupole seen in the mature phase (Fig. 4.6). The temperature pattern results from the adiabatic temperature change by vertical motion, and the vertical structure of the zonally averaged zonal wind results from the temperature pattern by thermal wind balance .

The strong westerlies near the tropospheric polar jet are maintained against the Coriolis forcing mainly by planetary wave forcing and partly by the weaker residual forcing. The eastward residual and wave forcings between the high latitude troposphere and the middle stratosphere are induced during a strong vortex and, at the same time, they strengthen the vortex further. Thus, there is a positive feedback between the polar vortex and these forcings. The increase of the tropospheric and stratospheric baroclinic wave activity due to the strong anomalous westerly wind shear can be important in this respect. This can be seen in Fig. 4.10, which shows the composite difference at lag 0 of tropospheric and lower stratospheric baroclinicity ($g\theta_y/\theta_0 N$). The latter is a good approximation to the largest growth rate of baroclinic waves [*Lindzen and Farrell*, 1980]. In general, the enhanced baroclinic instability during strong vortex is associated with an acceleration of the westerlies, which in turn leads to a positive feedback between the polar vortex and the baroclinic wave [*Tanaka and Tokinaga*, 2002]. This feedback contributes not only to the increase and persistence of the strong vortex but also to the downward propagation of the wind anomalies from the stratosphere into the troposphere. The enhanced westerly wave forcing near the tropospheric jet is, according to the quasigeostrophic momentum budget, associated with an anomalous equatorward motion from the stretched into the contracted tropospheric area (Fig. 4.9b), which dampens the high-latitude stretching and mid-latitude contraction in the troposphere. The increase of westerly wave forcing near the tropospheric jet can thus be seen as a quasigeostrophic adjustment of the troposphere to the changes induced by the stratosphere. As explained in chapter 2.5, the residual forcing in the extratropical lower stratosphere and upper troposphere can be explained by the combined contribution of gravity waves and non-quasigeostrophic component of the EP-flux.

The enhanced westerlies near the bottom are maintained mainly by the Coriolis forcing against westward planetary wave and residual forcing (Figs. 4.8a and b). Since the negative wave and residual forcing are caused during the strong NAM-westerlies and weaken the NAM-westerlies near the bottom even further, there is negative feedback between these forcings and the NAM wind-pattern in the lowermost boundary of the coupled system troposphere/stratosphere.

The strong stratospheric vortex is associated with an enhanced anomalous positive Coriolis forcing north of 20°N in the lower mesosphere, which together with the wave forcing, maintains the high latitude westerlies against the strong negative residual forcing. The net effect is an enhanced convergence of the anomalous Coriolis forcing in the polar mesosphere (Fig. 4.7a) and thus a stretching of the lower mesosphere (according to case 2b' in Fig. 4.1). This enhances, by continuity, the contraction of the polar upper stratosphere, as shown before, leading to stronger anomalous downward motion and adiabatic warming in both the lower mesosphere and upper stratosphere. This warming weakens the polar vortex and induces an anomalous negative shear of the zonal flow. The strong westward residual forcing between the high latitude upper stratosphere and lower mesosphere is induced during strong vortex and at the same time weakens and warms it, so that the residual forcing exercises negative feedback on the polar vortex at these altitudes. The residual forcing in the upper stratosphere and lower mesosphere can be explained by the non-orographic gravity wave drag, which according to Figs. 2.4(2), 2.5, 4.7 and 4.9a dominates the residual forcing and its change at these altitudes. The positive anomalies of the zonal wind and the anomalous easterly wind shear, as shown in Figs. 4.4(a) and 4.5, strengthen both the westerlies and the negative wind shear between the upper stratosphere and mesosphere seen in Fig. 2.2b. This leads, according to Lindzen's parameterization (see chapter 2.5), to a more easterly gravity wave drag than normal and can explain the high anomalous westward residual forcing seen in Fig. 4.7c. We can thus conclude that there is a negative feedback between the polar vortex and the residual forcing in the upper boundaries of the coupled system troposphere/stratosphere (i.e. upper stratosphere and lower mesosphere), which can be explained by the filtering of the gravity wave drag by the vertical structure of the stratospheric polar jet. In this feedback the strong vortex leads to an enhanced negative residual forcing (or gravity wave drag), which results in anomalous eastward Coriolis forcing (i.e. poleward motion) and thus in adiabatic warming by downward motion and a weakening of the vortex in both upper stratosphere and lower mesosphere. This result is supported by *Duck et al.* [2001], who proposed the same feedback, but in the context of the warming after late December.

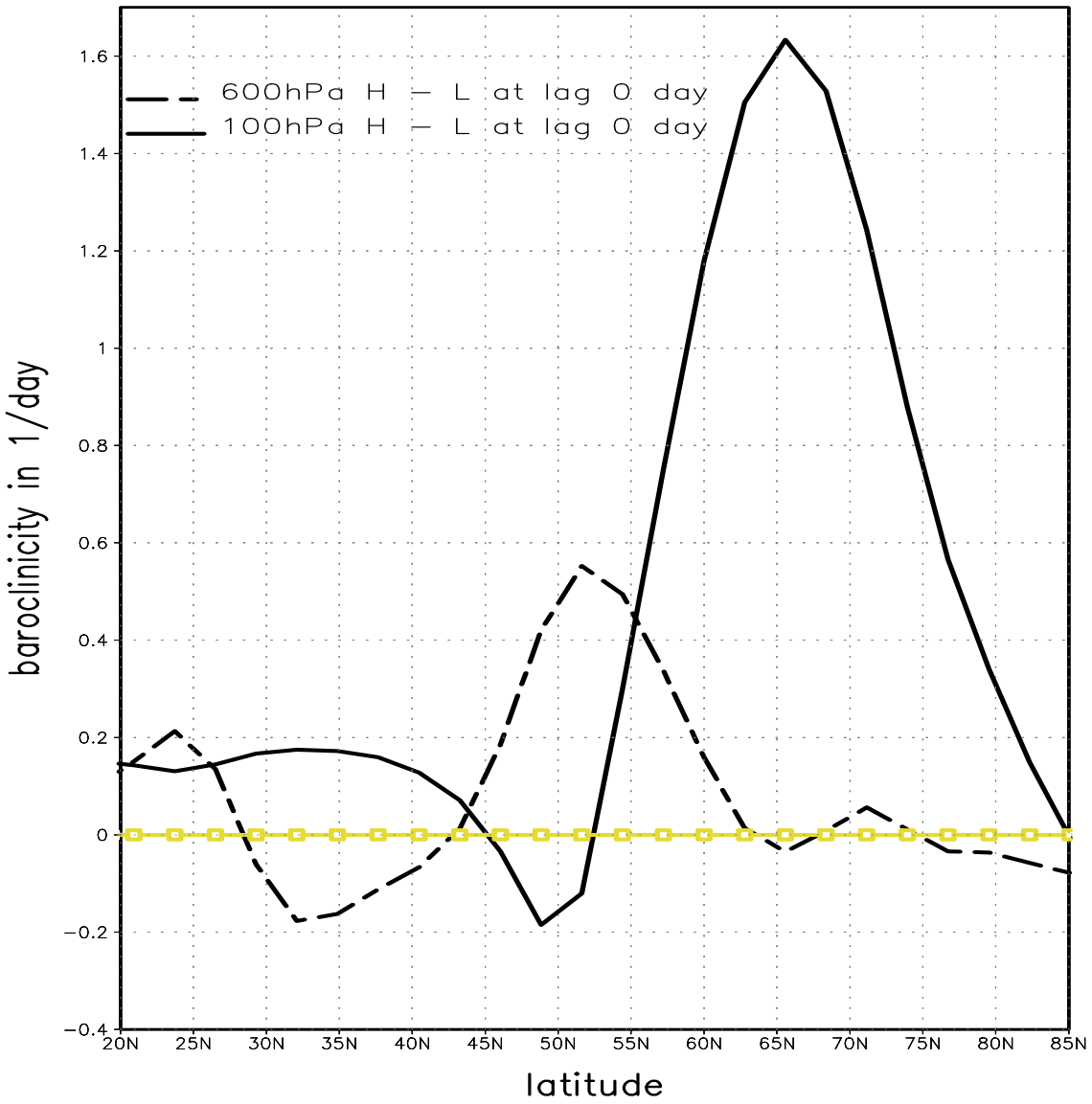

Figure 4.10: Differences between high and low (H - L) composite of the tropospheric (dashed line) and low stratospheric (solid line) baroclinicity at lag 0. The zero line is shown in yellow

The strong vertical velocity and temperature anomalies at the pole can be explained by the f-dependence of the residual Coriolis forcing, which (according to equation 9) makes the stretching vorticity and the resulting vertical motion and temperature change stronger there.

In summary, the vertical structure of the wind and temperature anomalies and their downward propagation during strong stratospheric NAM can be explained by the response of the stretching vorticity to the residual Coriolis forcing changes, which in turn are caused by planetary wave forcing in the middle and lower stratosphere and residual forcing in the lower mesosphere and upper stratosphere, as well as by quasigeostrophic adjustment of the troposphere to these changes. The persistent strengthening and downward propagation of the NAM-pattern is enhanced mainly by the planetary wave-vortex feedback that accelerates the westerlies within the coupled troposphere/stratosphere system. Thereby the strong vortex is strengthened further by the equatorward propagation of planetary waves and vice versa. There are two negative feedbacks acting in the upper and lower boundaries of the coupled system troposphere/stratosphere, which decelerate the westerlies and weaken the NAM-patterns. The first feedback, between residual forcing and polar vortex, acts above the stratospheric jet and can be explained by the filtering of gravity waves by the strong vortex and its vertical structure. The second feedback is driven by the residual and planetary wave forcing and acts near the surface.

4.3.2 The wave- zonal wind feedback

The impact of the planetary wave forcing on the stratospheric polar vortex is controlled by the tropospheric wave activity. An anomalous equatorward and/or downward propagation of the tropospheric waves leads to less wave breaking in the polar stratosphere and thus to an anomalous cooling and strengthening of the stratospheric westerlies by the resulting eddy heat and momentum fluxes (equation 4.1). In contrast, an anomalous poleward and upward propagation of the tropospheric waves leads to more wave breaking in the polar stratosphere and thus to an anomalous warming and weakening of the stratospheric westerlies. This connection between

the meridional propagation of the tropospheric waves and the stratospheric polar vortex can be seen in Fig. 4.11a. A strong vortex is associated with an increase of the anomalous equatorward and downward component of the tropospheric EP-flux and thus with less wave breaking in the polar stratosphere.

According to equations 4.1 and 4.2, the direction of the propagation of the tropospheric planetary waves, which modify the strength of the polar vortex, can be changed by the vertical and meridional structure of the zonally averaged zonal wind [*Hartmann et al.*, 2000; *Limpasuvan and Hartmann*, 2000]. Figs. 4.12a, b and 4.11b show the lag composite of the refraction index change caused by vertical curvature, vertical shear, and the sum of all terms of equation 4.1. The meridional curvature and the planetary term are small in the high latitudes compared to the other terms and thus not shown. The vertical curvature contributes to stronger equatorward propagation of the tropospheric waves and the vertical shear to stronger poleward propagation (Figs. 4.12a and b). The net effect of the zonally averaged zonal wind is a dipole structure in the refraction index between the troposphere and middle stratosphere north of about 35°N. This supports an anomalous equatorward propagation of tropospheric waves and is consistent with the direction of the EP-flux vector (Fig 4.11a). The negative pole in the polar troposphere results mainly from the vertical curvature; the positive pole to the south mainly from the vertical shear. The anomalous meridional propagation of waves, which drives the strong stratospheric NAM-phases results mainly from the vertical structure of the downward propagating anomalous zonal flow. This provides a positive feedback between the stratospheric polar vortex, and the meridional propagation of planetary waves, which contributes to the intensification and persistence of both stratospheric and tropospheric wind anomalies during the growing phase and to the decline during the decay phase.

In summary, there is a positive feedback between the planetary wave propagation and the stratospheric vortex, in which the stronger equatorward (poleward) wave propagation and thus less (more) wave breaking in the polar stratosphere is induced by an anomalous strong (weak) polar vortex and vice versa. This feedback explains the vortex-planetary wave forcing feedback shown above (Fig. 4.7b).

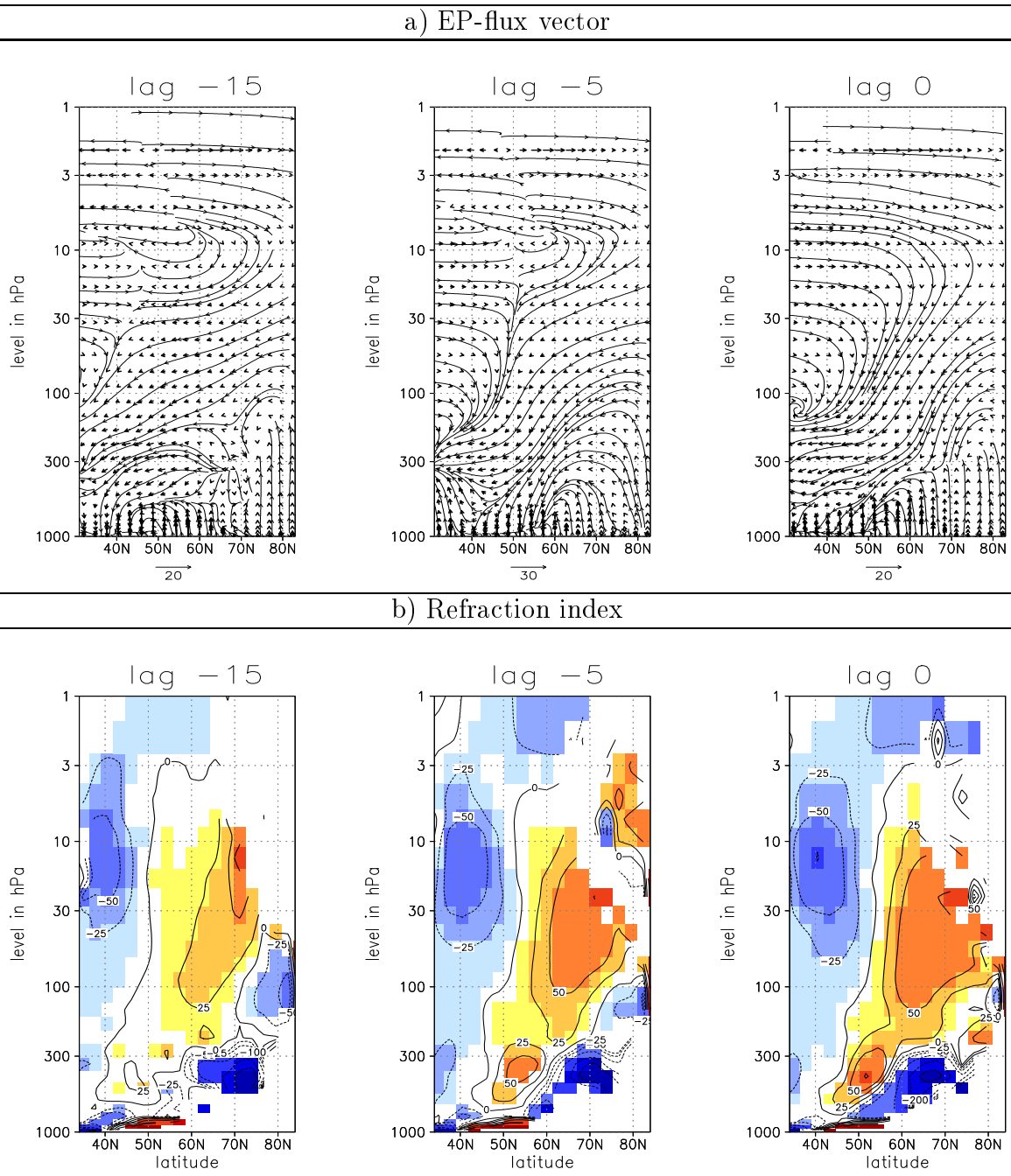

Figure 4.11: The differences between high and low (H - L) composite at lags -15, -5 and 0 of (a) the EP-flux vector and (b) the refraction index due to all changes of the zonally averaged zonal flow (equation 4.1). Positive (negative) values in (b) are represented by solid (dashed). Color indicates significance at the 95% level according to a t-test. The stream plot in (a) represents the EP-flux vector.

a) Effect of the vertical curvature of the zonal flow

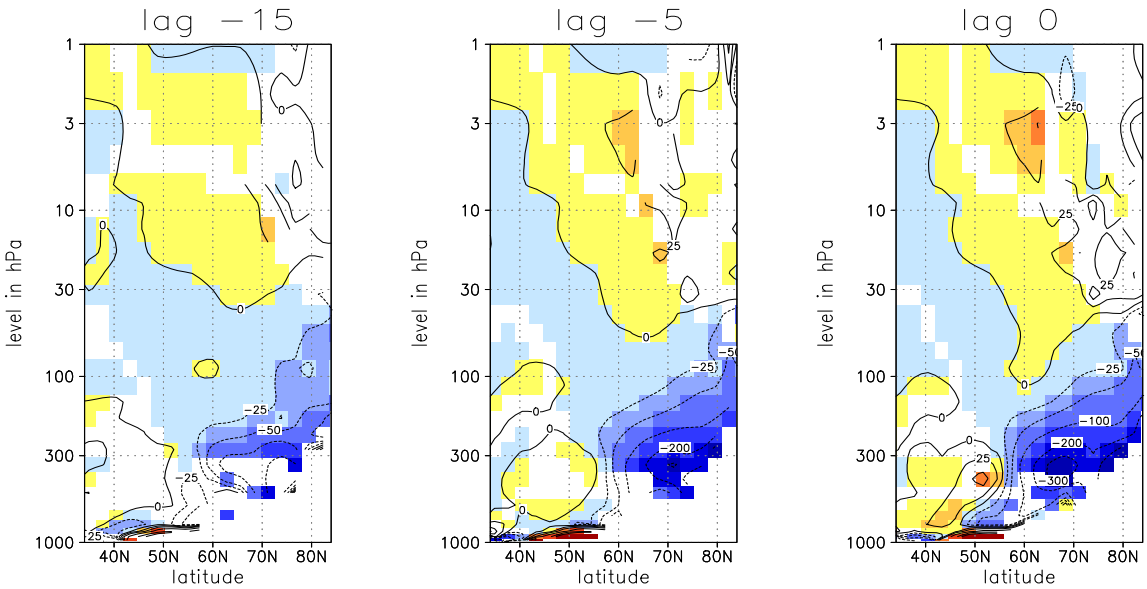

b) Effect of the vertical shear of the zonal flow

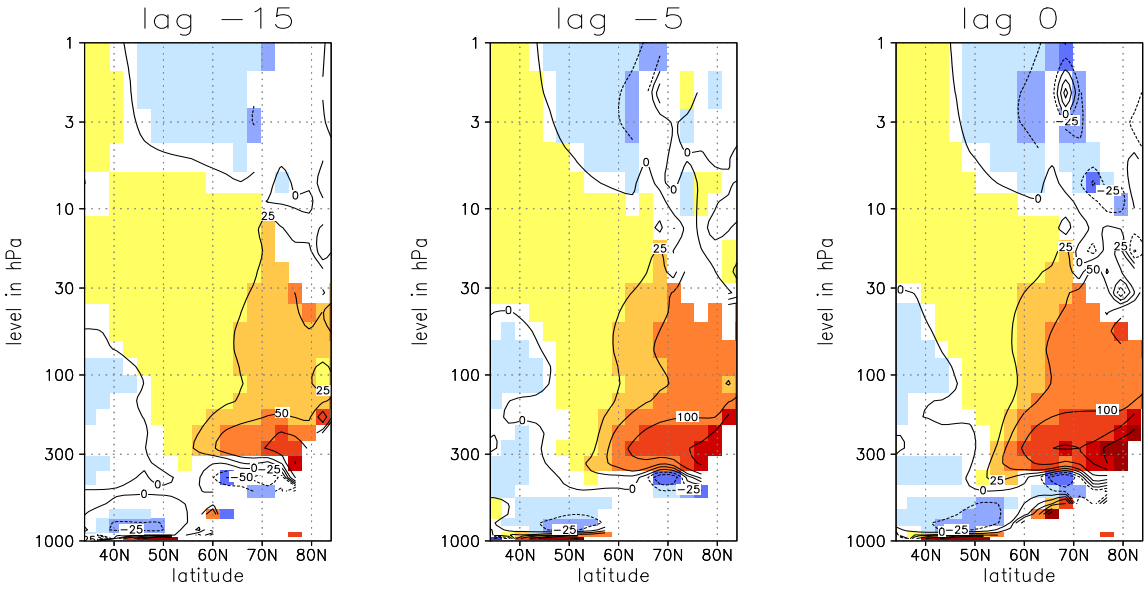

Figure 4.12: The differences between high and low (H- L) composite at lags -15, -5 and 0 of the effect on the refraction index of (a) vertical curvature and (b) vertical shear of the zonal mean of the zonal flow. Positive (negative) values are represented by solid (dashed) lines. Color indicates significance at the 95% level according to a t-test.

4.4 The dynamics of the evolution of the polar vortex

In order to understand the mechanism driving changes in the stratospheric polar jet, the TEM-terms were averaged between 55 and 70°N, where the wind anomalies are strongest. Again, a lag composite (+/-40 days) analysis based on the 50hPa NAMI was performed. Figs. 4.13a, b, and c show the high minus low composite difference of the resulting anomalous residual forcing, residual Coriolis forcing, and wave forcing between 100 and 0.1 hPa. Figs. 4.14a and b are similar, but they show the inverted scaled vertical residual velocity in p-coordinates and the adiabatic temperature change by vertical motion in the Arctic region. The growth and mature phase of the polar vortex is marked by a significant increase of the eastward planetary wave forcing over the entire stratosphere and lower mesosphere (Fig. 4.13c). This is balanced in the middle and lower stratosphere mainly by the enhanced westward Coriolis forcing (or equatorward motion, Fig. 4.13b). The strong anomalous westtward residual Coriolis forcing between 55 and 70°N induces a contraction of the polar stratosphere. This can be inferred from the anomalous adiabatic cooling by upward motion in the middle and low polar stratosphere and the anomalous adiabatic warming by downward motion in the upper polar stratosphere (Figs. 4.14a and b).

The high latitude lower mesosphere responds to the increase of the stratospheric NAM with an enhanced anomalous eastward residual Coriolis forcing (poleward motion), which together with the eastward planetary wave forcing balances the strongly negative residual forcing (Fig. 4.13). As mentioned above, the enhanced negative residual forcing can be explained by the filtering of gravity waves by the stratospheric jet an its vertical structure, which leads to more easterly gravity drag in the mesosphere and upper stratosphere and provides a negative feedback on the polar vortex. The enhanced eastward residual Coriolis forcing causes, according to case 2b' (Fig 4.1), a stretching of the polar mesosphere and enhances, by continuity, the downward motion in both polar mesosphere and upper stratosphere (Fig 4.14a). The

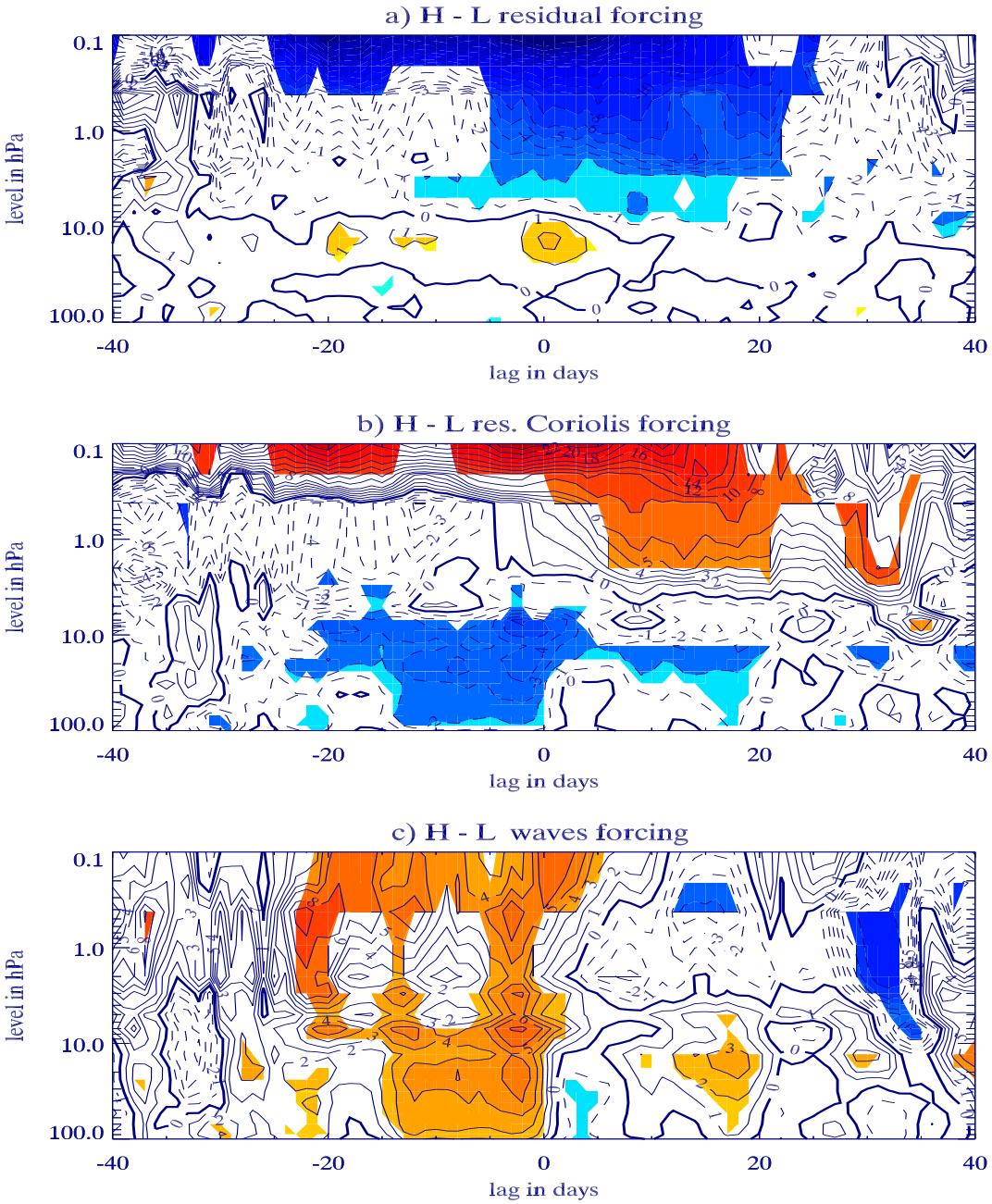

Figure 4.13: The difference between the high and low (H - L) lag composite of the averaged (a) residual forcing, (b) residual Coriolis forcing, and (c) planetary wave forcing between 55 and 70°N. Positive (negative) values are represented by solid (dashed) lines and zero by a thick line. Color indicates significance at the 95% level according to a t-test.

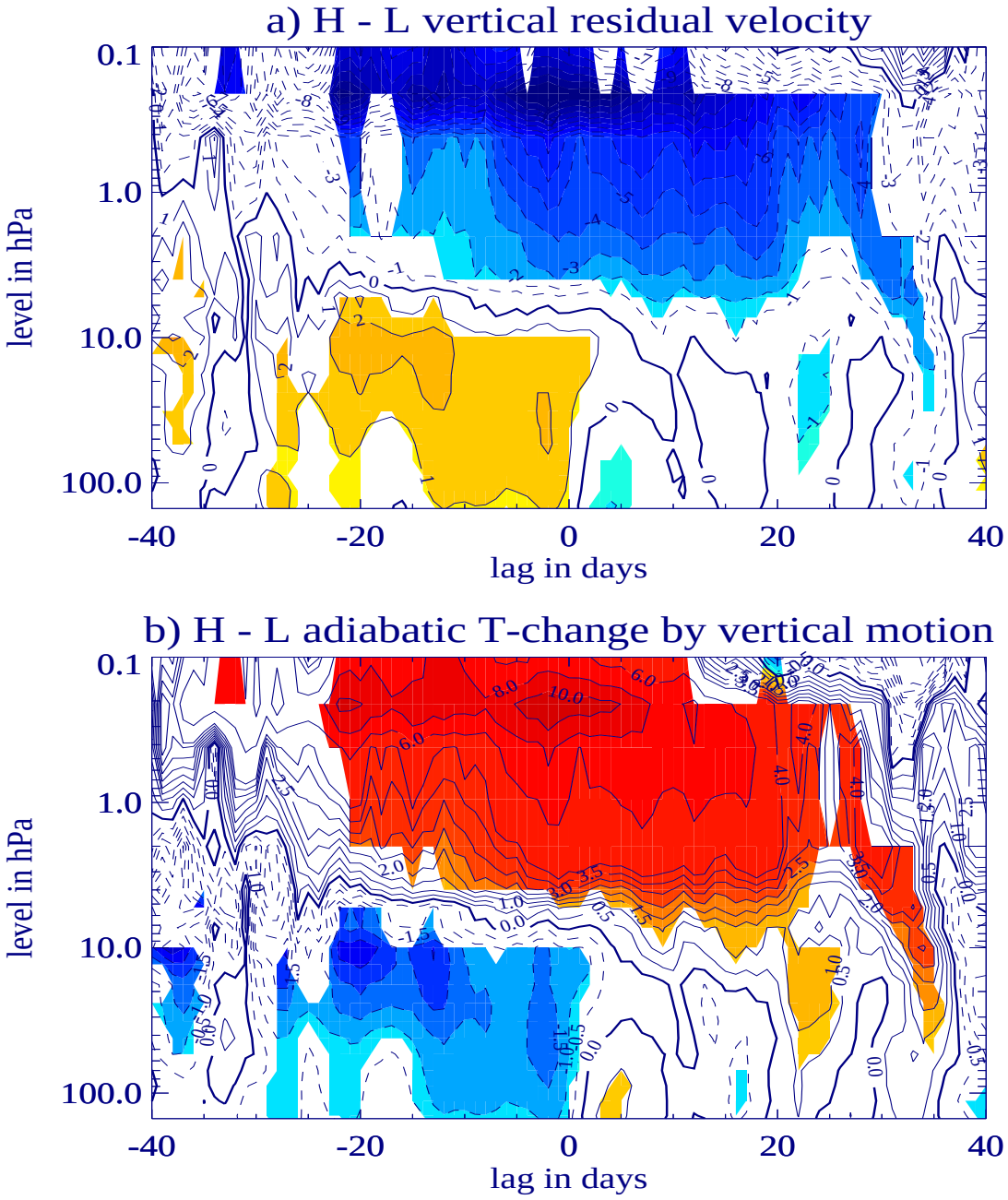

Figure 4.14: The difference between the high and low (H - L) lag composite of the (a) inverted omega residual velocity and (b) adiabatic temperature change by vertical motion north of 60°N. Positive (negative) values are represented by solid (dashed) lines and zero by a thick line. Color indicates significance at the 95% level according to a t-test.

net result is an anomalous adiabatic warming between the polar upper stratosphere and lower mesosphere that propagates downward and weakens the stratospheric vortex (Fig. 4.14b). The negative residual forcing provides thus a negative feedback that regulates the strength of the stratospheric vortex. This explains the amplification and downward propagation of the anomalous warming and easterlies from the mesosphere into the stratosphere and thus the weakening of the vortex there.

The weakening of the stratospheric jet in the decay phase leads to a strong decrease of the eastward planetary wave forcing that in turn weakens the polar vortex (Fig. 4.13c). This feedback can be explained by the positive planetary wave- vortex feedback discussed above, by which the weakening of the stratospheric jet and its shear and curvature lead to reduced anomalous equatorward wave propagation and thus to more wave breaking in the polar stratosphere. These changes induce, according to the momentum budget, a weakening of the anomalous westward Coriolis forcing (or equatorward mass transport, Fig. 4.13b), which, by continuity, results in reduced upward motion and adiabatic cooling in the lower and middle stratosphere (Fig. 14). The positive feedback between the planetary waves and the vortex contributes thus not only to the amplification of the NAM anomalies in the increase phase but also to their weakening in the decay phase.

The anomalous upward (downward) motion in the high (mid) latitude stratosphere is associated with a pressure increase (decrease), which begins in the stratosphere during the growth phase and reaches the troposphere during the mature phase (Fig. 4.15). These NAM-like patterns subsequently weaken strongly parallel to the wind and temperature anomalies.

In summary, the amplification of the strong polar jet is associated with an enhanced anomalous warming in the polar mesosphere and upper stratosphere that propagates downward and weakens the stratospheric vortex. The warming and weakening of the vortex can be explained by the negative feedback between vortex and residual forcing (mainly gravity wave drag). This negative feedback acts as a self-regulation mechanism of the middle atmospheric jet. The weakening of the vortex is accelerated also by the planetary wave-vortex feedback.

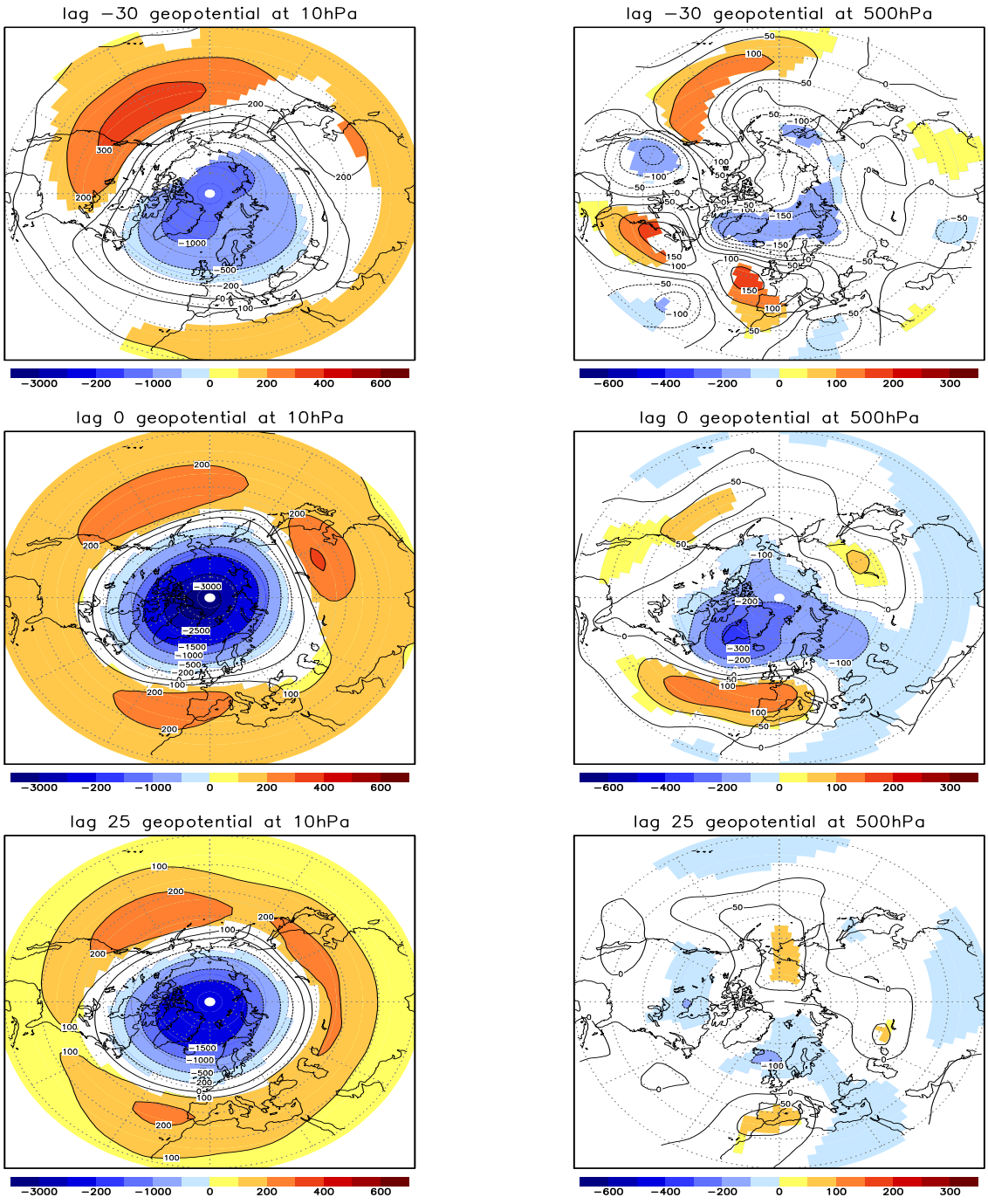

Figure 4.15: The differences between high and low (H - L) composite at lag -30, 0 and 25 of the geopotential height at the 10 and 500hPa levels. Positive (negative) values are represented by solid (dashed) lines. Color indicates significance at the 95% level according to a t-test.

5 The coupled system stratosphere/troposphere at strong tropospheric NAM

In this chapter, the dynamics of the coupling between troposphere and stratosphere during strong tropospheric Northern Annular Mode (in the following referred to as 'tropospheric mode') is investigated. The results of a lag-composite analysis using the 1000hPa-NAMI from the same run used in the last chapters are described. Even though the tropospheric NAMI is used less often than the NAO-Index (NAOI), it is equally suitable for the study of the extratropical variability, since it is strongly correlated to the NAOI: Both indices are related to the same physical processes and climatic changes as described by *Thompson and Wallace* [1998; 2000]. Analogous to the previous chapter, the wind and temperature patterns associated with the tropospheric NAM are diagnosed, as well as the forces driving these patterns. The focus will be on the differences between the stratospheric mode shown in the last chapter and the tropospheric mode obtained through the 1000hPa-NAMI-composite.

5.1 Wind and temperature anomalies during strong tropospheric NAM-phases

5.1.1 Time evolution

The evolution of the high minus low (H - L) lag composite of the NAMI at 1000hPa is shown in Fig. 5.1a. Fig. 5.1b shows the evolution of the H - L lag composite

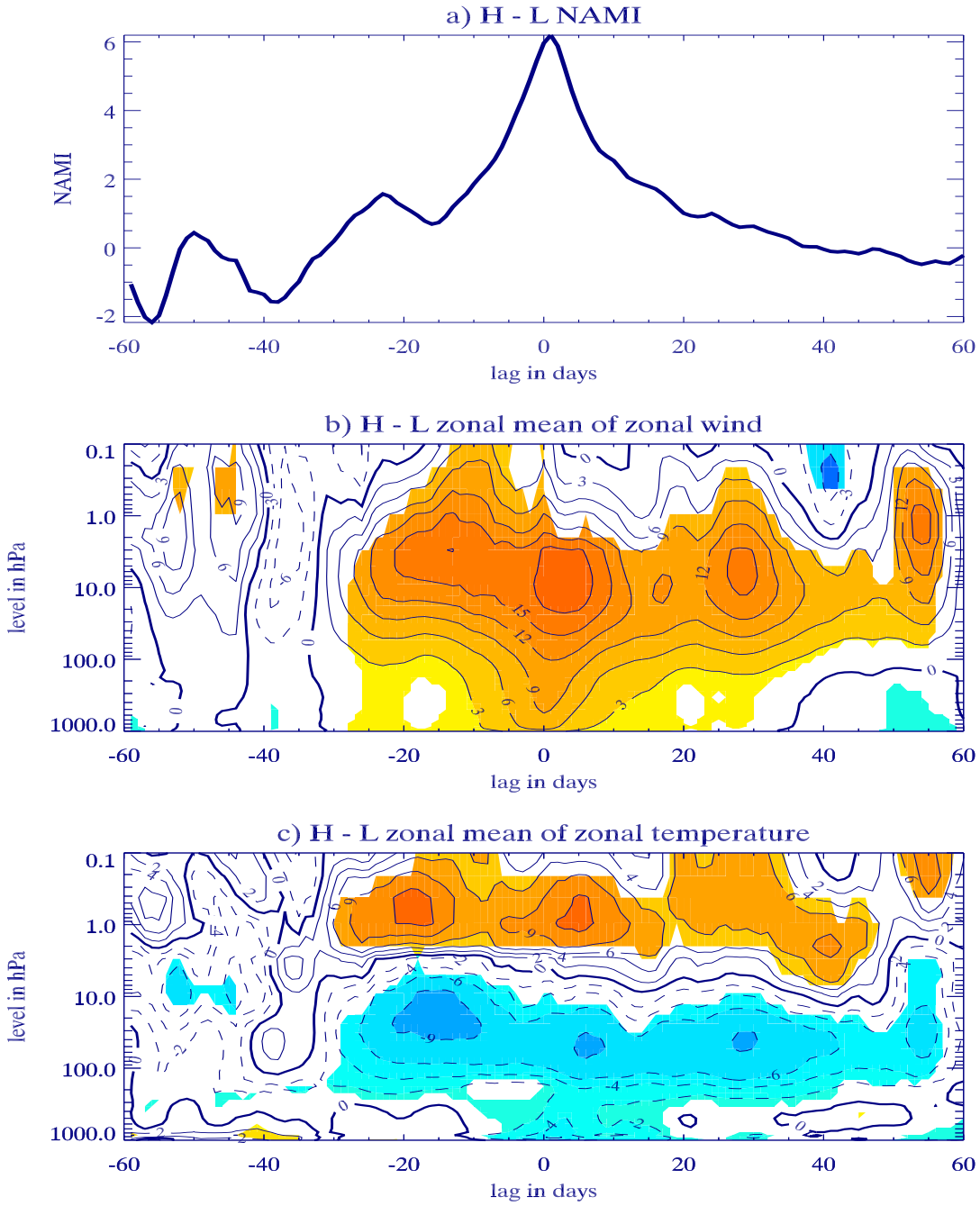

Figure 5.1: The difference between the high and low (H - L) lag composite in the tropospheric mode of (a) the NAMI at 1000hPa (b) the zonally averaged zonal wind between 55 and 70°N and (c) the zonally averaged temperature north of 60°N. Positive (negative) values are represented by solid (dashed) lines and zero by a thick line. Color indicates significance at the 95% level according to a t-test.

of the anomalous zonally averaged zonal wind between 55 and 70°N in the tropospheric mode. The statistical significance was estimated through a t-test. Fig. 5.1c shows the anomalous zonally averaged temperature between 60 and 90°N in tropospheric mode. Just as the vortex-evolution in the stratospheric mode is well described by the 50hPa-NAMI (see chapter 4), the evolution of the zonally averaged tropospheric zonal wind is well described by the 1000hPa-NAMI. The slow increase of the 1000hPa-NAMI between about lag -25 and lag -10 days characterizes the onset phase of the development of the tropospheric westerlies. The faster increase of the NAMI between lag -10 and 0 describes the growth and mature phases. The decrease of the 1000hPa-NAMI at positive lags indicates the decline and decay phases. Compared to the stratospheric NAM (Fig. 4.4), which is dominated by low frequency change, the tropospheric NAMI is dominated by high frequency fluctuations on synoptic time scales. These fluctuations are superimposed on low frequency variations having longer stratospheric time scales. This is consistent with the results of the wavelet and SSA analyses described in chapter 3.2.2. The change of the tropospheric NAMI and westerlies shows some correlation to that of the stratospheric westerlies during the whole life cycle, including the pre-onset and post-decay phases (Fig. 5.1). Such correlations can also be seen in Fig. 7 of *Ambaum and Hoskins* [2002], who used observational data and computed the lag/lead-correlation between NAOI and PV500-index. They defined the PV500-index as the first principal component of the potential vorticity on the 500°K isentropic surface. This index measures, like the stratospheric NAM, the strength of the stratospheric westerlies and polar vortex.

The life cycle of the strong tropospheric NAM is much shorter than the stratospheric one. This reflects the importance of the high frequency tropospheric variability associated with the local structure of the tropospheric circulation (see section 3.1.3). This finding is consistent with the observational results by *Ambaum and Hoskins* [2002], who found that the autocorrelation of the NAOI drops much more rapidly (after ca. 10-15 days) than that of PV500-index (after ca. 30-40 days).

The first increase of the middle atmospheric temperature and wind anomalies precedes the onset phase of the tropospheric NAMI. These anomalies reach a first

climax about 15 days before reaching the 1000hPA-NAMI-maximum. This behavior differs greatly from the stratospheric mode (Fig. 4.4), where the maximum in middle atmospheric wind and temperature anomalies is first reached at lag 0, when the stratospheric NAMI is also maximal. The growth and mature phases of the tropospheric NAMI are associated with an increase of the wind and temperature anomalies not only in the troposphere but also in the lower and middle stratosphere. The vortex and the cooling between lower and middle stratosphere become strongest about 4-5 days after the NAMI-maximum. This result is consistent with *Ambaum and Hoskins* [2002], who showed, from observations, that the increase in the NAO index is associated with a stronger stratospheric vortex about 4 days later. The increase and mature phases of the tropospheric NAMI are associated with a decrease of the wind anomalies and a warming between upper stratosphere and mesosphere.

5.1.2 Two-dimensional structure

The two-dimensional structure of the H - L lag composite of the zonally averaged zonal wind and the temperature anomalies is shown at six time lags (-30, -20, -10, 0, 20, and 50) in Figs. 5.2 and 5.3, respectively. This structure makes visible several differences between the tropospheric and stratospheric NAM-modes (Figs. 4.4, 4.5 and 4.6), especially in the increase and mature phases: While the tropospheric wind and temperature anomalies are much stronger in the tropospheric mode, the stratospheric anomalies are much stronger in the stratospheric mode; the tropospheric jet is shifted more poleward and the zero-line-temperature is shifted more downward in the tropospheric mode; the quadrupole structure of the temperature anomalies is more pronounced in the stratospheric mode. While in both modes the structure of the zonal mean of zonal flow is in thermal wind balance with the temperature pattern, the position of the wind maximum at lag 0 is much lower in the tropospheric mode than in the stratospheric mode.

In summary, a comparison between the results obtained with MAECHAM5 and those of *Ambaum and Hoskins* [2002], showed that MAECHAM5 captures several properties of the observed tropospheric NAM or NAO. The model shows several dif-

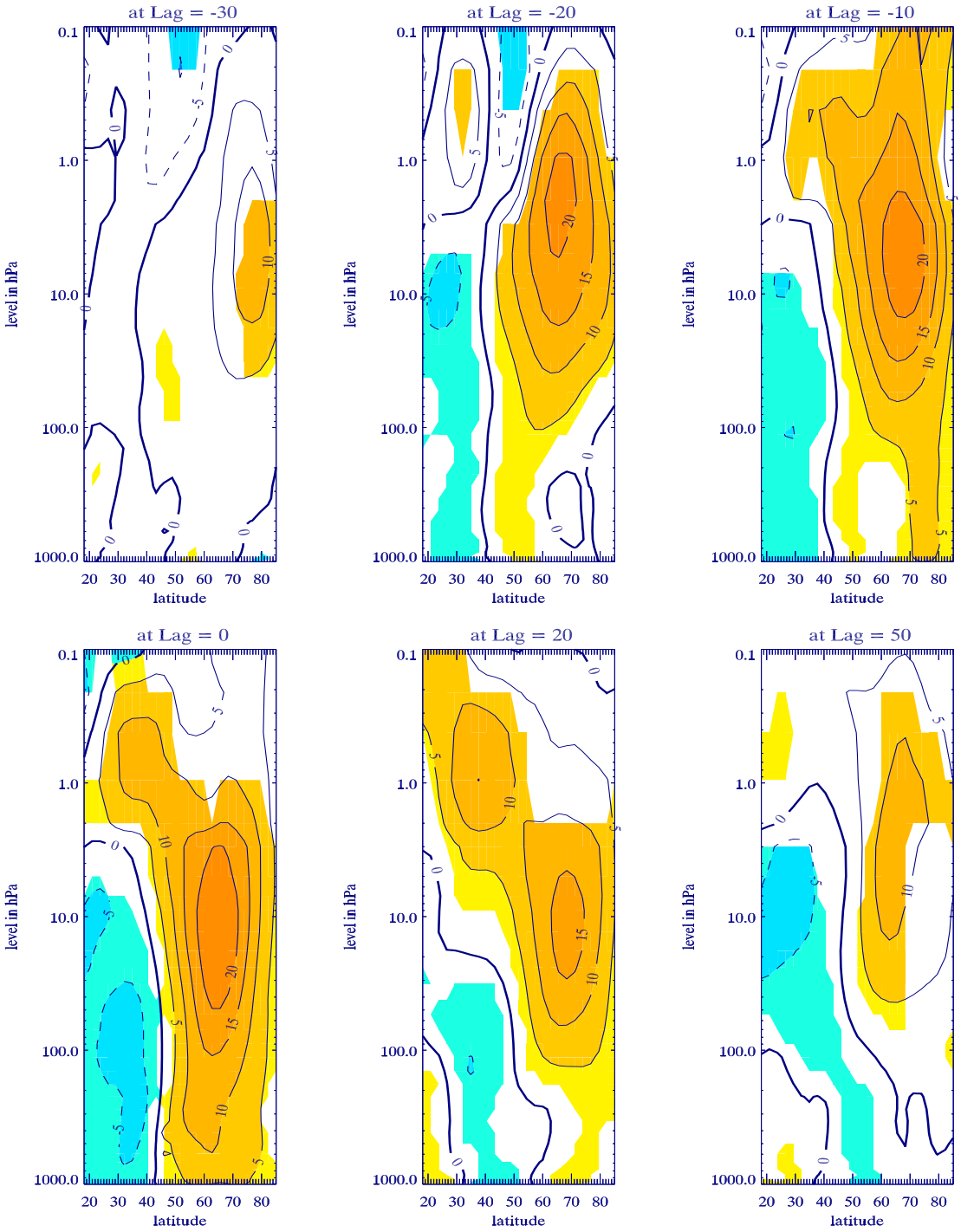

Figure 5.2: The differences between high and low (H - L) composite of the zonally averaged zonal wind at six different time lags. Positive (negative) values are represented by solid (dashed) lines and zero by a thick line. Color indicates significance at the 95% level according to a t-test.

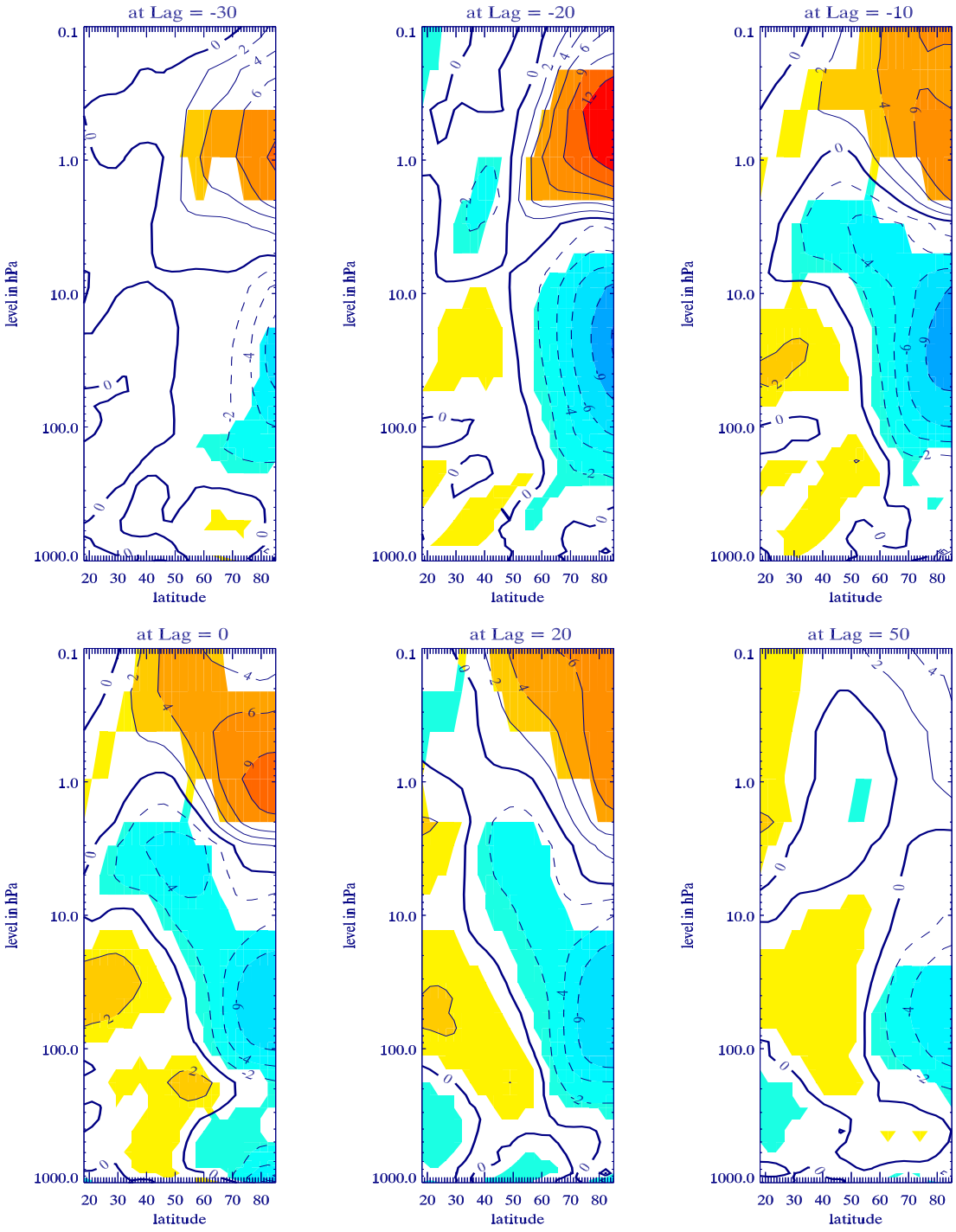

Figure 5.3: The differences between high and low (H - L) composite of the zonally averaged temperature at six different time lags. Positive (negative) values are represented by solid (dashed) lines and zero by a thick line. Color indicates significance at the 95% level according to a t-test.

ferences between tropospheric and stratospheric NAM: The life cycle of the tropospheric NAM-mode is much shorter and is dominated by high frequency fluctuation on the synoptical time scale. Onset, increase and maturation of the tropospheric mode are preceded and accompanied by a strong vortex indicating a possible impact of the stratosphere on the troposphere. The enhanced tropospheric westerlies at lag 0 are followed by a strong vortex and cooling 4-5 days later. The tropospheric anomalies are much stronger in the tropospheric mode than in the stratospheric mode, while the stratospheric anomalies are much weaker.

5.2 The forcing driving the tropospheric NAM

The TEM-formulation of the momentum budget is used to look at the forces driving the tropospheric NAM and to explain the differences between tropospheric and stratospheric NAM-mode discussed above. Fig. 5.4 shows the high minus low lag composite of the anomalous residual Coriolis (Fig. 5.4a), wave (Fig. 5.4b), and residual (Fig. 5.4c) forcing at lags -25, -5, 0, and 4. Fig. 5.5 shows the high minus low lag composite of tropospheric (at 600hPa) and stratospheric (at 100hPa) baroclinicity in the tropospheric mode. The composite of the anomalous residual vertical velocity and the meridional circulation at lags -25, -5, 0, 2 and 5 are plotted in Fig 5.6.

The structure of the stratospheric forcings before the onset phase of tropospheric NAM mode (see lag -25 in Fig. 5.4) is quite similar to their structure in the mature phase of the stratospheric mode (Fig. 4.7). At these time lags the strong stratospheric jet is maintained mainly by planetary wave forcing, which exercises a positive feedback on it and leads to a negative Coriolis force centered in the high latitude stratosphere. This results in a contraction of the polar stratosphere and thus a rising of the Arctic tropopause, which leads to adiabatic cooling by upward motion as well as anomalous westerly wind and wind shear in the upper troposphere (Figs. 5.6, 5.3, 5.2, and 5.1). This result is consistent with what *Ambaum and Hoskins* [2002] found through a lag-regression analysis. They showed a rising of the Arctic tropopause at

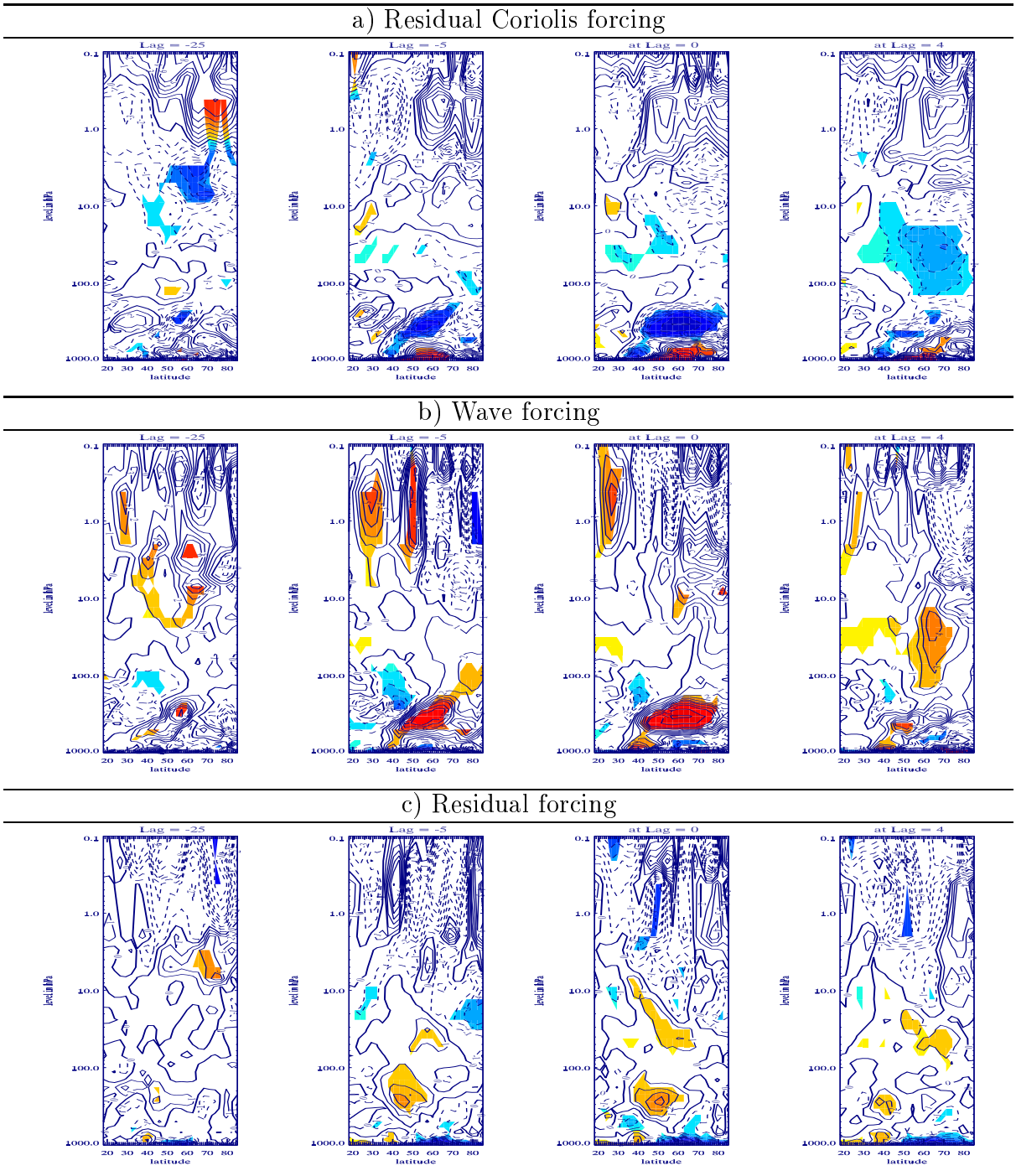

Figure 5.4: The differences between high and low (H - L) composite at lags -25, -15, -5 and 0 of (a) residual Coriolis forcing, (b) wave forcing, and (c) residual forcing. Positive (negative) values are represented by solid (dashed) lines and zero by a thick line. Color indicates significance at the 95% level according to a t-test.

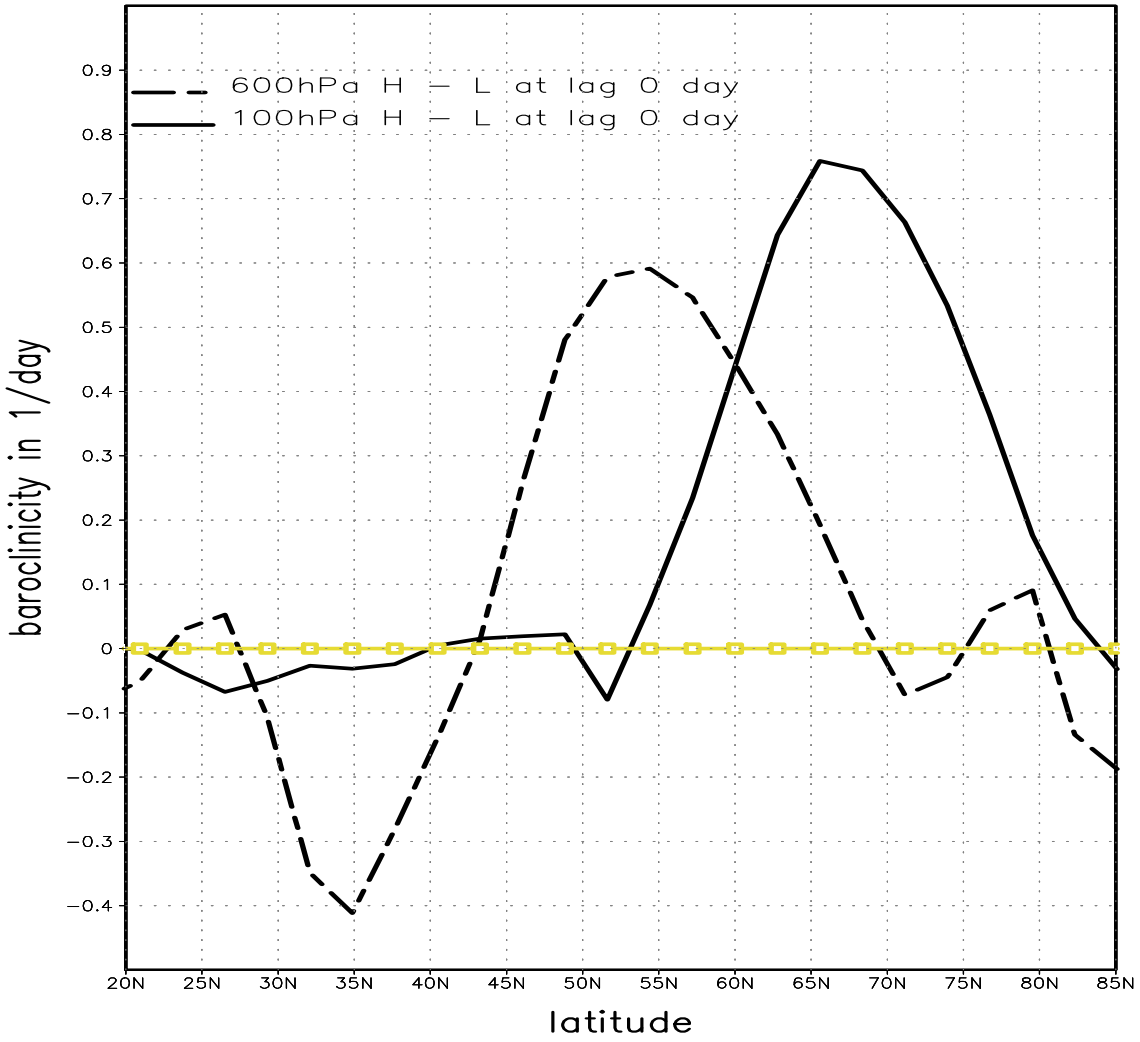

Figure 5.5: Differences between high and low (H - L) composite of the tropospheric (dashed line) and low stratospheric (solid line) baroclinicity at lag 0. The zero line is shown in yellow.

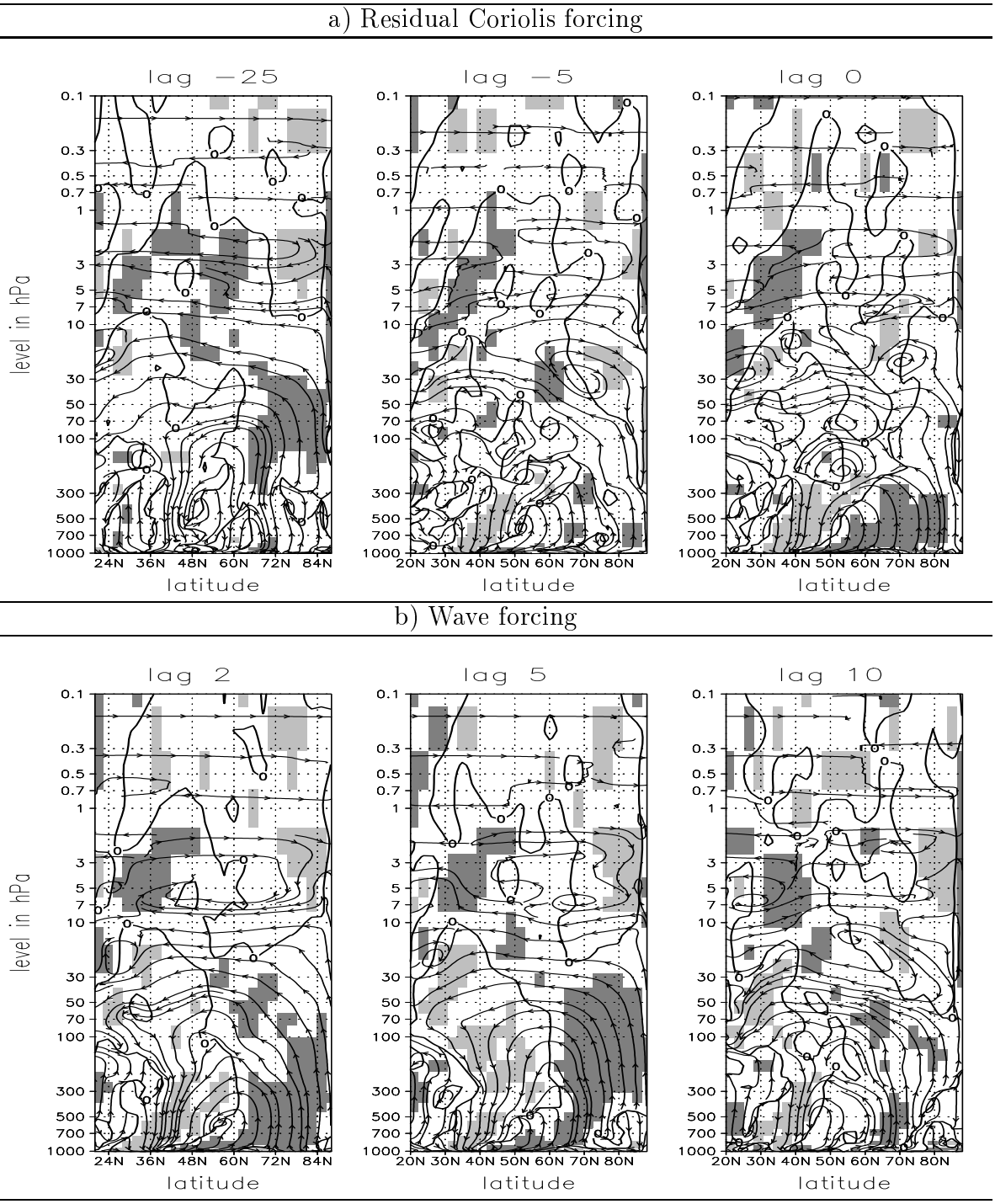

Figure 5.6: The differences between high and low composite (H - L) -in tropospheric mode- at six different lags (-25, -5, 0, 2, 5 and 10) of the inverted omega residual velocity in p-coordinate. The stream plot represents the meridional residual circulation. Shading indicates significant values at the 95% level according to a t-test. Dark (light) grey indicates upward (downward) motion.

positive NAO phase, which is related to the strong stratospheric vortex.

The net effect of the stratosphere-induced anomalous upward motion (Fig. 5.6 at lag -25) is in general a cyclonic pressure anomaly in the high latitude upper and middle troposphere (see Fig. 4.15) and an enhanced meridional temperature gradient (see Fig. 5.3 at lag -20), which increases the upper tropospheric baroclinicity before the increase and maturation phases. As described by *Hoskins et al.* [1985], the amplification of cyclonic anomalies in the troposphere can be accelerated by a combination of pre-existing lower-tropospheric baroclinicity (associated with the internal low tropospheric temperature change) and upper-tropospheric cyclonic anomalies (e.g. associated with stratospheric change). The high baroclinic wave activity in the extratropical troposphere can also be reproduced by prescribed mid-latitude SST-anomalies [e.g. *Inatsu et al.*, 2003].

As shown in Fig. 5.4, the increase and mature phases of the tropospheric NAMI are associated with a rapid and strong intensification of the internal tropospheric wave drag, which leads to rapid and strong increases of the westerly wind and its vertical shear (Figs. 5.1b and 5.2). The westerly wave forcing in the mature phase is associated with an enhanced baroclinicity due to the vertical wind shear (Fig. 5.5). The increase of tropospheric westerlies in the tropospheric mode results from the combined effect of both strong wave and much weaker residual forcing (Fig. 5.4), compared to the moderate effect of the wave forcing in the stratospheric mode (Fig. 4.7). This results in much higher tropospheric anomalies in the tropospheric than in the stratospheric mode.

In the mature phase of the tropospheric NAMI (near lag 0), the strong westerlies near the lower boundary are maintained mainly by the strong eastward Coriolis forcing or anomalous poleward motion. This poleward motion is in turn associated with a strong compensating equatorward motion (i.e. easterly Coriolis forcing) near the tropospheric jet, which balances both wave and residual forcing there (Fig 5.4). Poleward and equatorward motion together result, by continuity, in a strong anomalous upward motion (Fig. 5.6) and thus a stretching, adiabatic cooling and pressure lowering in the polar troposphere. This enhances afterwards, by continuity,

the upward motion and the adibatic cooling in the lower and middle polar stratosphere (Fig. 5.6), which explains the stratospheric temperature minimum and the vortex maximum 4-5 days after lag 0 (Fig. 5.1). This vortex maximum is associated with an enhanced wave forcing in the stratosphere (Fig. 5.4b at lag = 4), which increases as a result of the vortex-planetary wave feedback (equations 4.1 and 4.2, Figs. 4.11 and 4.12). As in the stratospheric mode, this induces a Coriolis forcing divergence (Fig. 5.4a at lag = 4) and thus a contraction of the polar stratosphere and a stretching of the underlying troposphere (Fig. 5.6) that lead to the persistence of the anomalous cooling and westerlies in both troposphere and stratosphere as seen in Fig. 5.1. This finding is consistent with *Ambaum and Hoskins* [2002], who showed that a strong NAO is associated with a strong polar vortex 4 days later and with a rising of the tropopause. This rising persists for a few weeks after reaching the NAO maximum and causes a lowering of the tropospheric pressure in the arctic. They also showed that the rising of the tropopause in the arctic is related to the strong vortex.

In summary, tropospheric and stratospheric NAM are two distinct modes with different time scales and driven by different mechanisms. In the stratospheric NAM mode, the tropospheric westerlies are driven non-locally by the stratospheric circulation and enhanced by the vortex-wave forcing feedbac. In the tropospheric mode, on the other hand, the tropospheric westerlies are induced by a strong internal wave and a much weaker residual forcing, which develops inside the troposphere on a synoptical time scale. This results in stronger tropospheric westerlies in the tropospheric than in the stratospheric mode. The stratosphere is also important in the tropospheric mode: It provides the upper troposphere with a low frequency westerly wind and wind shear and thus with enhanced baroclinicity. The stronger stratospheric westerlies in the stratospheric mode result from the more enhanced contribution of the wave forcing. This chapter also showed, through a comparison between the results obtained with MAECHAM5 and those of studies using observational data, that MAECHAM5 captures the basic dynamics of the observed tropospheric NAM or NAO.

6 Conclusion

In this study, MAECHAM5/ocean mixed layer coupled model was used to investigate the dynamics of the evolution of strong stratospheric NAM-phases and their impact on troposphere and lower mesosphere.

First, the model was compared to the observations and we looked at the dynamical consistence in MAECHAM5. The focus was on the function of the middle atmospheric meridional circulation and on the forcing driving it. The January climatology of the model wind and temperature proved to agrees quite well with the observations, especially in the extratropical region and outside the uppermost model levels (where the sponging effect is strong).

It was shown that MAECHAM5 reproduces both the middle atmospheric mean meridional residual circulation and its function, which consists in compensating the radiative cooling (warming) in the summer (winter) hemisphere, quite well (see ch.2). The dynamics that maintains the middle atmospheric circulation in MAECHAM5 proved to be consistent with previous studies. In accordance with the Charney-Drazin criterion, the strong tropospheric planetary wave activity propagates up- and poleward into the winter stratosphere, where the stratospheric wind is westerly. This results in the deceleration of the strong radiatively induced westerlies and the generation of the Brewer-Dobson circulation. The winter part of the Murgatroyd-Singleton residual circulation is induced both by planetary waves and residual forcing. The strong residual forcing in the winter mesosphere and upper stratosphere can be explained mainly by the gravity wave drag, and it contributes to the Murgatroyd-Singleton circulation much more than the planetary wave drag. This finding shows the importance of the gravity wave drag in the upper strato-

sphere and mesosphere and is consistent with *Holton* [1983], who showed that a realistic warming in the polar upper stratosphere can be simulated by using only the gravity wave drag, tuned to ensure a realistic mesosphere. The summer part of the Murgatroyd-Singleton residual circulation is induced exclusively by the residual forcing, which can be explained by the gravity wave drag.

Then the three-dimensional structure of the leading modes of the month-to-month winter variability and covariability in the stratosphere/troposphere coupled system was studied. It was shown that the three-dimensional structure of the model NAM (i.e. the leading EOF-mode of the extratropical geopotential height) is quite similar to that derived from the observational studies. This mode is much more important in the stratosphere than in the troposphere. The wavelet and SSA analyses of the NAMI showed that the stratospheric NAM is dominated by low frequency time scales. The same analysis showed that the synoptic and quasistationary time scales are much more important in the troposphere. This reflects the local structure of the tropospheric circulation. The SVD analysis of the geopotential height showed that the stratosphere and troposphere are strongly coupled through the NAM-patterns.

A lag composite analysis based on the 50hPa-NAMI showed enhanced anomalous westerlies and a temperature quadrupole between the troposphere and lower mesosphere that strengthen (weaken) during the increase (decrease) of the positive NAMI phase. The lower part of the NAM temperature quadrupole shows a downward propagating dipole with a cold pole in the polar and a warm pole in the mid latitude troposphere and stratosphere. At the same time it shows an anomalous westerly wind and wind shear that also strengthen and propagate downward, especially during the increase and mature phases. The upper part of the temperature quadrupole shows a downward propagating warm pole in the polar mesosphere and upper stratosphere and a cold pole in the mid latitudes at the same altitudes, and it is associated with an anomalous easterly wind shear that also strengthens and propagates downward, especially during the decline and decay phases.

In this study, an approach using the stretching vorticity was used to explain the mechanisms of the coupling between troposphere, stratosphere and lower meso-

sphere. As demonstrated in ch.4, the MAECHAM5/ocean mixed layer coupled model, NAM temperature, zonal flow and geopotential height patterns as well as their downward propagation can be explained by the response of the stretching vorticity to the residual Coriolis forcing changes and some feedbacks that contribute to the persistence and decay of those patterns during their increase and decrease phases, respectively. Fig. 6.1 summarizes the anomalous changes that contribute to the strengthening (6.1a) and weakening (6.1b) of the polar jet and resulting impact on the troposphere and mesosphere. Fig. 6.2 summarizes the anomalous changes at strong negative NAM-phases. Fig. 6.3a (b) illustrates the non-local forcings that drive the remote residual circulations and the NAM-patterns between the troposphere and lower mesosphere during strong positive (negative) stratospheric NAM. The dynamics of the strong negative NAM (Figs. 6.2 and 6.3b) can be derived by taking (L - H)-composites of the results shown in this study.

The dynamics driving a strong positive stratospheric jet and its coupling to the troposphere as shown in Figs. 6.1 and 6.3a can be summarized as follows: During the growth and the mature phases of the stratospheric jet (Fig. 6.1a) there is an anomalous equatorward deflection of the tropospheric planetary waves, which leads to reduced wave breaking in the polar stratosphere and thus to anomalous eastward planetary wave forcing. The middle and lower stratosphere respond to these changes by an anomalous westward residual Coriolis forcing that balances the eastward planetary wave forcing and weakens the Brewer-Dobson circulation. The strongest anomalous westward Coriolis forcing in the stratosphere is centered at 60-70°N. This results in an anomalous divergence (convergence) of the Coriolis forcing north (south) of 60-70°N and leads as in case 2a (2a') of Fig. 2 to a contraction (stretching) of the stratosphere in the high (mid) latitudes. By continuity, these changes contribute to an anomalous stretching of the high latitude upper troposphere and lower mesosphere, and a contraction of the mid-latitude upper troposphere and lower mesosphere. The net results are the NAM temperature, geopotential height and zonal wind patterns in which the anomalous cooling and pressure decrease are caused by upward motion and the anomalous warming and pressure increase by downward motion. The zonal wind structure results from the temperature pattern

by thermal wind balance. The persistence, strengthening, and downward propagation of the NAM patterns during the increase and mature phases are increased mainly by the positive vortex-planetary waves feedback, in which the strong stratospheric jet and the resulting wind shear and curvature are associated with less wave breaking into the stratosphere, which in turn strengthens the stratospheric jet and its vertical shear and curvature further [*Hartmann et al.*, 2000; *Limpasuvan and Hartmann*, 2000]. The increase of westerly wave forcing near the tropospheric jet is associated with anomalous equatorward motion from the stretched into the contracted tropospheric area and can thus be seen as a quasigeostrophic adjustment of the troposphere to the changes induced by the stratosphere.

The lower mesosphere and upper stratosphere respond to the strong stratospheric jet with a delayed strong negative residual forcing that weakens the stratospheric jet and exercises negative feedback on it (Fig. 6.1b). Both the enhanced residual forcing and the resulting feedback in these altitudes can be explained by the strengthening of the easterly gravity wave drag induced by the strong stratospheric jet and its vertical structure. The enhanced negative residual forcing results in an anomalous positive Coriolis forcing that- together with the wave forcing- maintains the westerlies against the strong easterly residual drag. The net effect is an anomalous convergence of the Coriolis forcing in the polar mesosphere, and thus a stretching of the mesosphere (according to case 2b' in Fig. 2). This enhances the anomalous downward motion in both lower mesosphere and upper stratosphere. The net effect is a delayed adiabatic warming and weakening of the polar vortex, which is strongest during the decline and decay phases. The vortex-residual forcing feedback, which can be explained by the gravity wave filtering through the stratospheric jet, acts as a self-regulation mechanism of the strong wind and temperature anomalies in the middle atmosphere. The weakening of the stratospheric jet in the decline and decay phases is accelerated and enhanced by the polar vortex-planetary waves feedback.

The essence of the dynamics represented in Figs. 6.1 and 6.2 is summarized in Fig.6.3: During strong stratospheric NAM-phases, stratosphere and troposphere can be seen as one coupled system, which interacts with its upper and lower boundaries.

The vertical and meridional structure of the NAM-wind-pattern inside this system controls several forcings, which in turn exercise a non-local control on the residual circulation and thus also on the wind and temperature patterns. This control results from the response of the Coriolis forcing to the induced planetary wave and residual forcing, and the resulting mass redistribution. The Coriolis forcing responds locally to these forcings in such a way that the momentum remains conserved. A net positive forcing drives a negative Coriolis forcing (i.e. equatorward motion) and thus, by continuity, a negative (positive) meridional circulation under (above) the forcing region. A net negative forcing drives a positive Coriolis forcing (i.e. poleward motion) and thus, by continuity, a positive (negative) residual circulation under (above) the forcing region. Only forcings acting away from the boundary layers (bottom, tropopause, stratopause) can control both circulations above and under the forcing source. Inside the troposphere/stratosphere system, planetary wave forcing and residual forcing control the residual circulation non-locally. At the same time they exercise positive feedback on the wind anomalies, in such a way that these forcings contribute to the strengthening and persistence of the NAM-patterns. In the upper boundaries of the troposphere/stratosphere system (mesosphere and upper stratosphere), the non local control of the circulation is driven by the residual forcing (i.e. the gravity wave drag). At the same time it exercises negative feedback on the zonal flow in such a way that the NAM-patterns are weakened and modulated by this forcing from above. In the lowermost boundaries of the system (i.e. near the bottom), planetary wave and residual forcing (mainly friction) control the residual circulation and exercise negative feedback on the wind anomalies in such a way that the NAM-patterns are weakened and modulated from below.

It should be noted, though, that by using the idealised MAECHAM5 simulation and not observational data, we excluded several factors that impact the circulation and wave forcing in both troposphere and stratosphere, e.g. solar cycle, dynamics-chemistry coupling, QBO, volcano eruption, and anthropogenic effects. These can modify the form, location and strength of the forcing sources shown in Fig. 6.3 and lead to a different picture. The exclusion of these effects makes the interpretation of our result easier, though, since the simultaneous impact of all these factors is still

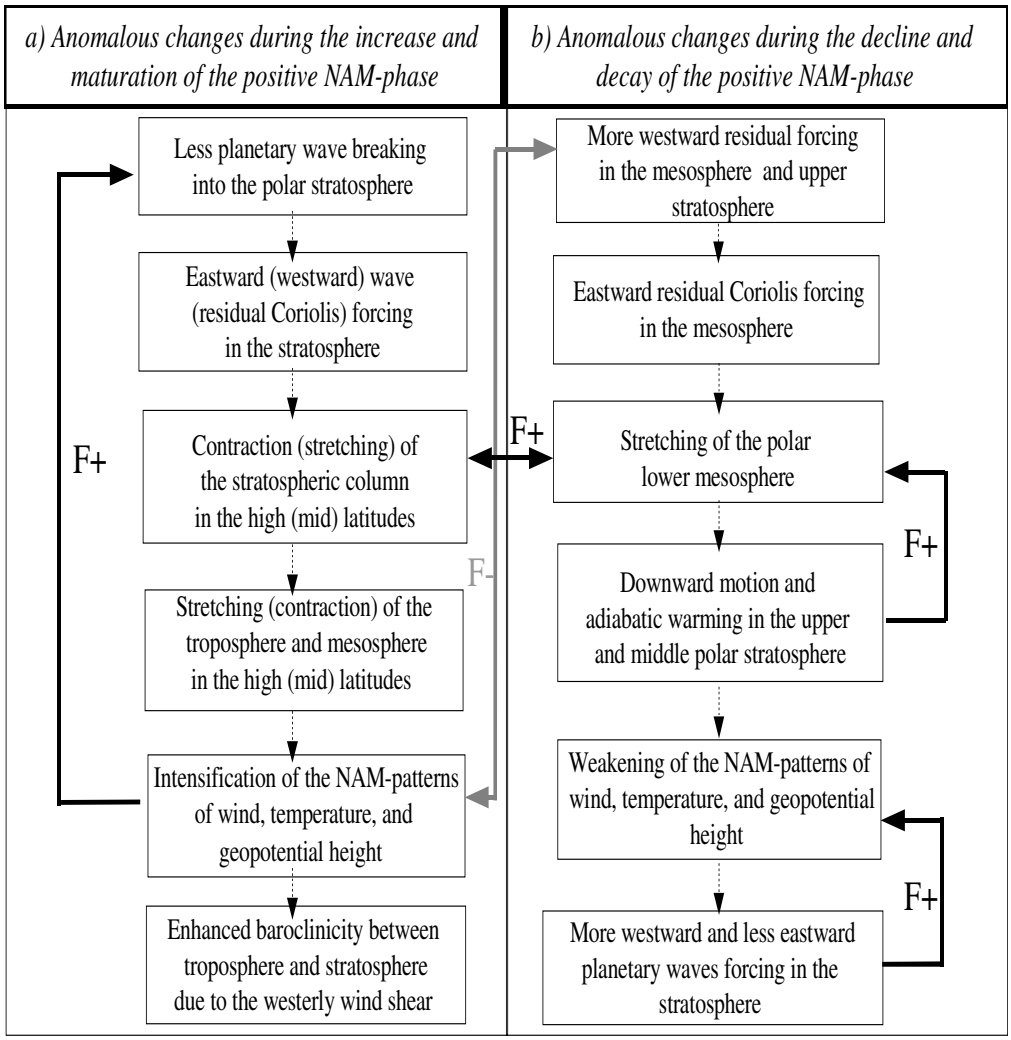

Figure 6.1: Schematic diagram showing the mechanisms that contribute to (a) the strengthening and (b) the weakening of the positive anomalies of the stratospheric polar jet and its impact on the tropospheric circulation during the evolution of the strong positive stratospheric NAM-phase. F+ (F-) represents positive (negative) feedback.

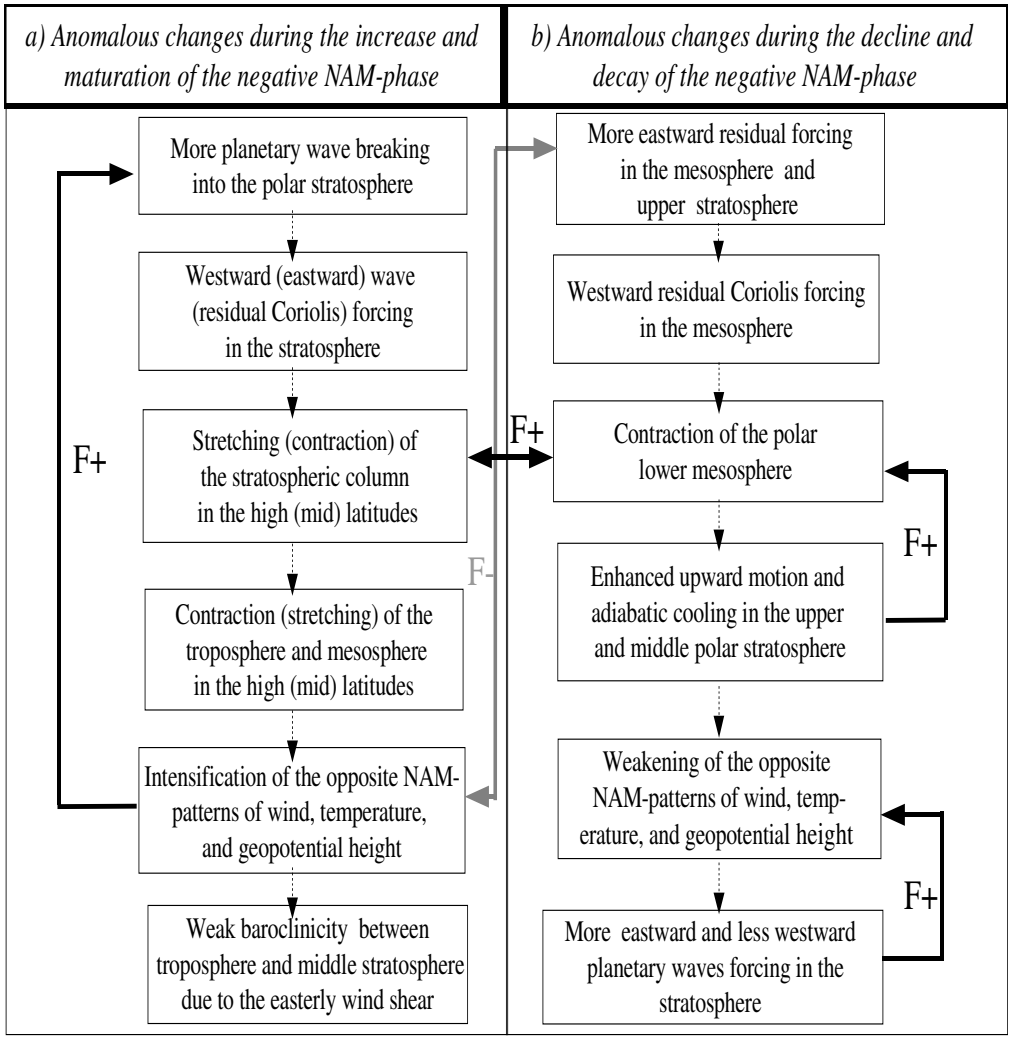

Figure 6.2: Schematic diagram showing the mechanisms that contribute to (a) the strengthening and (b) the weakening of the negative anomalies of the stratospheric polar jet and its impact on the tropospheric circulation during the evolution of the strong negative stratospheric NAM-phase. F+ (F-) represents positive (negative) feedback

unclear.

As shown in chapter 5, tropospheric and stratospheric NAM are two different modes having different time scales, and driven by different mechanisms: The life cycle of the tropospheric NAM-mode is much shorter and is dominated by high frequency fluctuation in the synoptic time scales superimposed to low frequency changes. Onset, increase, and mature phases of the tropospheric mode are preceded and accompanied by an enhanced vortex. The enhanced tropospheric westerlies at lag 0 are followed by a strong vortex and cooling 4-5 days later. The tropospheric anomalies are much stronger and the stratospheric anomalies much weaker in the tropospheric mode as compared to the stratospheric mode.

The differences in the structures and time scales between the tropospheric and stratospheric NAM reflect the different forcings driving these modes. In the stratospheric NAM mode, the tropospheric westerlies are driven non-locally by the stratospheric circulation and are enhanced by the vortex-wave forcing feedback. In the tropospheric mode, on the other hand, the tropospheric westerlies are induced by a strong internal wave and a residual forcing, which develop inside the troposphere in a synoptical time scale. This results in the tropospheric westerlies being stronger in the tropospheric than in the stratospheric mode. The stratosphere is also important in the tropospheric mode: It provides the upper troposphere with westerly wind and wind shear that can contribute to the internal amplification of the baroclinic wave in the troposphere. The amplification of the wave forcing in the maturation phase leads to an enhanced anomalous change in the tropospheric circulation, which results, by continuity, in a strong anomalous upward motion (i.e. adiabatic cooling) in the arctic and thus in a strong vortex that reaches its maximum 4-5 days later and contributes, through the stretching vorticity mechanism and vortex-planetary waves feedback, to the persistence of both tropospheric and stratospheric westerlies and cooling. The weak stratospheric westerlies in the tropospheric mode result from the weak contribution of the planetary waves to the enhanced westerlies in this mode.

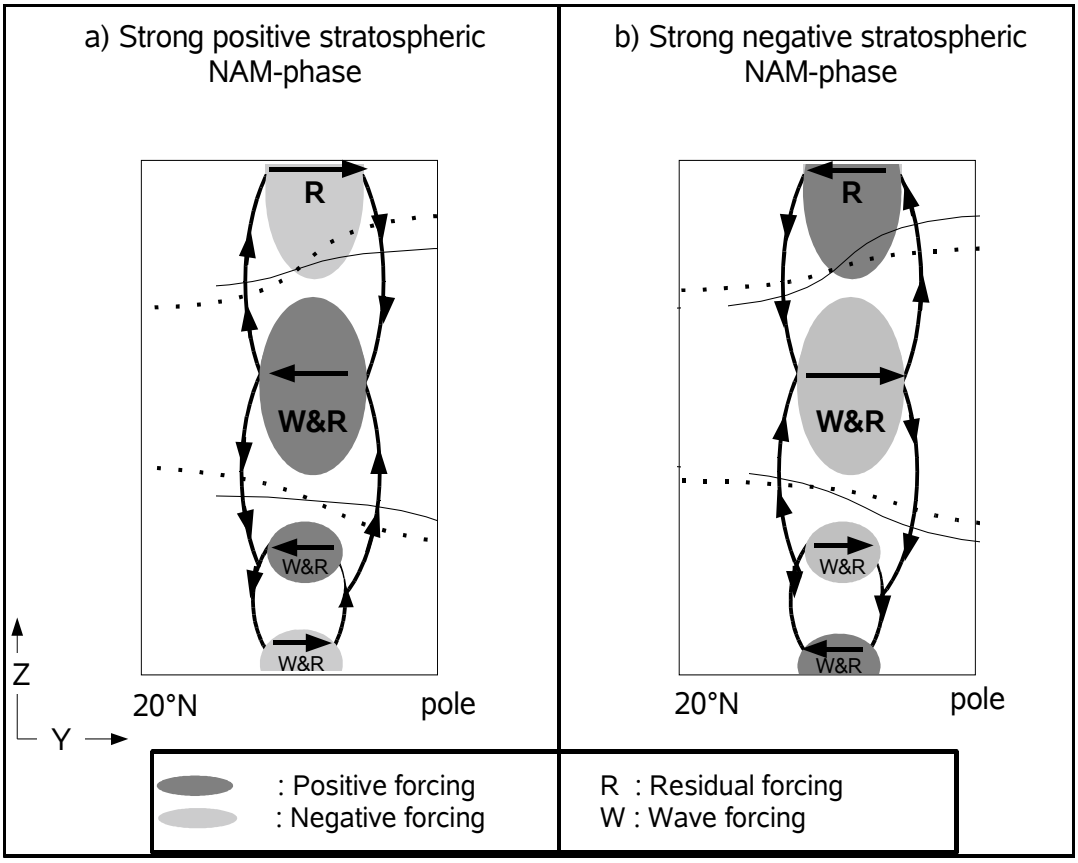

Figure 6.3: a (b) illustrates the non-local forcings driving the NAM residual circulation patterns between the troposphere and lower mesosphere during strong positive (negative) stratospheric NAM-phases. Positive (negative) forcing is shaded in dark (light) grey. Positive forcing drives equatorward motion and thus, by continuity, negative (positive) residual circulation under (above) the forcing source. Negative forcing drives poleward motion and thus, by continuity, positive (negative) residual circulation under (above) the forcing source. Only forcing acting away from the boundary layers can drive the circulation both above and under the forcing source. The residual effect (R) can be explained by the following forcings: gravity wave, non-quasigeostrophic component of the EP-flux and frictional forcing (see text). The non-local forcings exercise positive feedback on the NAM-wind patterns between the free troposphere and stratosphere but negative feedback in the upper and lower boundaries.

7 Appendix

APPENDIX A

The stretching or contraction of the stratosphere could lead, by continuity, to the change of temperature, pressure and wind in the troposphere and/or mesosphere through the resulting vertical motion. Processes that drive the change of the stretching vorticity can thus contribute to understanding the coupling among stratosphere, troposphere and mesosphere. A tendency equation of the stretching vorticity can be derived from the quasigeostrophic basic equations in z coordinates [e.g. *Andrews et al.*, 1987; *Holton*, 1992].

Using the zonal-mean quasigeostrophic potential vorticity equation in z coordinate:

$$\bar{q}_t \;\; = \left(-\overline{v'q'} - \overline{X}\right)_y + f_0\rho_0^{-1}\left(\rho_0\frac{\bar{Q}}{\theta_{0z}}\right)_z, \tag{A-1}$$

and the quasigeostrophic relation between the meridional eddy flux of the potential vorticity and the divergence of the EP-flux:

$$\overline{v'q'} = (\rho_0)^{-1}\underline{\nabla}.\underline{F}, \tag{A-2}$$

we can rewrite the potential vorticity equation A-1 in the following form:

$$\bar{q}_t \;\; = \left(-(\rho_0)^{-1}\underline{\nabla}.\underline{F} - \overline{X}\right)_y + f_0\rho_0^{-1}\left(\rho_0\frac{\bar{Q}}{\theta_{0z}}\right)_z. \tag{A-3}$$

In this equation,

$$\bar{q}_t \quad = \quad \left(-\bar{u}_y\right)_t + \left(\overline{q_s}\right)_t \tag{A-4}$$

is the local change of the potential vorticity, and $\left(\overline{q_s}\right)_t$ is the local change of the stretching vorticity defined as follows:

$$\left(\overline{q_s}\right)_t = \frac{f_0}{\rho_0}\left(\frac{\rho_0}{N^2}\left(\overline{\Phi}_z\right)_t\right)_z \ . \tag{A-5}$$

If we use the TEME,

$$\bar{u}_t - f_0\bar{v^*} = (\rho_0)^{-1}\underline{\nabla}.\underline{F} + \overline{X} \quad , \tag{A-6}$$

we can rewrite equation A-3 in this form:

$$\bar{q}_t \quad = \left(-\bar{u}_t + f_0\bar{v^*}\right)_y + f_0\rho_0^{-1}\left(\rho_0\frac{\bar{Q}}{\bar{\theta}_{0z}}\right)_z \ . \tag{A-7}$$

Using A-4 and A-7, we get the following tendency equation of the stretching vorticity:

$$\left(\overline{q_s}\right)_t = \left(f_0\bar{v^*}\right)_y + f_0\rho_0^{-1}\left(\rho_0\frac{\bar{Q}}{\bar{\theta}_{0z}}\right)_z \ . \tag{A-8}$$

According to A-8, the local change of the zonal mean stretching vorticity is controlled by the meridional divergence of the residual Coriolis forcing (first term on the right) and the vertical structure of the diabatic heating (second term).

Bibliography

Ambaum, M. H. P., and B. Hoskins, The NAO troposphere-stratosphere connection, *J. Climate*, *15*, 1969–1978, 2002.

Andrews, D., J. R. Holton, and C. B. Leovy, *Middle atmosphere dynamics*, Academic Press, London, 1987.

Appenzeller, C., J. R. Holton, and K. H. Rosenlof, Seasonal variation of mass transport across the tropopause, *J. Geophys. Res.*, *101*, 15,071–15,078, 1996.

Baldwin, M. P., and T. J. Dunkerton, Propagation of the Arctic Oscillation from the stratosphere to the troposphere, *J. Geophys. Res.*, *104*, 30,937–30,946, 1999.

Baldwin, M. P., and T. J. Dunkerton, Stratospheric harbingers of anomalous weather regimes, *Science*, *294*, 581–584, 2001.

Baldwin, M. P., D. B. Stephenson, D. W. J. Thompson, T. J. Dunkerton, A. J. Charlton, and A. O. Neill, Stratospheric memory and skill of extended-range weather forecasts, *Science*, *301*, 636–640, 2003.

Black, R. X., Stratospheric forcing of surface climate in the Arctic Oscillation, *J. Climate*, *15*, 268–277, 2002.

Boville, B. A., The influence of the polar night jet on the tropospheric circulation in a GCM, *J. Atmos. Sci.*, *41*, 1132–1142, 1984.

Brasseur, G. P., J. J. Orlando, and G. S. Tyndall, *Atmospheric Chemistry and Global Change*, Oxford University Press, Oxford, 1999.

Bretherton, C. S., C. Smith, and J. Wallace, An Intercomparison of Methods for Finding Coupled Patterns in Climate Data , *J. Climate*, *5*, 541–560, 1992.

Brönnimann, S., The impact of El Niño/Southern Oscillation on European climate, *Reviews of Geophysics (accepted)*, 2006.

Brönnimann, S., J. Luterbacher, J. Staehelin, T. M. Svendby, G. Hansen, and T. Svenoe, Extreme climate of the global troposphere and stratosphere in 1940-42 related to El Niño, *Nature*, *431*, 971–974, 2004.

Brönnimann, S., E. Xoplaki, C. Casty, A. Pauling, and J. Luterbacher, ENSO influence on Europe during the last centuries, *Climate Dyn.*, *28*, 181–197, 2007.

Charney, J. G., The dynamics of long waves in a baroclinic westerly current, *J. Meteor.*, *4*, 135–162, 1947.

Charney, J. G., and P. G. Drazin, Propagation of planetary-scale disturbances from the lower into the upper atmosphere, *J. Geophys. Res.*, *66*, 83–109, 1961.

Christiansen, B., Downward propagation of zonal mean zonal wind anomalies from the stratosphere to the troposphere: Model and reanalysis, *J. Geophys. Res.*, *106*, 27,307–27,322, 2001.

Danielsen, E., R. Bleck, J.Shedlovsky, A. Wartburg, P. Haagenson, and W. Pollok, Observed distribution of radioactivity, ozone, and potential vorticity associated with tropopause folding, *J. Geophys. Res.*, *75*, 2353–2361, 1970.

Duck, T. J., J. Whiteway, and A. Carswell, The Gravity Wave-Arctic Stratospheric Vortex Interaction, *J. Atmos. Sci.*, *58*, 3581–3596, 2001.

Dunkerton, T., On the Mean Meridional Mass Motions of the Stratosphere and Mesosphere, *J. Atmos. Sci.*, *35*, 2325–2333, 1978.

Fels, S. B., Radiative-dynamical interactions in the middle atmosphere, *Adv. Geophy*, *18A*, 277–300, 1985.

Fishbein, E., et al., Validation of the UARS Microwave Limb Sounder temperature and pressure measurements, *J. Geophys. Res.*, *101*, 9983–10,016, 1996.

Gouget, H., G. Vaughan, A. Marenco, and H. G. J. Smit, Decay of a cut-off low and contribution to stratosphere-troposphere exchange, *Quart. J. Roy. Meteor. Soc.*, *126*, 1117–1141, 2000.

Green, J. S. A., A problem in baroclinic stability, *Quart. J. Roy. Meteor. Soc.*, *86*, 235–251, 1960.

Hartmann, D. L., Baroclinic instability of realistic zonal-mean states to planetary waves, *J. Atmos. Sci.*, *36*, 2336–2349, 1979.

Hartmann, D. L., J. M. Wallace, V. Limpasuvan, D. W. J. Thompson, and J. R. Holton, Can ozone depletion and global warming interact to produce rapid climate change?, *P Natl. Acad. Sci. USA.*, *97*, 1412–1417, 2000.

Haynes, P. H., C. J. Marks, M. E., McIntyre, T. G. Shepherd, and K. P. Shine, On the downward control of extratropical diabatic circulations by eddy-induced mean zonal forces, *J. Atmos. Sci.*, *48*, 651–679, 1991.

Hays, P. B., et al., The high-resolution Doppler imager on the Upper Atmosphere Research Satellite, *J. Geophys. Res.*, *98*, 10,713–10,72, 2003.

Hervig, M. E., et al., Validation of temperature measurements from the Halogen Occultation Experiment, *J. Geophys. Res.*, *101*, 10,277–10,286, 1996.

Hines, C. O., Doppler-spread parameterization of gravity wave momentum deposition in the middle atmosphere. Part 1: Basic formulation, *J. Atm. Sol. Terr. Phys*, *59*, 371–386, 1997a.

Hines, C. O., Doppler-spread parameterization of gravity wave momentum deposition in the middle atmosphere. Part 2: Broad and quasi monochromatic spectra, and implementation, *J. Atm. Sol. Terr. Phys*, *59*, 387–400, 1997b.

Hirota, I., and J. J. Barnett, Planetary waves in the winter mesosphere Preliminary analysis of the Nimbus 6 PMR results, *Quart. J. Roy. Meteor. Soc.*, *103*, 487–498, 1977.

Hoerling, M. P., M.P., A. Kumar, and M. Zhong, El Niño, La Niña, and the Nonlinearity of Their Teleconnections, *J. Climate*, *10*, 1769–1786, 1997.

Holton, J. R., The influence of gravity wave breaking on the general circulation of the middle atmosphere, *J. Atmos. Sci.*, *40*, 2497–2507, 1983.

Holton, J. R., *An Introduction to Dynamic Meteorology*, 3dr Ed., Academic Press, San Diego, 1992.

Holton, J. R., and H.-C. Tan, The influence of the equatorial quasi-biennial oscillation on the global circulation at 50 mb, *J. Atmos. Sci.*, *37*, 2200–2208, 1980.

Holton, J. R., P. H. Haynes, M. E. McIntyre, A. R. Douglass, R. Rood, and L. Pfister, Stratosphere troposphere exchange, *Rev. Geophys.*, *33*, 403 39, 1995.

Hoskins, B. J., M. E. McIntyre, and . A. W. Robertson, On the use and significance of isentropic potential vorticity maps, *Quart. J. Roy. Meteor. Soc.*, *111*, 877–946, 1985.

Inatsu, M., H. Mukougawa, and S. Xie, Atmospheric Response to Zonal Variations in Midlatitude SST: Transient and Stationary Eddies and Their Feedback, *J. Climate*, *16*, 3314–3329, 2003.

Kodera, K., K. Yamazaki, M. Chiba, and K. Shibata, Downward propagation of upper stratospheric mean zonal wind perturbation to the troposphere, *Geophys. Res. Lett.*, *17*, 1263 66, 1990.

Krüger, K., B. Naujokat, and K. Labitzke, The Unusual Midwinter Warming in the Southern Hemisphere Stratosphere 2002, *J. Atmos. Sci.*, *62*, 603–613, 2005.

Labitzke, K., The interaction between stratosphere and mesosphere in winter, *J. Atmos. Sci.*, *29*, 1395–1399, 1972a.

Labitzke, K., Temperature Changes in the Mesosphere and Stratosphere Connected with Circulation Changes in Winter, *J. Atmos. Sci.*, *29*, 756–766, 1972b.

Lau, K. M., and H. Weng, Climate Signal Detection Using Wavelet Transform: How to Make a Time Series Sing, *Bull. Am. Meteorol. Soc.*, *76*, 2391–2402, 1995.

Limpasuvan, V., and D. Hartmann, Eddies and the annular modes of climate variability, *Geophys. Res. Lett.*, *26*, 3133–3136., 1999.

Limpasuvan, V., and D. Hartmann, Wave-Maintained Annular Modes of Climate Variability, *J. Climate*, *13*, 4414–4429, 2000.

Lindzen, R. S., Turbulence and stress due to gravity wave and tidal breakdown, *J. Geophys. Res.*, *86*, 9707–9714, 1981.

Lindzen, R. S., and B. Farrell, A simple approximate result for the maximum growth rate of baroclinic instabilities, *J. Atmos. Sci.*, *37*, 1648–1654, 1980.

Lorenz, D. J., and D. L. Hartmann, Eddy-Zonal flow feedback in the Northern Hemisphere Winter, *J. Climate*, *16*, 1212–1227, 2003.

Lorenz, E. N., *Empirical Orthogonal Functions and Statistical Weather Prediction*, Scientific Report 1, Statistical Forecasting Project, Mass. Inst. Tech., Cambridge, Mass, 1957.

Lott, F., and M. J. Miller, A new subgrid-scale orographic drag parameterization: Its formulation and testing, *Quart. J. Roy. Meteor. Soc.*, *123*, 101–127, 1997.

Manzini, E., and N. A. McFarlane, The effect of varying the source spectrum of a gravity wave parameterization in middle atmosphere general circulation model, *J. Atmos. Sci.*, *103*, 31,523–31,539, 1998.

Matsuno, T., Vertical propagation of stationary planetary waves in the winter Northern Hemisphere, *J. Atmos. Sci.*, *27*, 871–883, 1970.

Matsuno, T., A quasi one-dimensional model of the middle atmosphere circulation interacting with internal gravity wave, *J. Meteor. Soc. Japan,*, *60*, 215–226, 1982.

Mechoso, C. R., and D. L. Hartmann, An Observational Study of Traveling Planetary Waves in the Southern Hemisphere, *J. Atmos. Sci.*, *58*, 3581–3596, 1982.

Murgatroyd, R. J., and F. Singleton, Possible meridional circulation in the stratosphere and mesosphere, *Quart. J. Roy. Meteor. Soc.*, *87*, 125–135, 1961.

Norton, W. A., Sensitivity of Northern Hemisphere surface climate to simulation of the stratospheric polar vortex, *Geophys. Res. Lett.*, *30*, 2003GL016,958, 2003.

Orsolini, Y., C. Randall, G. Manney, and D. Allen, An Observational Study of the Final Breakdown of the Southern Hemisphere Stratospheric Vortex in 2002, *J. Atmos. Sci.*, *62*, 735–747, 2005.

Perlwitz, J., and N. Harnik, Observational evidence of a stratospheric influence on the troposphere by planetary wave reflection, *J. Climate*, *16*, 3011–3026, 2003.

Perlwitz, J., and N. Harnik, Downward Coupling between the Stratosphere and Troposphere: The Relative Roles of Wave and Zonal Mean Processes, *J. Climate*, *17*, 4902–4909, 2004.

Pfister, L., Baroclinic instability of easterly jets with application to the summer mesosphere, *J. Atmos. Sci.*, *42*, 313–330, 1985.

Plumb, R. A., Baroclinic instability of the summer mesosphere: A mechanism for the quasi-two-day wave?, *J. Atmos. Sci.*, *40*, 262–270, 1983.

Polvani, L. M., and P. J. Kushner, Tropospheric response to stratospheric perturbations in a relatively simple general circulation model, *Geophys. Res. Lett.*, *29*, 2001GL014,284, 2002.

Quiroz, R. S., The warming of the upper stratosphere in February 1966 and the associated structure of the mesosphere, *Mon. Wea. Rev.*, *97*, 541–552, 1969.

Quiroz, R. S., The tropospheric-stratospheric polar vortex breakdown of January 1977, *Geophys. Res. Lett.*, *4*, 151–154, 1977.

Rodgers, C. D., and A. J. Prada, Evidence for a traveling 2-day wave in the middle atmosphere, *J. Geophys. Res.*, *86*, 9661–9664, 1981.

Roeckner, E., et al., *The atmospheric general circulation model ECHAM-4: model description and simulation of present-day climate*, Report 218, Max-Planck-Institut für Metoerologie, Hamburg, 1996.

Roeckner, E., et al., *The atmospheric general circulation model ECHAM5. Pt. 1: Model description*, Report 349, Max-Planck-Institut für Metoerologie, Hamburg, 2003.

Roeckner, E., et al., *The atmospheric general circulation model ECHAM5. Pt. 2: Sensitivity of simulated climate to horizontal and vertical resolution*, Report 349, Max-Planck-Institut für Metoerologie, Hamburg, 2004.

Rood, R. B., A. R. Douglass, M. A. Cerniglia, and W. Read, Synoptic scale mass exchange from the troposphere to the stratosphere, *Geophys. Res. Lett.*, *102*, 23,467–23,485, 1997.

Russell, J. M., et al., The Halogen Occulation Experiment, *J. Geophys. Res.*, *98*, 10,777– 10,979, 1993.

Strauss, D. M., Long wave baroclinic instability in the troposphere and stratosphere with spherical geometry, *J. Atmos. Sci.*, *38*, 409–426, 1981.

Swinbank, R., and A. O'Neill, A stratosphere-troposphere data assimilation system, *Mon. Wea. Rev.*, *122*, 686–702, 1994.

Swinbank, R., and D. Ortland, Compilation of wind data for the UARS reference atmosphere project, *J. Geophys. Res.*, *108*, D19, 4615, doi:10.1029/2002JD003,135, 2003.

Tanaka, H. L., and H. Tokinaga, Baroclinic instability in high latitudes induced by polar vortex: A connection to the Arctic Oscillation, *J. Atmos. Sci.*, *59*, 69–82, 2002.

Thompson, D. W. J., and J. M. Wallace, The Arctic Oscillation signature in the wintertime geopotential height and temperature fields, *Geophys. Res. Lett.*, *25*, 1297–1300, 1998.

Thompson, D. W. J., and J. M. Wallace, Annular Modes in the Extratropical Circulation Part I: Month- to-month variability, *J. Climate*, *13*, 1000–1016, 2000.

Torrence, C., and G. P. Compo, A practical guide to wavelet analysis, *Bull. Am. Meteorol. Soc.*, *79*, 61–78, 1998.

von Storch, H., and A. Navarra, *Analysis of climate variability. Applications of Statistical techniques*, Springer-Verlag, 1995.

von Storch, H., and F. Zwiers, *Statistical Analysis in Climate Research*, Cambridge University Press, Cambridge, 1999.

Wallace, J. M., C. Smith, and C. Bretherton, Singular Value Decomposition of Wintertime Sea Surface Temperature and 500-mb Height Anomalies, *J. Climate*, *5*, 561–576, 1992.

Wang, B., and Y. Wang, Temporal Structure of the Southern Oscillation as Revealed by Waveform and Wavelet Analysis, *J. Climate*, *9*, 1586–1598, 1996.

Wu, D. L., et al., Mesospheric temperatures from UARS MLS: Retrieval and validation, *J. Atmos. Solar-Terr. Phys*, *65 (2)*, 245–267 JAN, 2003.

Zhang, K.-S., and T. Sasamori, A Linear Stability Analysis of the Stratospheric and Mesospheric Zonal Mean State in Winter and Summer, *J. Atmos. Sci.*, *42*, 2728–2750, 1985.

Acknowledgements

I am very grateful to Prof. Dr. Mojib Latif and Dr. Marco Giorgetta for supervising this thesis, and for their guidance during the evolution of this work.

Special thanks to my wife Christine for the enormous amount of support, patience and encouragement all along. I also thank my parents and all my family in Morocco for supporting the choices I have made. Special thanks to my brothers Hamid and Fouad and to Amal, Mohcine and Hanan for their support at the beginning of my studies in Germany. Without them this thesis would never have become possible. Many thanks also to Ingrid and Karen- my "German mothers."

Thanks also go to Drs. Jürgen Bader and Elisa Manzini and Profs. Drs. Axel Timmermann, Kirstin Krüger and Eberhard Ruprecht for many fruitful discussions. Special thanks to Dr. Noel Keenlyside for helpful comments, discussions and suggestions on earlier versions of the manuscript. I also thank Drs. Monika Esch and Wonsun Park for the Model support.

Last but not least, many thanks to Cornelia Schuster, Kai Grunau, Joachim Herrmann and all the other people at our institute, be it in our department, in other departments or in the library, who have in one way or another contributed to this thesis.

The financial support of this work was provided by the German Climate Research Programme DEKLIM and the European Climate Research Programme DYNAMITE.